Use Of Impedance Spectroscopy As A Probe Of Mitochondrial Membrane Potential

by
Pavithi Nishani Weerasinghe

A dissertation submitted to the Department of Physics,
College of Natural Sciences and Mathematics
in partial fulfillment of the requirements for the degree of

DOCTOR OF PHILOSOPHY

in PHYSICS

Chair of Committee: John H. Miller, Jr., Professor

Committee Member: Jarek Wosik, Research Professor

Committee Member: Gemunu Gunaratne, Professor

Committee Member: Claudia Ratti, Professor

Committee Member: Wanda Zagozdzon-Wosik, Professor

Committee Member: Dale Hamilton, M.D.

University of Houston
December 2019

DEDICATION

I dedicate this dissertation to the most inspiring people in my life,

my father and mother.

ACKNOWLEDGMENTS

I would like to express my sincere gratitude to my advisor, Dr. John H. Miller, Jr., for his guidance and support during the course of my study. His insightful knowledge in the area of experimental Biophysics enabled a vast understanding during my study. I would also like to extend a sincere thanks to Dr. Jarek Wosik, for the motivation, guidance and profound knowledge during the entirety of my multi-disciplinary study that involved Physics and Engineering experimental techniques. My sincere thank you to Dr. Wanda Zagozdzon-Wosik, for the resources she helped me acquire for my study, and the advice and support throughout this study. I would also like to express a sincere thanks to Dr. Dale Hamilton, for providing me with the necessary resources at the Bioenergetics lab, and the constant guidance in a field of study that was unfamiliar as a Physicist. My sincere thanks also go to Dr. Claudia Ratti and Dr. Gemunu Gunaratne for serving on my committee.

A special mention and thanks to my close friend and colleague Dr. Martha Villagrán, whose determination, support and constant encouragement has driven me to continuously achieve my goals. My sincere thanks to previous students of my research group, Dr. Camilia Prodan, Dr. Rooplekha Mitra, and Dr. Divya Padmaraj. I would also like to thank Dr. Uday Kiran, Dr. Kuang Qin, and Dr. Sladjana Maric for the insightful discussions, advice, and help.

I would like to thank the researchers and staff at the Bioenergetics lab at Houston Methodist Research Institute, especially, Dr. Anisha Gupte, Dr. Aijun Zhang, Indira Vendula, and Robin Smith for providing me with mitochondria samples required for my study, and for the help and support during the time I worked at the Bioenergetics lab.

I would also like to extend my thanks to Randy Clark for helping with the fabrication of my device and also Indika Deepal Weerasinghe for the support in basic electronics. My sincere thanks to Dr. Jiefu Chen and his students, who allowed me to use equipment from his lab for my study, and to Dr. Joe Charlson for permitting use of equipment from his lab at the initial stage of this study. I would

also like to sincerely thank Jennifer Chin-Davis and Naomi Haynes for their support throughout my graduate career.

My most sincere gratitude goes to my parents, my brother, and my sister-in-law, for the motivation, inspiration, and endless encouragement in pursuing a career in Physics, and for extending it to a doctorate. My sincere thank you to my uncle and aunt, Srilal and Krisanthi, and cousins, Sonali and Savin for their kindness and generosity when we came to live in Houston. I would also like to thank my family-in-law, relatives, and friends.

Finally, my extreme gratitude to my husband, without whose constant encouragement, and moral support, I would not be where I am today.

ABSTRACT

A key element in mitochondrial metabolism, the synthesis of adenosine triphosphate (ATP), is driven by an electrochemical potential and a proton concentration gradient across the inner mitochondrial membrane. The electrical properties of mitochondrial suspensions thus provide vital information into internal metabolic processes. This study reports on measurements of frequency- and time-dependent electrical impedance of mitochondrial suspensions as a non-invasive and label-free method of probing mitochondrial membrane potential, and other aspects of mitochondrial activity. We designed and fabricated an effective and sensitive probe to study changes in electrical properties of live mitochondrial suspensions involving basic bioenergetic respiratory protocols, to monitor the activity of the electron transport chain. Several substrates, inhibitors, and uncouplers were used to stimulate the electron transport mechanism in mitochondria, and study the oxygen consumption changes. These observed oxygen consumption changes were correlated with measured impedance changes of mitochondrial suspensions of various concentrations, by studying their dielectric properties.

Our measurements of complex impedance were used to calculate relative dielectric permittivity and conductivity of mitochondrial suspensions, and to obtain admittance data that allowed analysis of the effects of interactions between substrates and mitochondria. Our results indicate that changes in relative dielectric permittivity for mitochondria in the presence of pyruvate and malate correlate with the increased oxygen intake of mitochondria. Our findings show that these two substrates, which trigger activation of the electron transport chain and increase the membrane potential, are shown to increase the effective relative dielectric permittivity, correlating with the expected membrane potential change. Thus, an impedance sensing method can be adapted for in-vitro studies of biological processes, such as those that take place within mitochondria. The method discussed in this dissertation could eventually be developed into tools that monitor mitochondrial diseases and dysfunction, and help enable development of treatment methods, such as new drugs that target metabolism.

TABLE OF CONTENTS

LIST OF TABLES

LIST OF FIGURES

Chapter 1: Introduction

1.1 Motivation

Mitochondria play a key role in providing energy and in modulating the cell's central pathways and processes. The mitochondrion is called "the powerhouse of the cell," and provides chemical energy for cellular functions in the form of ATP (adenosine triphosphate), via oxidative phosphorylation of ADP (adenosine diphosphate).

Oxidative phosphorylation occurs along the electron transport chain (ETC), a series of protein complexes in the inner mitochondrial membrane. These protein complexes use energy from donated electrons to pump protons, from the mitochondrial matrix to the intermembrane space across the inner mitochondrial membrane, building up a proton concentration gradient and an electrochemical membrane potential. During respiration, most of the oxygen breathed into the lungs is consumed at complex IV, otherwise known as cytochrome c oxidase in the electron transport chain, providing a correlation between electron transport and proton pumping mechanisms to the rate of oxygen consumption. The proton concentration gradient and membrane potential drives ATP synthesis from ADP and inorganic phosphate (P_i), within the ATP synthase enzyme (complex V). The electron transport mechanisms are discussed further in chapter 2.

An impedance sensing method has been adapted for in-vitro studies of mitochondrial processes of those that take place within the mitochondrion. Label-free biosensors provide a means to probe biological micro-mechanisms by providing higher throughput, lower cost, and smaller sample size. Mitochondrial dysfunction has been found to affect a vast array of diseases, including cardiac diseases, diabetes, and neurodegerative diseases, as well as aging and cancer. The technique discussed

in this dissertation could eventually be developed into tools that probe mitochondrial diseases and dysfunction, and help determine the effectiveness of treatment methods, such as new drugs targeting mitochondria.

The mitochondrial membrane potential ($\Delta\psi_m$), plays a key role in driving ATP synthesis and is a significant indicator of the health and state of functional mitochondria. Recent work of Prodan *et al.* [1, 2], Bot *et al.* [3], and Mitra *et al.* [4] has shown that changes in cellular membrane potential correlates with changes in impedance of cell suspensions. Frequency dependent studies of mitochondrial suspensions can provide vital information on temporal changes that take place within these mechanisms, and can be helpful for extensive studies for development of diagnostic treatments.

1.2 Electrical Properties of Biological Materials

Biological cells and tissues are characterized by frequency dependent dielectric properties with a high permittivity at low frequency, which decays as the frequency increases. The relaxation phenomena that take place at different frequency ranges in biological systems are results of the underlying processes. Studies of biological systems based on their electrical properties enable investigation of the response of living organisms to an applied electric field. All biological cells contain intracellular fluids and are suspended in an extracellular fluid matrix, and respond with complex frequency dependent electrical impedance that can be used as a biomarker to distinguish between normal and abnormal tissue [5].

A generic circuit description of biological samples in suspension consists of an impedance of the extracellular fluid, in parallel with a series combination of the membrane capacitance and resistance of the intracellular fluid. The electrical components are given by a combination of relaxation processes due to the polarization of the cell membrane suspending medium, and the polarization between the suspending medium and the cytoplasm. The general behavior of biological samples exhibit complex behavior. Here, the current passes through the extracellular fluid at low frequencies, with the cell close to being an insulator. However, for higher frequencies, the capacitance is close to being ideal and the resistance contribution is from both the extracellular and intracellular components.

In recent years, techniques of studying biological systems have emerged as an extremely popular analytical technique for various biological applications that include characterization of batteries, fuel cells, ceramics, coatings, semiconductors, sensors, and corrosion. Biological systems are basic biochemical systems that respond to an applied electric field over a frequency range, and can be used to obtain details of the minute processes taking place within their structures.

1.3 Electrical Impedance Studies

Electrical Impedance Spectroscopy (EIS) can be generically described as a method to study electric or dielectric properties of materials under the influence of an electric field. Electrical impedance signifies the "complex" resistance which resists the flow of electrons through a material, and is important to understand fundamental microscopic processes in an experimental point of view.

The influence of an applied electric field to a biological system can be studied by analyzing the response at a range of frequencies. An alternating electric field generates a dipole moment on charges that arise due to the relative motion of particles. The impedance and phase angle are measurable quantities that explain properties of the particles and medium of a biological system. Impedance spectroscopy is a technique that relies on electrical measurement of resistance, capacitance, and inductance, and the observed spectral data depend on equivalent circuits consisting of various combinations of such electrical components that represent the biological mechanisms being studied.

The formula for the frequency dependent impedance is given by,

$$Z(\omega) = Z' + jZ'', \tag{1.1}$$

where Z' and Z'' are the real and imaginary components of impedance, respectively.

Mitochondrial membranes exhibit resistive and capacitive properties that can be compared with electrical circuits. Analysis of impedance and phase for a frequency range can be used to evaluate the resistive, capacitive, and inductive behavior of a biological medium, eventually explaining the underlying transport processes and reactions in the medium.

1.4 Objectives and Goals

Mitochondria are organelles vital to the functionality of the human body. Numerous diseases have been found to target mitochondria in different parts of the human body, some more common than others. Diseases such as heart disease and diabetes are widespread diseases that have been found to be linked to mitochondrial dysfunction. Complex diseases such as Alzheimer's, Parkinson's, cancer, and others also involve impaired functionality of mitochondria.

Electrical impedance spectroscopy is a powerful capable technique of probing changes in dielectric properties of suspensions, which can correlate with changes in mitochondrial membrane potential [1, 2, 3, 6, 7].

The goals of this project are to: (1) study real-time impedance variations of mitochondrial suspensions with frequency, and measure how impedance and dielectric response change with addition of various substrates; and (2) correlate measured changes in dielectric response and conductivity with changes in oxygen consumption rate, expected changes in mitochondrial membrane potential, and other properties of the mitochondria, buffer, and added substrates.

1.5 Dissertation Overview

The remainder of this dissertation is organized in the following order. Chapters 2 and 3 provide a broad background into the study, by discussing the mitochondrial structure and function and the theory of mitochondrial membrane potential with relation to oxygen consumption. Chapters 4 and 5 focus on electrical properties of biological materials and methods of electrical impedance spectroscopy. Chapter 6 discusses the experimental methods with analysis and interpretation of data, and chapter 7 provides the concluding remarks.

Chapter 2: Mitochondria and Membrane Potential Studies

2.1 Mitochondrial Structure and Function

Mitochondria are present in all eukaryotic cells, and are double-membrane-bounded organelles that transform energy into forms that can be used to drive cellular reactions. In general, they occupy a large portion of the cytoplasmic volume of eukaryotic cells, and play an essential role in energy metabolism and evolution of complex mammals. These organelles represent α-proteobacteria, from which they have originated 1.6 billion years ago [8]. Mitochondria have their own Mitochondrial DNA (*mtDNA*) that encodes 37 genes in its proteins, while some genes involved in mitochondrial metabolism are encoded by nuclear DNA (*nDNA*) [9].

Depicted as stiff, elongated cylinders with a diameter of 0.5 to 1 μm, mitochondria closely resemble bacteria, from which they evolved (Figure 2.1). They are mobile and flexible organelles, constantly changing their shape and referred to as the powerhouses of the cell [8]. Mitochondria are vital for cell survival, cell signaling, modulation of oxidative stress and maintaining cell apoptosis (controlled cell death), and they are the primary source of adenosine triphosphate (ATP), an energy-rich compound that drives most fundamental cellular functions. ATP is produced on a substantial scale in the human body, amounting to around 50 kg per day in a healthy adult [10]. Most of the ATP required for cellular functions is generated via oxidative phosphorylation (oxphos) in the ATP synthase protein complex, from adenosine diphosphate (ADP) and inorganic phosphate (P_i). Mitochondria also perform cell-specialized functions that are different from each other, depending on each cell in the tissue or organism. For instance, cardiac cells have a high quantity of mitochondria due to increased energy demand, and are responsible for approximately 6 kg of ATP to maintain its function [11].

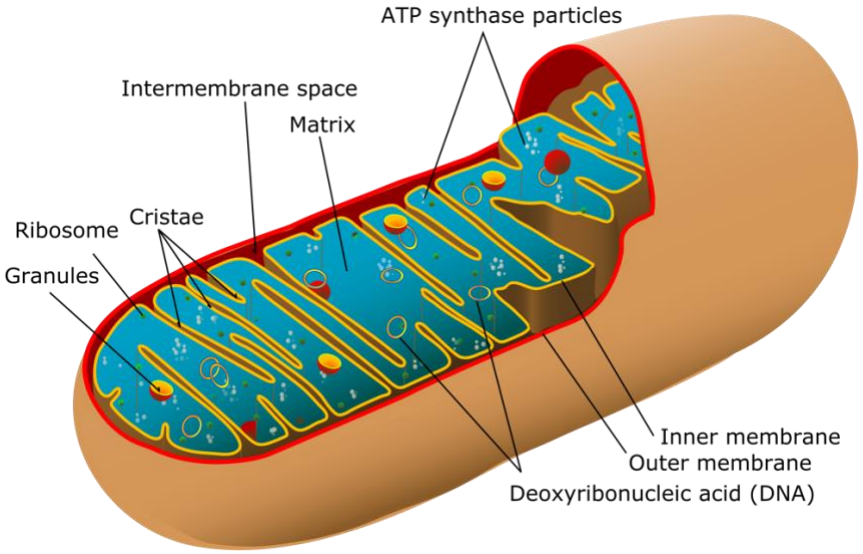

Figure 2.1: Structure of the mitochondrion [12].

The mitochondrion is bounded by two highly specialized membranes that create two separate mitochondrial compartments: the internal matrix space, and an intermembrane space. The outer membrane contains many transport proteins called *porin*, and is permeable to small molecules, by forming large aqueous channels for transport. The inner membrane is highly-specialized, and contains a fairly high portion of the double-phospholipid *cardiolipin*. This makes the membrane impermeable to ions, while the transport proteins make it selectively permeable to small molecules that are required to channel through the many mitochondrial enzymes in the matrix space. The inner membrane is folded into numerous *cristae*, which are folds in the inner mitochondrial membrane, increasing its total surface area, allowing more productivity from the mitochondria. Apart from the transport proteins that regulate the passage of metabolites in and out of the matrix, the inner membrane contains a series of principal proteins that carry out the oxidation reactions of the respiratory chain, and the synthesis of the molecule ATP. The five protein complexes that make up the respiratory chain, (also known as the electron transport chain) are essential to the process of oxidative phosphorylation, and for maintaining the electrochemical gradient across the inner membrane, which is essential for driving ATP synthesis.

The intermembrane space is the space between the inner and outer mitochondrial membranes, and is the space that necessarily allows protons to accumulate during the proton pumping mechanism of oxidative phosphorylation. The mitochondrial matrix is the innermost compartment of the mitochondrion, containing several highly concentrated enzymes and proteins that are essential for energy production. These include enzymes required for the oxidation of pyruvate and fatty acids, and for the citric acid cycle.

Mitochondria are highly dynamic organelles that form interconnected networks, whose structure and biogenesis are vastly influenced by the requirements of a cell [13]. The cellular distribution and shape of the mitochondrial network is supported greatly by regulating mitochondrial division, fusion, motility and tethering. The in-depth study of these critical cellular structures and processes is achieved by using *isolated mitochondria*, where mitochondria are extracted and purified by mechanical homogenization and differential centrifugation [14, 15]. Mitochondrial research has benefitted greatly from the accessibility of preparing organelles that can be isolated from tissues. The pioneers George Palade and coworkers, developed a protocol to isolate mitochondria, and paved the way for the extensive discoveries on mitochondrial biology, especially the *chemiosmotic theory of oxidative phosphorylation* and the explanation of the tricarboxylic acid cycle and other cyclic processes [14, 16, 17].

2.2 Mitochondrial Bioenergetics

Chemiosmotic theory is the fundamental mechanism of energy regulation in mitochondria, where the oxidation of carboxylic acids utilizes the synthesis of ATP by oxidative phosphorylation in the inner mitochondrial membrane. The respiratory enzymes embedded in the inner membrane of the mitochondria first catalyze the oxidation reactions that generate an electrochemical gradient of protons (H^+ ions) across the inner membrane. The membrane-bound F_1F_0-type proton ATPase (or ATP synthase) enzyme drives the endergonic reaction of producing ATP from ADP and P_i, using the energy of this proton gradient. The chemiosmotic process of ATP generation takes place over several steps [18].

The inner mitochondrial membrane contains a series of protein complexes that form the electron transport chain (ETC), where high-energy electrons enable protons to be pumped across the membrane, while generating a proton concentration gradient. This gradient generates a difference in the pH between the matrix and the intermembrane space, which then modulates a molecular motor F_0F_1 in the ATP synthase enzyme, to generate ATP by transporting H^+ ions back into the mitochondrial matrix. Figure 2.2 shows the process of oxidative phosphorylation, initiated by the functional acetyl molecules in the citric acid cycle that produce NADH (nicotinamide adenine dinucleotide) and $FADH_2$ (flavin adenine dinucleotide), the molecules that transfer highly energetic electrons to protein complex I and complex II. These highly energetic electrons then pass through the protein complexes and coenzymes via the ETC, yielding water and ATP molecules.

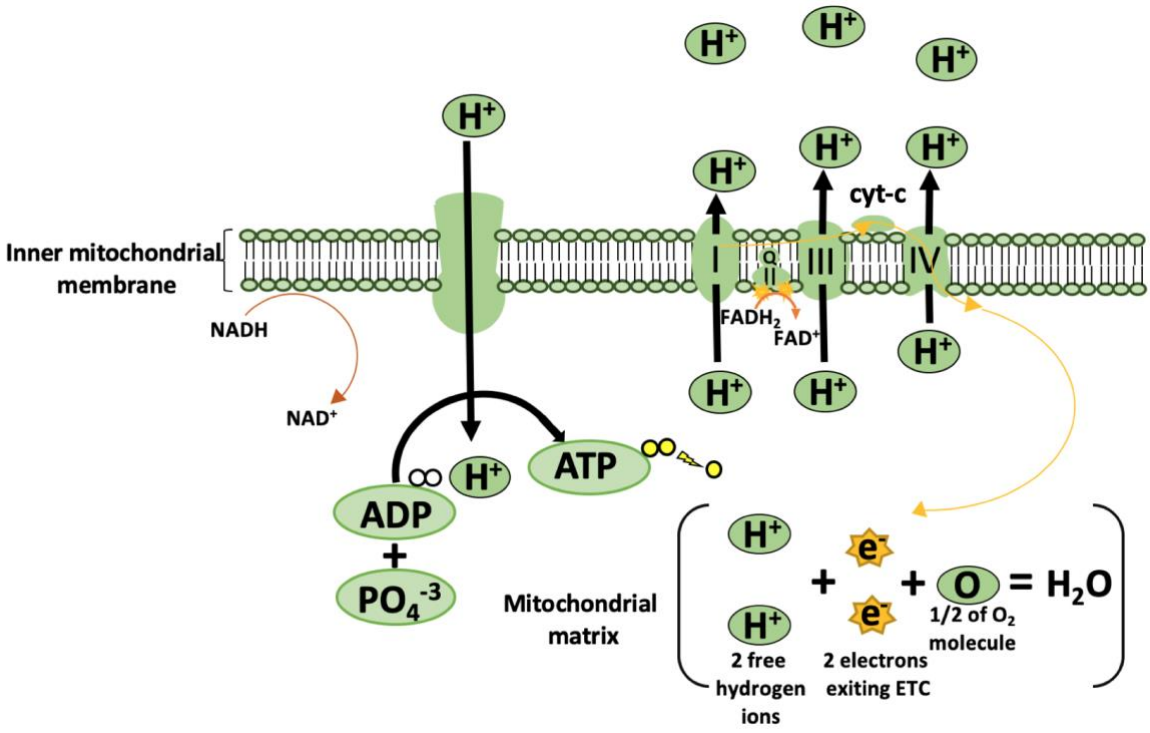

Figure 2.2: The mitochondrial respiratory chain. Image adapted from *Biology Dictionary* [19].

Adenosine triphosphate, widely known as ATP is one of the most important and versatile carrier molecules in cells. ATP serves as a convenient storage of energy that drives numerous chemical reactions in cells. The synthesis of ATP is an energetically unfavorable reaction, in which a phosphate group is added to adenosine diphosphate (ADP), while ATP hydrolysis is energetically favorable and breaks down to generate ADP and inorganic phosphate (Figure 2.3). Many chemical reactions such as, the synthesis of biological molecules, active molecular transport across cell membranes, and the generation of force and movement, are energetically unfavorable reactions that are driven by the energy released during ATP hydrolysis, and coupled through enzymes.

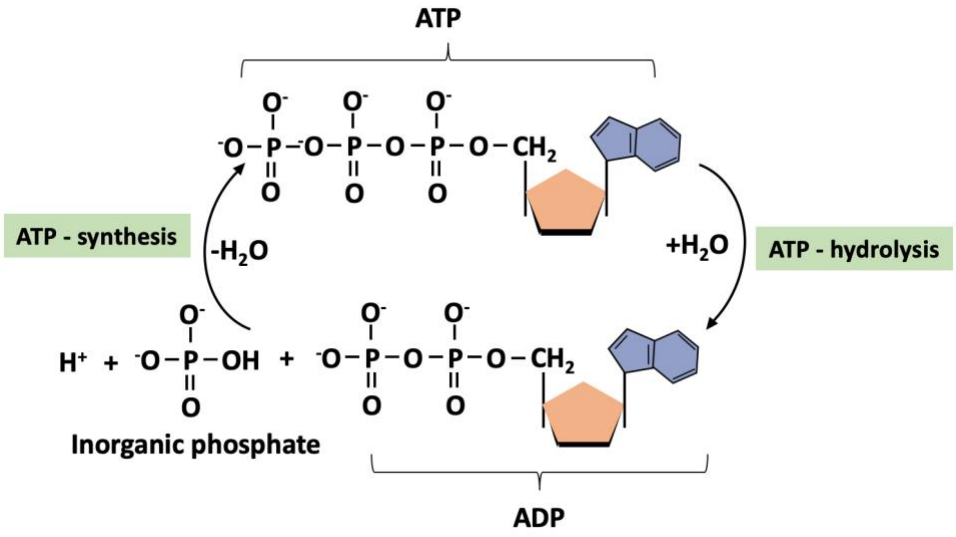

Figure 2.3: The ATP cycle. Hydrolysis of the highly energetic bond in ATP releases energy, forming ADP and inorganic phosphate. Image adapted from *Chemistry Libretexts* [20].

A major part of the food we consume contains proteins, lipids, and polysaccharides, and must be broken down into smaller molecules for cellular use. The first stage of catabolism is the breakdown of these large macromolecules into smaller subunits. Enzymes play an important role in the breakdown of, proteins into amino acids, polysaccharides into sugars, and fats into glycerol and fatty acids. The second stage of enzymatic breakdown occurs in the cytoplasm of cells, where most of the carbon and hydrogen atoms from the sugars are converted into *pyruvate*, and then enters the mitochondria, converting to *acetyl coenzyme A (acetyl CoA)*. The final stage in catabolism is the complete oxidation of acetyl CoA to H_2O and CO_2, and is the stage when most of the ATP is generated.

The key process in the second stage of catabolism is the sequence of reactions knows as *glycolysis*. Glycolysis initiates aerobic oxidation of glucose, yielding two molecules of NADH, two molecules of ATP and two molecules of pyruvate. The next step is the *citric acid cycle* (also known as the tricarboxylic acid cycle, or the Krebs cycle) shown in Figure 2.4, where the acetyl groups from acetyl CoA are oxidized to produce CO_2 and NADH, ending with oxidative phosphorylation, where the generated NADH reacts with molecular oxygen (O_2) to produce ATP and H_2O in a series of steps

that rely on the electron transport mechanism in the mitochondrial membranes. NADH, a reduced molecule of NAD_+ plays a central role in energy metabolism, and is a molecule with low stability and a convenient source of readily transferable electrons.

The primary function of the citric acid cycle is oxidizing acetyl groups in the form of acetyl CoA molecules produced from pyruvate. The carbon atoms of the acetyl groups are converted to CO_2, while the hydrogen atoms are transferred to the carrier molecules NAD_+ and FAD to convert them to their reduced forms, of NADH and $FADH_2$. The highly energetic electrons on these carrier molecules will subsequently harness their energy through the reactions of *oxidative phosphorylation*.

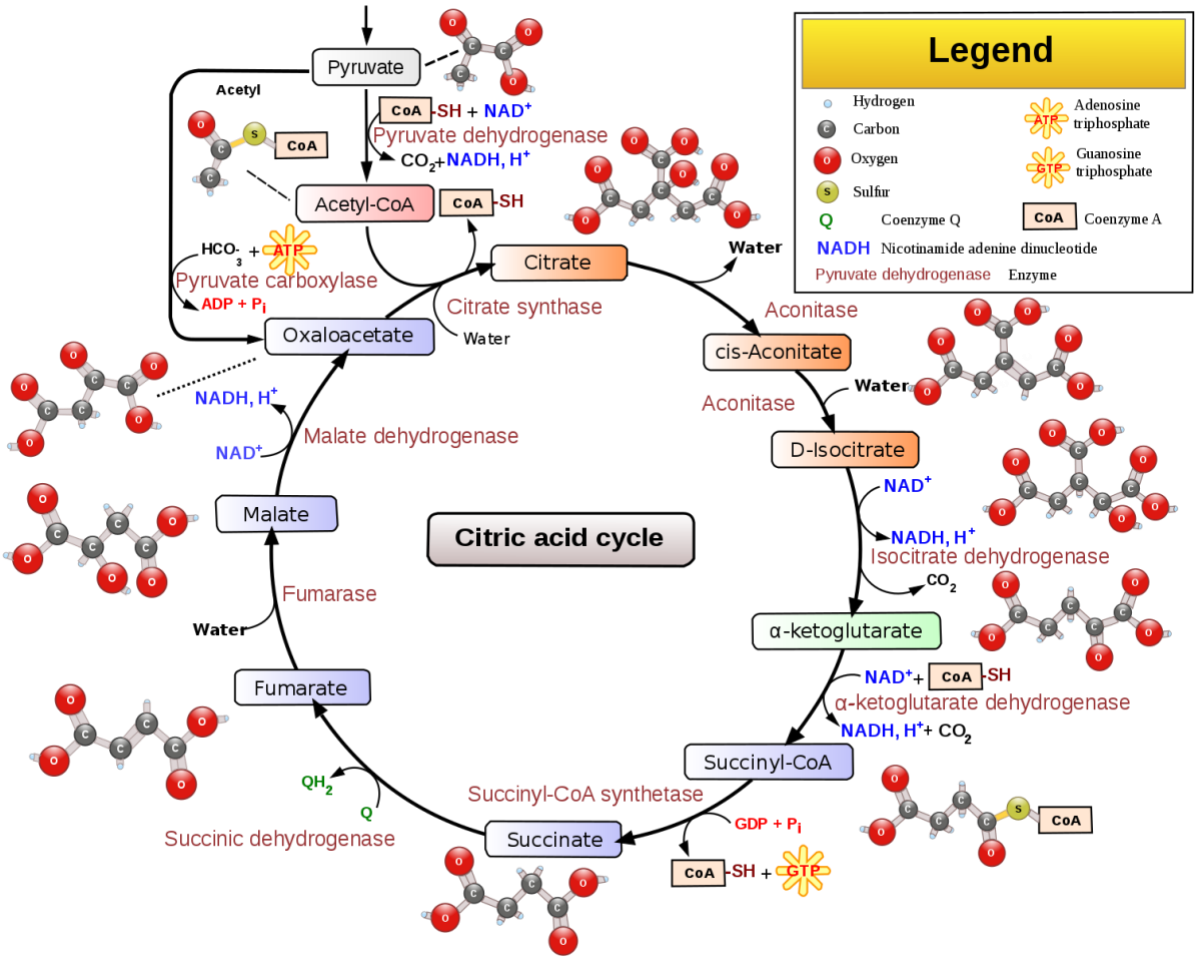

Figure 2.4: The complete citric acid cycle [21].

Oxidative phosphorylation is the final step of metabolism, and the point at which most metabolic energy is released. The carrier molecules produced during the citric acid cycle NADH and $FADH_2$, transfer the highly energetic electrons that were gained from oxidation of food molecules, to molecular oxygen, forming H_2O. This reaction, releases a vast amount of chemical energy formally equivalent to combustion of hydrogen in air to form water. It occurs in several steps by gradually passing these highly energetic electrons along protein complex carriers in the electron transport chain. This process enables the energy to be stored in molecules of ATP, rather than being lost to the environment as heat.

The respiratory chain, also called the electron transport chain, is unique, and is where the energetically favorable reaction of hydrogen forming water occurs, after hydrogen atoms are separated into protons and electrons first. These electrons pass through a series of electron carriers in the mitochondrial inner membrane, while they combine with protons transiently during several steps along the way. These protons and electrons permanently combine at the end of the electron transport chain by combining with an oxygen molecule, thereby producing a water molecule [8].

The electron transport contains four major mammalian respiratory complexes and the ATP synthase complex enzyme. Electron microscopic imaging of individual electron transfer complexes and structural data have led to detailed understanding of the electron and proton transfer mechanisms involved in the respiratory chain. Each complex of the electron transport chain can exist in either an oxidized form, in which it is capable of receiving a pair of electrons from another component, or in a reduced form, in which a complex with a pair of electrons is capable of donating them to an oxidized component [22]. When electron carrier molecules extracted from food molecules oxidize and transfer highly energetic electrons to the electron carriers in the protein complex enzymes, the H^+ removed from the carrier molecules are coupled, and pumped across the protein complexes in the inner mitochondrial membrane, from the matrix to the intermembrane space. These protons are thought to

move across a protein pump embedded in the lipid bilayer membrane, by transferring from one amino acid side chain to another, following special channels across the protein.

Complex I, also known as the NADH dehydrogenase complex (NADH:UQ oxidoreductase), is the largest of the respiratory enzyme complexes, and is the complex that begins the electron transport chain. Complex I accepts electrons from NADH and passes them through a flavin and several iron-sulfur clusters (electron carriers in the protein complex that accept electrons) to ubiquinone, a small hydrophobic molecule that is freely mobile in the lipid bilayer. Ubiquinone can combine with a proton from the medium for each electron it accepts. The electrons carried by ubiquinone are then transferred to complex III, the cytochrome *b*-c_1 complex. Cytochrome *c*, a single electron carrier in the inner mitochondrial membrane, then transfers electrons from the cytochrome *b*-c_1 complex to complex IV (cytochrome *c* oxidase) as the final step of the ETC. In this step, reduced cytochrome *c* transfers an electron to cytochrome *c* oxidase, and four such electron transfers lead to the conversion of an oxygen molecule to water.

Each of these complexes, I, III and IV act as electron-transport-driven H^+ pumps, and allow passage for H^+ in the mitochondrial matrix across the inner membrane into the intermembrane space, increasing its H^+ concentration, thereby generating a proton concentration gradient across the inner membrane. Complex II of the respiratory chain, the succinate dehydrogenase complex (succinate:UQ oxidoreductase) also plays a unique role in setting the rate of respiration by accepting electrons donated by succinate, an electron carrier molecule that is produced during the citric acid cycle. The oxidation of succinate to fumarate is catalyzed through complex II, where its prosthetic group flavin (FAD) is reduced by accepting electrons and passing them on to the mediator ubiquinone, and contributing electrons to the electron transport chain. However, in contrast with the other complexes, electron transfer through complex II is not coupled with proton translocation across the inner membrane to generate the proton concentration gradient [8, 23].

Peter Mitchell played a significant role in describing the *chemiosmotic hypothesis*, which explains the link between the mitochondrial membrane potential generated by the proton pumping mechanism of the electron transport chain, to ATP synthesis by the ATP synthase protein enzyme [16, 24]. The proton concentration gradient (or pH gradient) drives the H^+ back into the matrix and OH^- out of the matrix, and thereby generates the effect of the electrochemical potential change (ΔV) across the inner mitochondrial membrane, which attracts positive ions into the matrix and pushes negative ions out. The constituent of both the proton concentration gradient (ΔpH) and the membrane potential change (ΔV) is the electrochemical proton gradient across the inner mitochondrial membrane, which generates a proton motive force (pmf) that is key to the synthesis of ATP.

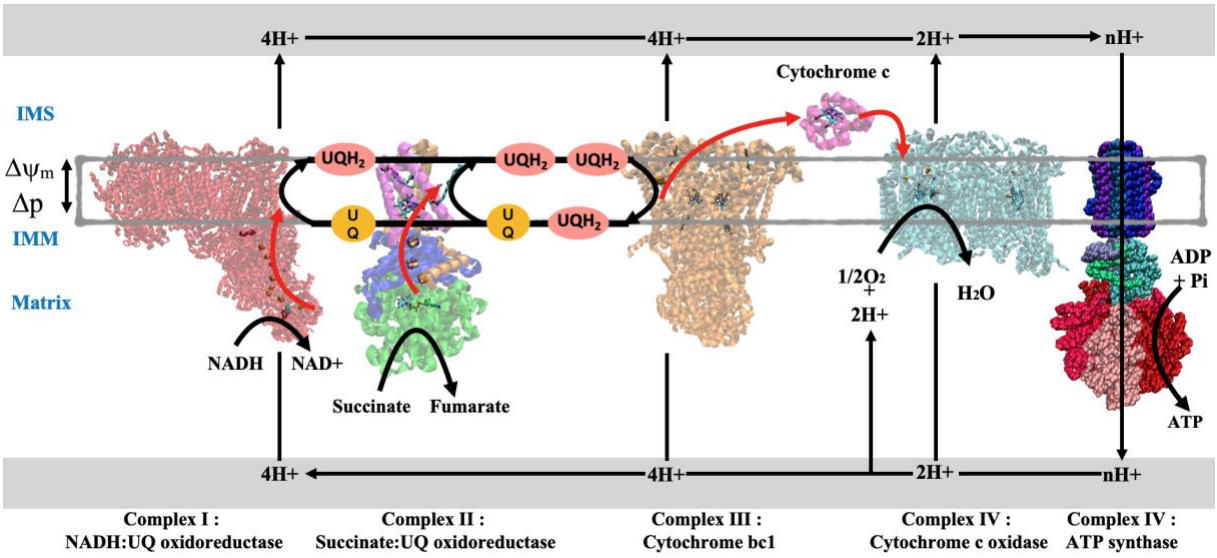

Figure 2.5: Protein complexes of the electron transport chain: the red lines indicate the electron pathways across complexes and ubiquinone molecules, ultimately combining with oxygen to produce water molecules. Image generated by molecular dynamic data structures from *RCSB Protein Data Bank* [25].

Complex V, the ATP synthase (also known as the F_1F_0-ATPase) is the final component in the oxidative phosphorylation process, and catalyzes ATP synthesis. The ATP synthase forms about 15% of the total inner membrane protein and have similarly representative complexes present in chloroplast

and bacterial membranes. The ATP synthase has two major subunits, F_0 and F_1. The transmembrane portion of the protein, the F_0 subunit is a H^+ carrier, while the F_1 subunit is involved in the synthesis of ATP, when protons are passed through this subunit down the electrochemical gradient. However, when the two portions are separated, the F_1 subunit goes into reverse to catalyze only ATP hydrolysis. The ATP synthase is a *reverse coupling device*, and can either use the energy of ATP hydrolysis to pump H^+ across the inner mitochondrial membrane, or harness H^+ flow down the electrochemical gradient to generate ATP. The direction that the complex operates depends on the net-free energy change of the coupled processes of H^+ translocation across the inner membrane. Figure 2.6 shows the structure of ATP synthase, which includes an assembly of two rotary motors with a shared common rotor shaft, while being stabilized by an exterior stalk [26].

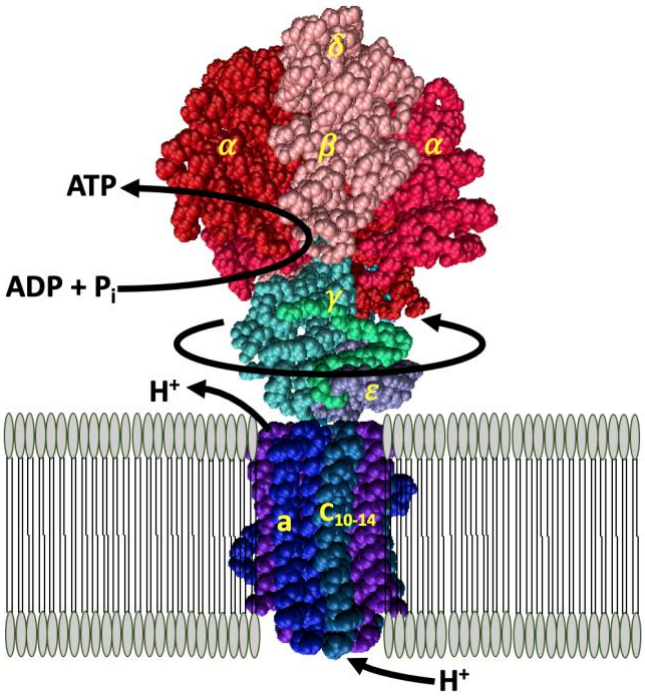

Figure 2.6: Structure of *E. coli* F_1F_0-ATP synthase. There are three catalytic sites, situated at interfaces of α- and β-subunits, where ATP is synthesized and hydrolyzed. Image generated by molecular dynamic data structures from *RCSB Protein Data Bank* [38] and adapted from Weber *et al.* [27].

2.3 Mitochondrial Membrane Potential

A cell membrane is a dynamic entity that controls the interior components of the cell by controlling the membrane permeability. A membrane has selective permeability to ions, displaying its properties as an *electrochemical membrane*. A cell membrane is composed of a bilayer lipid membrane (BLM) with parallel embedded protein and ionic channels (Figure 2.7). A membrane potential rises from a difference in electrical charge on the two sides of a membrane. Active electrogenic pumping and ion diffusion can cause this difference in charge [28].

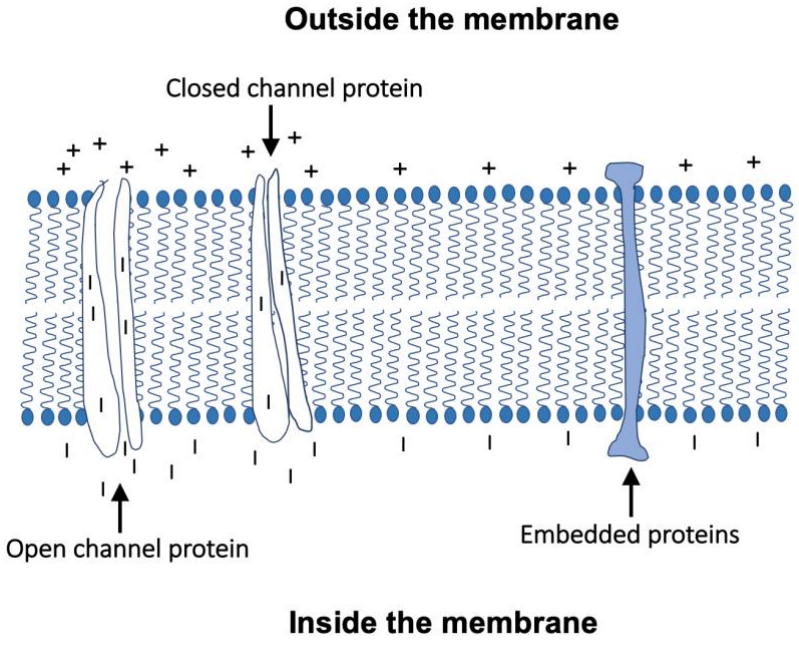

Figure 2.7: Bilayer lipid membrane with embedded proteins and sodium channels. Image adapted from Grimnes *et al.* [28].

For mitochondria, the charge difference across the inner membrane is generated by electrogenic H^+ pumps that allow accumulation of H^+ ions during the electron transport chain. The

mitochondrial membrane potential ($\Delta\psi_m$), the electrochemical potential difference generated by the proton pumps through complexes I, III and IV during oxidative phosphorylation, is an essential component for the intermediate storage of energy. The transmembrane proton gradient ($\Delta\mu H^+$) that contributes in providing the energy for the synthesis of ATP is a combination of the proton gradient across the inner mitochondrial membrane (ΔpH_m), and the mitochondrial membrane potential ($\Delta\psi_m$). The transmembrane proton gradient is expressed by the equation:

$$\Delta\mu H^+ = -F\Delta\psi_m + 2.3RT\Delta pH_m, \tag{2.1}$$

where *F* is Faraday's constant, *R* is the universal gas constant, and *T* is the absolute temperature.

The "*protonmotive force*" is also directly proportional to the free energy change, $\Delta\mu H^+$, where,

$$\Delta p = \Delta\psi_m - 59\Delta pH \tag{2.2}$$

where *F* is the Faraday's constant. A higher $\Delta\psi_m$ postulates a higher energy capacity of the inner mitochondrial membrane, and increases the synthesis of ATP. Although the inner membrane is an excellent electrical insulator, the high electric field is difficult to maintain with the various membrane proteins that are capable of transporting different solutes across the membrane, creating ion leaks across the inner membrane that exponentially change depending on $\Delta\psi_m$. An optimal value of $\Delta\psi_m$ is required to be maintained across the membrane, since high $\Delta\psi_m$ can lead to significant generation of reactive oxygen species (ROS), while extremely low values of $\Delta\psi_m$ can lead to the insufficient ability of the mitochondria to produce ATP [29, 30, 31]. The depolarization and opening of an ion channel can cause the mitochondria to release or accumulate unwanted substances, including some cations that are vital for maintaining the potential balance across the membrane. However, the time period a mitochondrion stays in a state of depolarization is a critical factor. Short episodes of depolarization

may not lead to significant changes in mitochondrial functioning, while depolarization prolonged for an appropriately longer time can lead to death of the mitochondrial functionality [32, 33].

Measurements of $\Delta\psi_m$ can be made by studies of suspensions of mitochondria, where most often changes in the energization of these structures, cause changes in the incubation medium, and can be probed. Measurements are often made using selective electrodes, such as TPP_+-sensitive electrodes, voltage clamping methods, and using fluorescent probes that carry delocalized positive charge [34, 35, 36, 37].

The patch clamping technique allows the study of a single or small number of ion channels, where a thin glass or quartz pipette with a blunt end is sealed onto the membrane. By applying suction and high-resistance seal, this method allows ions fluxing the membrane patch to flow into the pipette and are recorded by an electrode. Although there are advantages, this method has a low throughput and is less efficient [37, 38].

Fluorescent methods are more optical based methods that use voltage sensitive dyes to observe the changes in ionic currents that flux across channels in the membrane. This method has a relatively higher readout, however has an issue with dye calibration leading to problematic determination of the membrane potential.

Mitochondrial membrane permeability is a vital component in cell function related to survival and apoptosis. Disregarding the morphology of the cell or its functionality, the membrane potential plays an even significant role in controlling the permeability and ion transfer across it. $\Delta\psi_m$ has a role in the enhanced generation of reactive oxygen species, which can induce mitochondrial damage as well. Increased membrane potential enables generation of reactive ion species accumulation, by generating ATP synthase inhibitors such as oligomycin, that disrupt the oxidative phosphorylation mechanism, leading to unstable energy mechanisms in the mitochondria. Thus, we can clearly illustrate a scheme of diagnostic markers for cellular pathophysiology by studying mitochondrial membrane potential [2, 39].

Chapter 3: Mitochondrial Oxygen Consumption Studies

3.1 Mitochondrial Diseases

The principal function of the mitochondria is the generation of ATP by oxidative phosphorylation. However, the mitochondria are also vital for cell apoptosis (also understood as controlled cell death), cell signaling, as mediators protecting the cell, modulation of intracellular Ca^{2+} fluxes, balancing of oxidative stress by generation of ROS (reactive oxygen species), and aging, as well as numerous diseases. Research studies have indicated that many serious diseases such as Alzheimer's, Parkinson's, Pearson's syndrome, and also diabetes, heart disease, genetic diseases, and psychiatric disorders have been linked to the dysfunction of mitochondria [40 - 50].

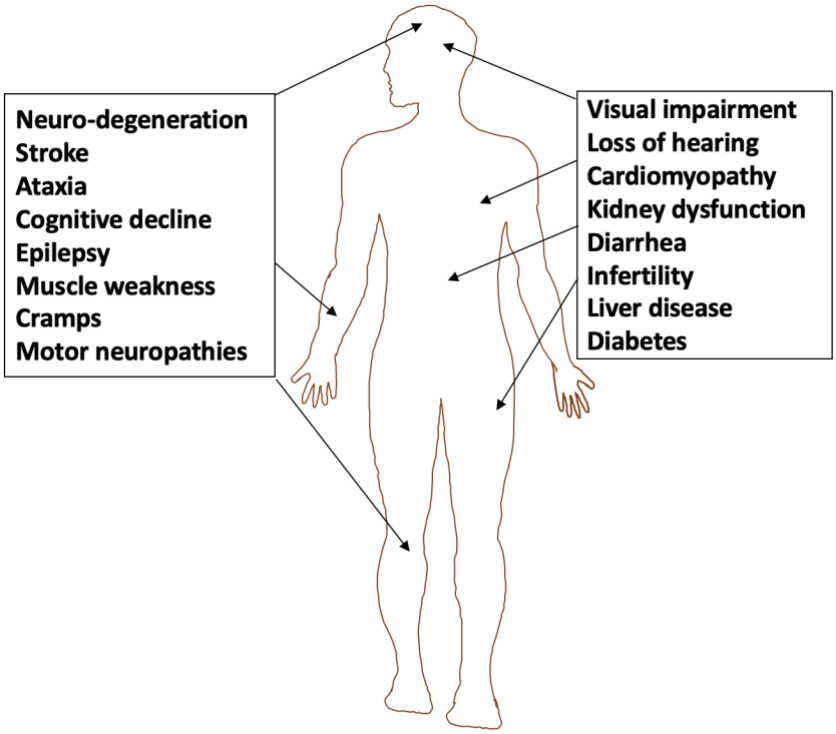

Figure 3.1: Mitochondrial diseases that affect numerous parts of the human body. Image adapted from Suomalainen *et al.* [51].

The distinction between healthy mitochondria, and dysfunctional or abnormal mitochondria can be marked via mitochondrial membrane potential. The membrane potential, explained thoroughly in chapter 2, is able to indicate the energetic state and permeability of normal cells [52 - 55]. Some studies have established that mitochondria of malignant phenotypes have much lower ATP synthesis rates and lower hydrolysis capacity [56, 57]. Thus, studies of membrane potential are a promising step to developing tools that provide biomarker capabilities. It is widely believed that the permeability of the mitochondrial membrane plays a decisive role in the survival of the cell, and regulates apoptosis, irrespective of the cell morphology and functionality.

Mitochondrial dysfunction can be assessed by using isolated mitochondria, *in vivo* or in intact cells, by precise control of experiments and understanding the relevance physiologically [58]. Several methods have been utilized to study functional and dysfunctional properties of mitochondria. Studies of measurement fluxes generally provide more information on the mitochondria's ability to produce ATP than by measurements of potentials and intermediate molecules that are generated. For isolated mitochondria as well as intact cells, the best assay is studying the mitochondrial respiratory control whereby titrations of external components provide the ability to identify the various sites in the mitochondrial membranes where primary complex sites are affected. Studying and measuring oxygen consumption rates offer a steady method of isolating each protein complex by controlling added effective substrates, and observing how the functionality of mitochondria is affected.

3.2 Oxidative Phosphorylation Studies

Peter Mitchell's *chemiosmotic theory* explains the process of electron transport that occurs across the electron transport chain, while hydrogen ions are transferred to the intermembrane space [16]. As explained in section 2.2, the resulting difference in proton (hydrogen ion) concentration and the generation of the membrane potential across the inner mitochondrial membrane provides the energy required to produce ATP from ADP and inorganic phosphate [59].

Each pair of electrons passing through the entire ETC releases energy to generate ATP molecules, and are then accepted by an oxygen atom to make a molecule of H_2O at complex IV. Numerous cells require the extensive maintenance of oxidative metabolism, by utilizing oxygen and glucose during this mechanism. The measure of oxygen molecules consumed during the ETC, is a direct measure of the membrane potential change. Studying oxygen consumption of mitochondria is an effective way to validate the functionality of protein complexes in the ETC, and observe the changes that take place in dysfunctional or diseased, or even cancerous mitochondria.

The in-depth analysis of mitochondrial function in muscle tissue is often achieved by using one of two types of preparations:

- *isolated mitochondria*, where mitochondria are extracted and purified by mechanical homogenization and differential centrifugation; or
- *permeabilized myofibres*, where the myofibre plasma membrane is selectively permeabilized, leaving the mitochondria intact within their environment and in direct contact with the incubation medium.

The major task of both methods of study is to preserve the structural integrity of the mitochondria for analysis, by allowing direct manipulation of mitochondrial function through the insertion of specific substrates and inhibitors to the incubation medium. However, the widely used

method of investigating mitochondrial function in skeletal muscle cell is by using isolated mitochondria. The membranes of the mitochondrial network are ruptured during muscle homogenization and must rapidly re-seal to yield apparently ‘intact’ organelles [14, 15, 60, 61].

During the process of mitochondrial isolation, the muscle is homogenized using scissors and a Teflon pestle, separating mitochondria and rupturing mitochondrial membranes. The isolation of mitochondria inevitably comes along with the disruption of the mitochondrial morphology, possibly leading to a partial loss of soluble mitochondrial proteins [62]. Despite the limitations, isolated mitochondria keep their properties and provide a powerful tool for in-depth analysis of mitochondrial functionality.

After isolation of mitochondria from cells, they still retain the ability to perform electron transport. The isolated mitochondria are suspended in a respiration buffer (Mir05), with an osmolarity of 330 mOsm, that maintains a suitable environment for the functionality of mitochondria [63, 64]. The electron transport process is then manipulated by experimenters, by adding substrates that donate electrons at different levels in the chains, or uncouplers and inhibitors that depolarize or hyperpolarize the generated membrane potential. Since the ultimate electron acceptor at the end of the chain is oxygen, which is converted to water, the flow of electrons can be measured by monitoring oxygen consumption of the isolated mitochondrial suspension.

Real-time analysis of the oxidative phosphorylation process is done by studies based on high-resolution respirometry, by using an extensive amount of basic bioenergetic respiratory protocols that provide insight into oxygen consumption in isolated mitochondria. The Oroboros Oxygraph-2k high-resolution respirometer is an instrumental part in measuring oxygen consumption rates of isolated mitochondrial suspensions [65]. Equipped with polarographic oxygen sensor electrodes, the respirometer is able to measure the oxygen concentration in mitochondrial suspensions and calculate the oxygen flux per volume inside its chambers [66, 67].

The Oroboros Oxygraph-2k respirometer is designed as a titration-injection respirometer containing two individual chambers designed with sensors that can be inserted externally through the stoppers, and angularly inserted polarographic oxygen sensors into the glass chambers [67, 68]. The glass chambers of diameter 16 mm are equipped with PEEK stirrer bars that keep the incubation medium stirring at all times to avoid precipitation of samples of mitochondria, and are temperature regulated electronically, in the range of 2 ^{0}C to 47 ^{0}C.

At the polarographic oxygen sensor (POS), oxygen is diffused from the sample to the cathode surface, through an unstirred layer of the sample at the outer membrane surface, the membrane, and the electrolyte layer. It is required that the sample in the chamber is constantly stirred by PEEK stirrer bars. The POS is a Clark-type oxygen sensor, and produces the recorded electrical signal by consuming the oxygen that diffuse through the oxygen-permeable membrane to the cathode. The POS consists of a gold cathode and a Ag/AgCl anode, connected by a KCl electrolyte [67].

At a given concentration of oxygen in the sample, the POS signal depends on the properties of the membrane thickness, and diffusion coefficient and oxygen solubility. The cathode and anode reactions are given by,

$$O_2 + 2\,H_2O + 4\,e^- \rightarrow\ 4\,OH^-, \tag{3.1}$$

$$4\,Ag \quad \rightarrow\ 4\,Ag^+ + 4\,e^-. \tag{3.2}$$

The oxygen concentration, and the oxygen flux, per sample quantity or per chamber volume, are recorded for data analysis and displayed on the DatLab software. The software provides an objective basis for prolonging particular experimental sections until stability is reached, before the next titration is made.

Assessing mitochondrial function and understanding its complex structure involves manipulation of isolated mitochondria by titrations of various substrates, inhibitors, and uncouplers. The Oroboros Oxygraph-2k respirometer is feasible in measuring changes observed in oxygen

concentration when being manipulated by such compounds, providing a comprehensive analysis and identifying normal and abnormal functionality of mitochondria [65].

A range of electron donors (glutamate/pyruvate and succinate) can be added in titrations to isolated mitochondrial suspensions to initiate electron transport at specific complexes on the ETC. Palmeira *et al.* [69] discusses protocols with various substrates used to study respiration.

Glutamate (or malate) and pyruvate are two substrates that are used simultaneously to generate NADH via the TCA cycle. Electrons are donated to complex I (NADH dehydrogenase complex) by oxidizing of NADH to NAD^+, initiating the ETC. Succinate is also a substrate that yields $FADH_2$ and donates electrons to complex II (succinate dehydrogenase), oxidizing to FAD^+. These substrates are added to a suspension of isolated mitochondria in respiration buffer, to initiate the transport of electrons across the ETC in the inner mitochondrial membrane, and exhibits an increase in the oxygen flux in the oxygraph [22].

Adenosine diphosphate (ADP) is a substrate that is used for determining the rate of electron transport in isolated mitochondria. As discussed in section 2.2, ADP is the principal molecule that is involved in the synthesis of ATP, via complex V (or the ATP synthase). Thus, the addition of ADP couples the rate of endergonic electron transport to the phosphorylation of ADP into ATP, and increases the influx of oxygen molecules to mitochondria.

Inhibitors are substrates that affect particular protein complexes in the ETC, and block the transport of electrons. Since there are no electrons flowing toward complex IV (cytochrome oxidase), oxygen consumption also stops, and the oxygen flux into mitochondria decreases rapidly. Oligomycin is an inhibitor that binds to the ATP synthase, and prevents the synthesis of ATP. Another inhibitor of mitochondrial functionality, rotenone, blocks the electron transport between complex I and ubiquinone, the mobile carrier in the inner mitochondrial membrane.

Uncouplers are an important indicator of the electron transport rate as well. They are molecules that affect oxidative phosphorylation by depolarizing the mitochondrial membrane. FCCP is

an uncoupler that leaks protons across the inner membrane, thereby depolarizing and decreasing the membrane potential, and can be observed to increase the oxygen flux in mitochondria rapidly.

The effect that substrate, uncoupler, or inhibitor titrations have on respiration of isolated mitochondria, or permeabilized cell suspensions is studied by the information provided by an oxygraph. Figure 3.2 shows an oxygraph obtained in an experiment for isolated mitochondria from cultured HeLa cells.

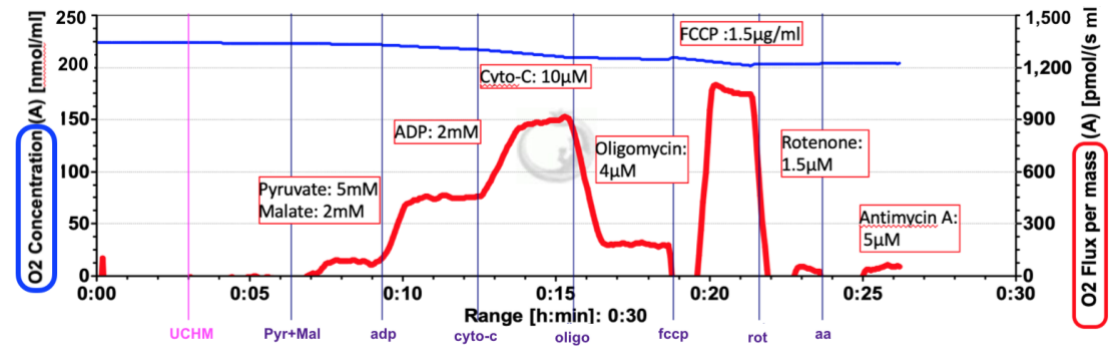

Figure 3.2: Oxygraph exhibiting oxygen concentration and volume-specified oxygen flux as a function of time. The protocol has been followed for isolated mitochondria from cultured HeLa cells with pyruvate + malate, 2 mM ADP, 10 µM cytochrome c (Cyto-c), 4 µM oligomycin, 1.5 µg/ml FCCP (F), 1.5 µM rotenone and 5 µM antimycin A.

The respiratory rates of mitochondrial suspensions shown by Figure 3.6, reflect the mitochondrial functionality as a structurally intact organelle, by calculating oxygen consumption rates in nmoles of O_2/min/mg.

State 1: Oxygen consumption rate of mitochondria prior to addition of substrate ADP, where the oxygen consumption rate is minimal.

State 2: Oxygen consumption rate in the presence of substrates, with the added ADP consumed.

State 3: Maximally simulated respiration rate initiated by adding 1 mM of ADP.

State 4: Respiration rate after addition of 2 µM of FCCP, when ATP synthesis discontinues. An increase in state 4 respiration would indicate uncoupling of the mitochondrial inner membrane.

Respiratory control ratio (RCR): Ratio of state 3 to state 4 respiration rates, which is used as an index to examine the viability of prepared mitochondria. Typical values are in the range of 3 – 10, while low rates of RCR indicate possible mitochondrial damage.

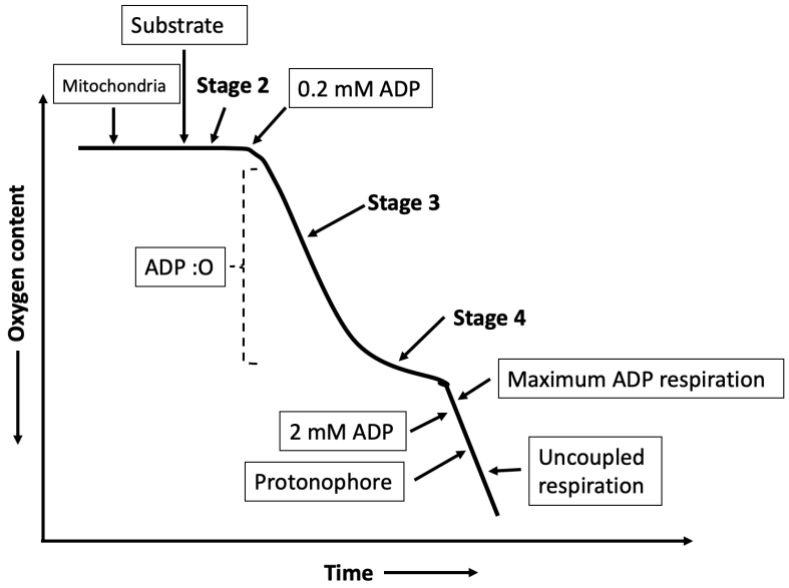

Figure 3.3: The polarographic study of oxphos using an oxygen electrode chamber. Substrate addition of a substrate will initiate state 2 respiration. ADP activates oxidative phosphorylation, consuming oxygen (state 3 respiration. After the exogenous ADP is consumed, the oxygen consumption rate is slowed (state 4 respiration). The ADP:O ratio indicates the efficiency of oxidative phosphorylation. The addition of saturating amounts of ADP results in maximal rates of oxidative phosphorylation. A protonophore will uncouple respiration and the maximal rate of oxygen consumption can be observed. Image adapted from Lesnefsky *et al.* [70].

Respiration rates with subsequent manipulation of mitochondrial function provides a viable indicator for the functionality and the state of mitochondria, and provides detailed analysis of oxygen consumption within the inner mitochondrial membrane.

Chapter 4: Electrical Properties of Biological Materials

4.1 Dielectric Phenomena

The dielectric response of a material is its response to an electric field. A dielectric does not exhibit a dc (direct-current) conductivity, but acts as an electrical capacitance by storing charge. An applied electric field can illustrate two very distinct properties: a) the energy in the electric field is lost to dissipation by the motion of the charge carriers, or b) the energy is stored through polarization. An applied electric field creates a displacement of bound charges in a region in the material, inducing a dipole moment. Polarization is the electric field induced separation of charges, and depends on the build-up of charges. The polarization of a material is described by the vector polarization P, defined as the electrical dipole moment per unit volume. The induced dipole moments align depending on the direction of the applied external field (Figure 4.1). The polarization P is given by,

$$P = D - \varepsilon_0 E, \tag{4.1}$$

where D is the displacement charge density (C/m2) and ε_0 is the permittivity of vacuum, and E is the applied electric field. The expression for D is given by,

$$D = \varepsilon E, \tag{4.2}$$

where, $\varepsilon = \varepsilon_r \varepsilon_0$ and ε_r is the relative permittivity of the material. From these relationships, the permittivity is found to be directly proportional to the polarization, and can be described as the dipole moment density built by an electric field.

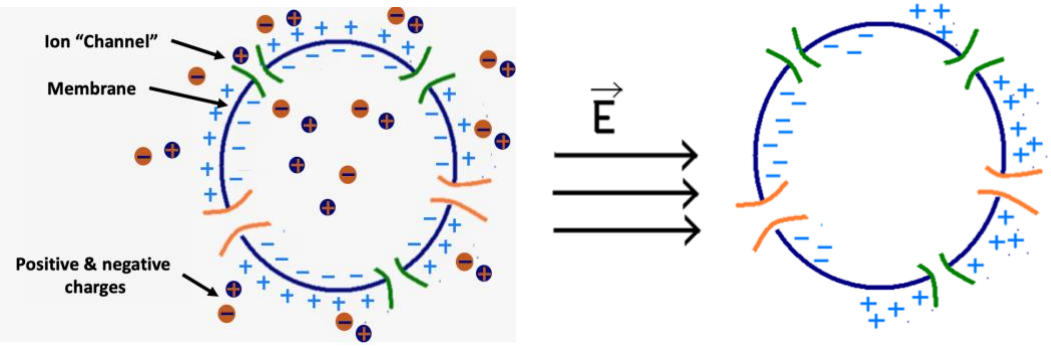

Figure 4.1: Polarization in an electric field.

For a time-varying electric field, the polarization phenomena can be observed as relaxation, due to the time required for charges to move with the varying electric field. This time-domain concept is described as the influence of a step function of the excitation signal on the material, and the time it takes to relax the system to equilibrium. A material's response to an applied electric field is controlled by two fundamental parameters, the conductivity σ, and the dielectric permittivity ε. Conductivity is determined by the mobility of the charges, while the permittivity is a measure of the material's polarizability, and are observed as a function of frequency as dispersion [28].

Conductivity σ, and dielectric permittivity ε can be studied as complex quantities in the time domain, in order to incorporate the dielectric losses. Then we define, the complex conductivity as:

$$\boldsymbol{\sigma} \equiv \sigma' + j\sigma'', \tag{4.3}$$

and the complex permittivity as:

$$\boldsymbol{\varepsilon} \equiv \varepsilon' - j\varepsilon'' \equiv \varepsilon_r'\varepsilon_0 - j\varepsilon_r''\varepsilon_0, \tag{4.4}$$

where, σ' and ε' are the real values of conductivity and permittivity respectively, σ'' and ε'' are the imaginary values of conductivity and permittivity respectively, and ε_0 is the permittivity of the

vacuum. For a material considered as a dielectric with losses (an insulator with losses), $\varepsilon''(\omega)$ is related to the conductivity of the material given by the dielectric loss factor,

$$\varepsilon'' = \frac{\sigma'}{\varepsilon_0 \omega}, \tag{4.5}$$

that indicates energy dissipation. Here, $\omega = 2\pi f$ is the frequency. A parametrization of the dielectric loss factor is described in terms of the loss angle δ, where $\tan\delta = \varepsilon''/\varepsilon'$.

For a dielectric with only bound charges, let us assume that the material has a relaxation process with a single characteristic time constant, and that the polarization increases exponentially as a function of time. This is called the *Debye single dispersion*. The polarization in the dielectric causes the surface charge density *D(t)* to increase from one value of D_∞, to D_0 as the material relaxes and reaches equilibrium [28].

This can be expressed as a function of time by,

$$D(t) = D_\infty + (D_0 - D_\infty)\left(1 - e^{-t/\tau}\right), \tag{4.6}$$

where D_∞ is the surface charge density starting from $t = 0$, D_0 is the charge density after the new equilibrium is obtained and the charging current is zero, and τ is the relaxation time constant.

In the frequency domain, the Debye single dispersion equation becomes,

$$\boldsymbol{\varepsilon}(\omega) = \varepsilon_\infty + \Delta\varepsilon/(1 + j\omega\tau), \tag{4.7}$$

and,

$$\boldsymbol{C}(\omega) = C_\infty + \Delta C/(1 + j\omega\tau), \tag{4.8}$$

where $\Delta\varepsilon' = \varepsilon_s' - \varepsilon_\infty'$.

The *quadrature* and *in-phase* components are,

$$\boldsymbol{\varepsilon}' = \varepsilon_\infty' + \Delta\varepsilon'/(1 + \omega^2\tau^2), \tag{4.9}$$

and,

$$\boldsymbol{\varepsilon}'' = \Delta\varepsilon'\tau\omega/(1 + \omega^2\tau^2). \tag{4.10}$$

The values of the *quadrature* component decrease with increasing frequency, while the *in-phase* component values go through a maximum which can be seen in Debye singe dispersion relaxations shown in Zivkovic *et al.* [71].

There are three major mechanisms of electric polarization that occur at moderate electric fields, and for materials with low conductivity.

- **Electronic polarization (optical polarization):** The electric field deforms the originally symmetrical distribution of the electron clouds of atoms or molecules.
- **Atomic or ionic polarization (vibrational polarization):** The electric field causes the atoms or ions of a polyatomic molecule to be displaced relative to one another.
- **Orientational polarization:** For materials with molecules or particles with a permanent dipole moment, the electric field causes the dipoles to reorient toward the direction of the field.

The mechanisms of polarization discussed above and shown in Siddabattuni *et al.* [72] are due to the bound positive and negative charges within an atom or molecule itself. However, electronic polarization can also occur for mobile and trapped charges. This polarization is referred to as space charge polarization. Charge carriers (electrons, holes, or ions), that may be injected from electrical contacts, can be trapped in the bulk or at interfaces, forming positive and negative space charges in the bulk of the material, or at the interfaces between different materials. These space charges can modify the field distribution, and are referred to as interfacial polarization [73].

Different polarization mechanisms respond at different frequency ranges, and therefore have a timescale characteristic to the mechanism. As the frequency increases, the dielectric constant decreases, since most processes cannot respond to electric fields at higher frequencies. Study of wide frequency dielectric properties of materials can provide information about the physical structure of the material, and potential applications.

4.2 Dielectric Properties of Biological Materials

Biological systems interact with electromagnetic energy through the dielectric properties of biological materials. Measuring the electrical properties provides understanding of the underlying biophysical processes that take place in these materials. A biological sample can be interpreted as a conductor made up of tissues with different electrical properties. This makes investigation of biological specimens through the technique of characterization of electrical properties, a promising method, both from a diagnostic and fundamental point of view.

As discussed in section 4.1, the response to an applied electric field is described by the conductivity, σ and dielectric permittivity, ε. The dielectric behavior of biological samples is mainly due to the mobility of the ions and bound charges within the tissues. The living cell is surrounded by aqueous electrolytes, with cations such as, H^+, Na^+, K^+, Ca^+, Mg^+ and anions such as HCO_3^-, Cl^-, HPO_4^{2-}, SO_4^{2-} in human blood. The ionic motion in an aqueous environment generates a conduction current I_c within the cells due to the motion of the ions affected by thermal fluctuations.

The cell membrane is a dynamic component in a living cell, and is considered an *electrochemical membrane*, due to its selective permeability to ions. The passive part of the cell membrane is the bilayer lipid membrane (BLM), that contains proteins, transport organelles, and ionic channels in parallel, which represent electrically shunt pathways. The thickness of the membrane is very small, giving a high capacitance with a low breakdown potential. An electrical double-layer covers the wetted outer cell membrane surface, and affects the flow of charge through the cell. At dc and low frequencies, current must pass around the cells, due to the conductance in the double-layers. However, at higher frequencies, the membrane capacitance allows the ac current to pass through, removing the effect of the membrane [28].

The polarized bound charges at the membrane surfaces give rise to complex dielectric behavior through the displacement current I_d, which gives rise to Maxwell-Wagner and counterion polarization effects. Maxwell-Wagner effects affect processes at the interface of different dielectrics and display different dielectric relaxations.

Biomaterials have a distribution of relaxation responses, and the electrical properties of biomaterials can be analyzed as a function of frequency. This is called *Dielectric Spectroscopy*, and is used to study dispersions of biomaterials. The frequency dependence of the relative dielectric permittivity ε_r and the conductivity σ of tissue and cell suspensions change with frequency in three distinct steps [74 - 76]. The observed responses describe different mechanisms that reflect numerous components of the biological material.

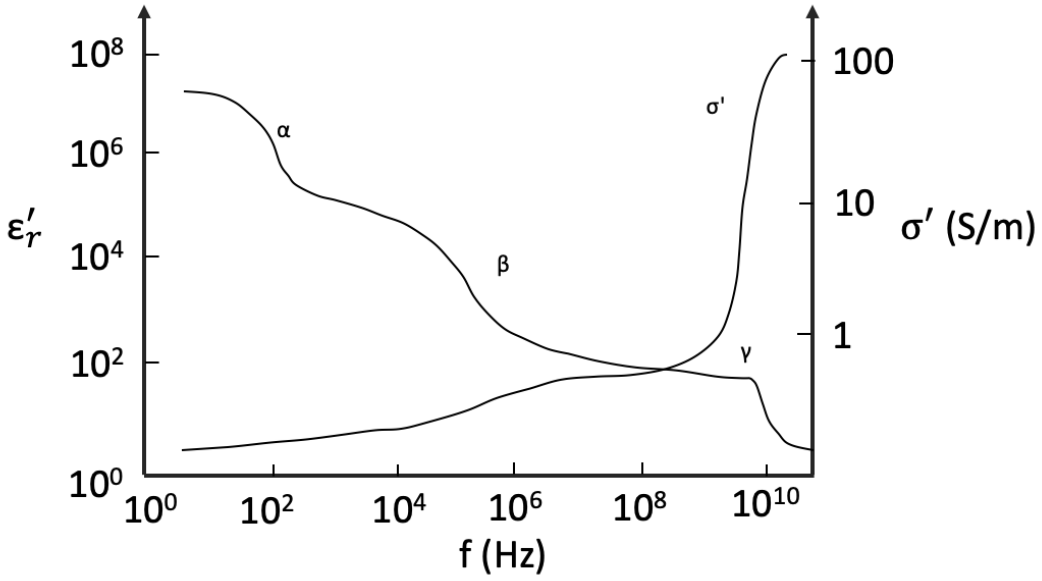

Figure 4.2: Dielectric dispersion regions. Image adapted from Grimnes *et al.* [28].

The frequency response occurs in three distinct steps as shown in Figure 4.2, in the low, RF and GHz frequency ranges and are classified as α, β, and γ dispersions.

- **α dispersion:**

The underlying mechanisms for α dispersion include the effects of electrical double-layers and the motion of charges near membrane surfaces and occurs in the mHz-kHz frequency range. The ambiguity of a double-layer due to the electrode polarization can cause α dispersion due to the ion charge distribution at the electrode surface. This is in addition to the membrane surface polarization, and can cloak the dispersion of the cell suspension, leading to a high dielectric constant at low frequencies. The overall dipole moment of each cell and organelle, due to the membrane potential and resulting charge imbalance, also affects the α dispersion [1 – 4].

- **β dispersion:**

β dispersion results from the passive cell membrane capacitance due to the accumulation of ions on the membrane surface. The response of the electric field on the protein molecules can also be observed by β dispersion, and occurs in a mid-frequency range of 1 kHz – 100 MHz.

- **γ dispersion:**

Dipolar mechanisms that arise in polar media, such as water, salts and proteins can be observed by γ dispersion. Relaxation of water molecules occurs at about 20 GHz, and is a result of its dipolar response. The frequency range for γ dispersion is 0.1 – 100 GHz, and in this particular frequency range, the conductivity from the dielectric relaxation of conducting water molecules is enhanced. Biological environment with very high-water content exhibits a comparable dispersion with that of water.

As seen in Figure 4.2, the permittivity decreases with increasing frequency, and therefore charges are not able to respond to the applied field. The dc conductivity generated from free charge carriers becomes problematic when purely dielectric measurements are considered. As shown in equation (4.10), for a suspension with constant conductivity, ε'' diverges at low frequencies. This can be dealt with, by either subtracting the measured dc conductivity, or by using in-phase conductivity.

Studying the frequency dependence of the dielectric properties of biological suspensions can provide the characteristic timescales and instrumental details to understand the functionalities of biological systems. In this context, impedance measurement techniques can be utilized to understand the dielectric response of biological materials. For biological suspensions, the membrane potentials that change the net negative charge inside the cell or mitochondria, give rise to electric dipole moments when an electric field is applied. For a higher bulk average dielectric constant, equation (4.1) becomes,

$$P = D - \varepsilon_0 E = \varepsilon_r \varepsilon_0 E - \varepsilon_0 E \approx \varepsilon_r \varepsilon_0 E , \tag{4.11}$$

for $\varepsilon_r \gg 1$. Therefore, an increase in the dipole moments of mitochondria in suspension will increase P, and increase ε_r of the suspensions as well [1, 2]. We will discuss the dependence of ε_r on the impedance being measured in chapter 5.

4.3 Dielectric Spectroscopy of Mitochondria

Dielectric spectroscopy of mitochondria provides an understanding into their structure and features. Pauly *et al.* [77] studied passive electrical properties of biological components, and observed that the mitochondrial matrix was highly conductive, with a limiting membrane that has a capacitance C_m, similar to the value of the cell membrane. The dispersion curves for swollen and shrunken mitochondria were obtained, and the membrane capacity of guinea pig heart mitochondria was calculated to be about 1.1 o 1.3 μF/cm2.

Dielectric spectroscopy has been proved to be an effective technique to measure the frequency dependent dielectric permittivity of mitochondrial suspensions in order to study changes that occur in samples due to various mechanisms. This non-invasive method can be applied to study mitochondrial suspensions, in which the frequency response strongly depends on the membranes and important cell parameters. However, the interpretation of dielectric spectroscopic measurements is limited by the polarization effects at the interface between the electrode and the medium, inherently called the electrical double-layer. The strong influence of double-layer polarization at low frequencies interferes with accurate measurement capabilities when studying complex biochemical systems, such as mitochondrial suspensions.

Studies by Asami *et al.* [78] show experimental data for mitochondrial suspensions, that agree with expected theoretical dispersion responses where the polarization effect at low frequencies can be seen. Such data plots can be used to compare experimental data obtained in this study.

A method to eliminate the effect of polarization was used based on studies conducted by Bot *et al.* [3, 79] and Prodan *et al.* [80]. They observed the response of polarization impedance, and used methods to remove it from experimental data [79]. Here, the complex impedance of the measured

medium is considered as a series combination of the ideal impedance Z_S of the medium and the polarization Z_P, where,

$$Z_m = Z_S + Z_P. \tag{4.12}$$

The correct impedance measurements for the medium being measured without the influence of polarization, can be calculated by subtracting Z_P from measured values. This method was used to calculate and eliminate the effect of polarization of measured data and will be discussed in detail in a later chapter.

Chapter 5: Electrical Impedance Spectroscopy (EIS)

5.1 Basics of EIS

Electrical Impedance Spectroscopy is a powerful method of characterizing electrical properties of materials and their interfaces with electronically conducting electrodes. The dynamics of bound or mobile charge in the bulk or interfacial regions in solids or liquids can be investigated using EIS. The general approach of EIS is to apply an electrical stimulus to the electrodes (a voltage or current stimulus), and observe the voltage or current response as a result.

Several fundamental microscopic processes follow when electrodes in such a system are electrically stimulated, leading to the complete electrical response. These microscopic processes include, the transport of electrons through electronic conductors, the transfer of electrons at the electrode-electrolyte interfaces, and the flow of charged atoms through the electrolyte defects. The rate of the flow of charged particles depend on the ohmic resistance of the electrodes and the electrolyte, and the reaction rates at the electrode-electrolyte interfaces [81].

The most common and standard type of electrical stimuli used in EIS, is the measure of impedance by applying a single-frequency voltage or current to the interface, and measuring the amplitude and phase-shift or the real and imaginary parts of the resulting current. This approach has the advantage of allowing the experimentalist to achieve a better signal-to-noise ratio in the frequency range of interest. EIS is accessible to study intrinsic properties that influence the conductivity of an electrode-material system, and can derive two categories of parameters, (a) those relevant to the material itself, such as conductivity, dielectric constant and charge mobility, and (b) those relevant to the electrode-electrolyte interface, such as capacitance of the interface region and diffusion coefficient

of materials of the electrode. EIS has been a useful approach pursued by many investigators since its discovery in 1925, to investigate polarizations across biological membranes.

The complex quantity $\boldsymbol{Z(\omega)}$, is defined as the "impedance function", and its value at a particular frequency is the "impedance" of the electric circuit, taking into account not only amplitude, but also phase difference. Impedance is generally defined as the total opposition an electronic device or circuit offers to the flow of an ac current at a given frequency. In the frequency domain, the voltage/current relation is $I(\omega) = V(\omega)/Z(\omega)$. The complex quantity for a capacitance is $1/(\omega.C)$, and for an inductance is $\omega.L$. The concept of electrical impedance was first introduced by *Oliver Heaviside* in the 1880s, and later developed to study using complex vector diagrams by *A. R. Kennelly and C. P. Steinmetz* [82]. The vector equation for impedance is given by,

$$Z(\omega) = Z' + jZ'', \tag{5.1}$$

and can be represented quantitatively as seen in Figure 5.1. Here the polar coordinates are,

$$Z' \equiv Re\,(Z) = |Z|\cos\theta, \tag{5.2}$$

and,

$$Z'' \equiv Im\,(Z) = |Z|\sin\theta, \tag{5.3}$$

where, the phase angle is,

$$\theta = \tan^{-1}(Z''/Z'), \tag{5.4}$$

and the magnitude is,

$$|Z| = \sqrt{(Z')^2 + (Z'')^2}. \tag{5.5}$$

Most electrode–material systems are non-linear systems, and thus, EIS measurements in either the time or the frequency domain are meaningful to study signals of magnitude, such that the overall electrode–material system response is electrically linear [83].

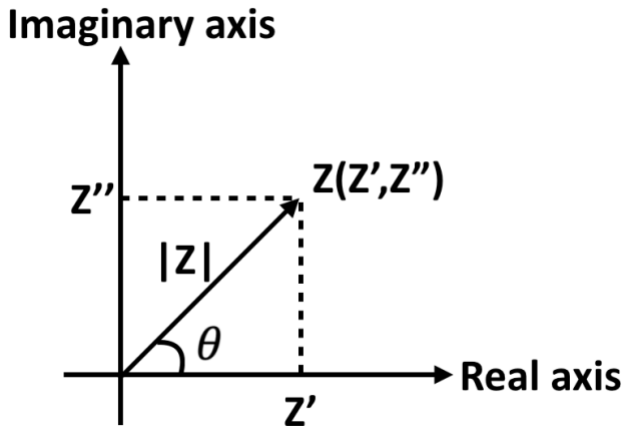

Figure 5.1: Complex impedance (Z) with a real part (Z') and an imaginary part (Z'').

5.2 Electrolytics

An *electrolyte* is a substance that has an ionic conductivity. Intracellular and extracellular living tissue cells are considered to be electrolytic conductors, that contain ions with freedom to migrate. Two current-carrying electrodes in an electrolyte are the source and sink of electrons, from the *electrons* of the metal, to the *ions* of the electrolyte.

Electron transport in a metal does not involve transport of metal ions, and has a much lower migration velocity of electrons, in the order of 0.3 mm/s at high current densities [28]. However, electric current flow in an ionic solution is a more complex event. In the bulk electrolyte, conductivity is composed of separate contributions from cations (+) and anions (-). For a homogeneous and isotropic medium, the current density of a single anion-cation pair is given by,

$$\boldsymbol{J} = \sigma \boldsymbol{E}, \tag{5.6}$$

where, σ is the conductivity, and $\boldsymbol{E}$ is the applied electric field. Equation (5.6) shows that the bulk electrolyte solution obeys the linear Ohm's law.

5.3 Interface phenomena: The Electrical Double-layer

The electrochemical processes that take place at the electrodes are significantly different from the processes in the bulk of the solution. The field of bioimpedance and bioelectricity is considerably interested in cell suspensions and tissue compositions that have membranes as well as electrolytic components. These membranes show distinct surface phenomena due to the electric dipoles that form from the applied electric fields, but also exhibit polarization processes that exist between the interfaces of electrodes with cell suspensions and tissue samples.

The transformation from *electronic* to *ionic* conduction occurs at the electrode-liquid interface, between the electrode, the source or sink of electrons, and the solution, by which electron transfer follows. A non-uniform distribution of charges forms in the transition zone between the electrode metal and the electrolyte, triggering an electric potential between the interfaces. Between a solid and a polar medium, the interface effect becomes particularly prominent, since the polar medium is liquid with a high ion mobility [28].

The double-layer is similar to a molecular capacitor, where one *capacitor plate* characterizes the charges in the metal, and the other *capacitor plate* characterizes the ions in close proximity to the electrode in the solution. The distance between these "*capacitor plates"* is in the order of 0.5 nm, thereby forming enormous capacitance values [28]. In electrochemical studies, the most widespread studies have been for surfaces of Hg, Ag, Au, Pt and various forms of carbon [84].

Many models were developed over the years to understand the electrical processes that take place between a solid conductor and an electrolyte. Helmholtz was the first to introduce a simple model of the electric double-layer in 1879. His proposal was, that all the charges in the metallic conductors stay at its surface, whereas the counter-ion charge in the solution also exists at the surface to maintain electro-neutrality. Thus, two separate layers of charge are formed at the electrode/

electrolyte interface with opposite polarity, and separated by a distance in the order of a few angstroms [85]. The theory of Gouy and Chapman, in the early 1900s, takes into account the exchange of counter-ions between the double-layer and the solution and proposes the idea of the diffuse layer. Both coulombic forces and thermal motion affect the equilibrium distribution of the counter-ions giving rise to a *diffuse double-layer*. Then, in 1924, Stern modified the Gouy-Chapman model by including both the diffuse layer and a compact layer. In this model, the ions are considered to have a finite size, and can approach the surface depending on the ionic radius and the solvation of the ion in the solvent. The centers of the ions absorbed by the surface form an *inner Helmholtz plane* (IHP), and the centers of the solvated ions form an *outer Helmholtz plane* (OHP). Krishnamoorthy *et al.* [85] show several models developed for the electrical double-layer.

A small-signal current that passes through an electrode-electrolyte interface causes the current to encounter the faradaic impedance due to the exchange of electrons, as well as due to the capacitive current flow and diffusive ion transport via the double-layer formed at the interface. The double-layer impedance is inversely proportional to the electrode area, and is also frequency dependent. Thus, the total measured impedance of the electrochemical system includes the impedance of the electrical double-layer, in series with the resistance of the solution. The effect of the capacitive double-layer between the electrode-electrolyte interphase dominates the observed impedance at low frequencies, while the solution resistance dominates at higher frequencies [86].

The impedance effect of the electrical double-layer, especially at low frequencies, can cause concern for impedance measurements performed for electrolytes and biological suspensions. The double-layer can introduce thermal noise in the circuit, aggregating the measured impedance values [87].

5.4 Equivalent Circuit Models

Electrical Impedance is an important parameter used to characterize electronic circuits and components, as well as several biochemical, thermal, and vibrational mechanisms. Standard circuit components such as resistors, capacitors, and inductors can be used in electronic circuits that can provide models for real-world systems that respond to varying electric fields. However, the components of an electronic circuit model of a real system such as a biological suspension, can be accurately predicted only up to a certain limit. Each component in the electronic model may not explain how a biological system can interact with an applied electric field.

The impedance is a complex quantity given by,

$$Z(\omega) = Z' + jZ'', \tag{5.7}$$

where Z' is the real part, and Z'' is the imaginary part, also known as the reactance (X). The quantity of reactance for different circuit components can justify how each depends on the ac frequency of the applied electric field.

Impedance analyzers are instruments that are capable of measuring impedance of an electronic circuit component or a material, by allowing different configurations of test leads or probes to be connected directly or indirectly. However, incorrect measurement techniques or instrumentational errors can cause impedance measurements of passive electronic circuit components to show unnatural behavior in the real world as compared to their ideal behavior.

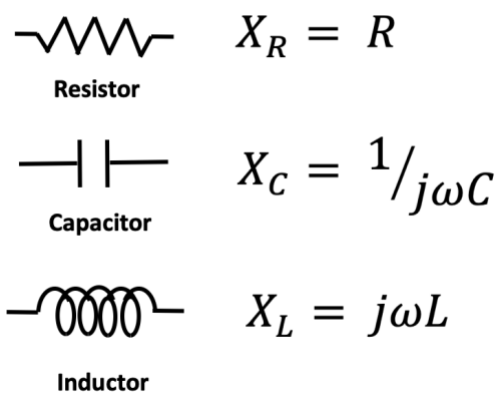

Figure 5.2: Reactance of electronic circuit elements. Here, R is the resistance, C is the capacitance, L is the inductance and $\omega = 2\pi f$ is the frequency.

It is important to thoroughly understand what an impedance value for a circuit component (resistor, inductor, or capacitor), indicates in reality. The *parasitics* of the component, and the measurement error sources such as the test fixture's residual impedance, affect the value of the impedance.

- An ideal value is the value of the component without parasitic effects. The model for an ideal component is purely resistive and has no frequency dependence. The ideal value is the theoretically calculated value of an electrical component.
- A real value represents effective impedance, and includes the effect of the component's parasitics. Thus, it depends on the frequency of the applied electric field.
- The measured value is the value of the component measured by the use of an external instrument, and reflects the residual impedances and inaccuracies of the instrument. The accuracy of the measurements can be judged by comparing how close the measured value is to the ideal value of a component.

Frequency dependency is a common factor that plays a part in all real-world component measurements of impedance because of the existence of parasitics [88]. The parasitics can define the component's frequency characteristics for real-world resistors, capacitors and inductors. The

frequency response of an electronic component that depends on the parasitics can change the measured value of the resistor.

Electrical impedance spectroscopy (EIS) measurements for biological suspensions can be analyzed by fitting the data to an equivalent circuit model, consisting of resistances and capacitances in series and parallel combinations such that its impedance matches the measured data [89, 90]. An equivalent electrical circuit is a relatively simple way to model even complex biological systems. However, it should be noted that models cannot describe any biological system with complete accuracy.

Many reports can be used to study the response of biological cells and membranes under the effect of electric fields. For example, Radke *et al.* [91] have developed an equivalent circuit model for immobilized bacteria with series and parallel combinations of resistors and capacitors where the dielectric behavior of the solution is represented by a combination of resistances and capacitances, and the cytoplasm and membrane components are also described as resistors and capacitors with well-defined values. The double-layer capacitance at the electrode surface and the capacitance created from the oxide separation of the gold electrodes and the silicon is described by a capacitance. Cai *et al.* [92, 93] have developed an equivalent circuit model for NaA zeolite membranes, with resistive and capacitive components describing the solution and membrane separately, and also included components that represent the resistive and capacitive properties of the ionic double-layer at the electrode-electrolyte interface.

More complex and detailed models have also been developed by several research groups. An electrical model has been modified and developed by Schoenbach *et al.* [94] where the suspension medium as well as inner and outer membranes are represented by resistive and capacitive components.

The mitochondrial suspension can be modeled as a leaky capacitor that consists of a parallel configuration of a capacitance C and a conductance G as shown in Figure 5.3.

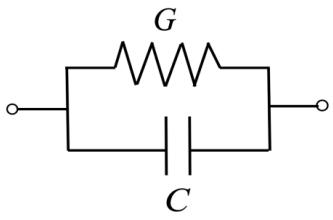

Figure 5.3: A simple electronic equivalent model for a mitochondrial suspension.

The conductance and capacitance of the measured biological suspension are given by,

$$G = \frac{\sigma A}{d} = \frac{1}{R}, \tag{5.8}$$

$$C = \frac{\varepsilon_r \varepsilon_0 A}{d}, \tag{5.9}$$

where σ is the electrical conductivity, ε_0 is the permittivity of free space, ε_r is the relative dielectric permittivity of the suspension, A is the area of the electrodes, R is the resistance and d is the distance between the electrodes. The complex impedance for the suspension model can be derived as,

$$Z = \frac{1}{G + j\omega C}. \tag{5.10}$$

Here, |Z| becomes,

$$|Z| = \frac{R}{\sqrt{1 + \omega^2 R^2 C^2}}. \tag{5.11}$$

In the high frequency limit, $\omega^2 R^2 C^2 \gg 1$,

$$|Z| = \frac{1}{\omega C}. \tag{5.12}$$

Thus, under these limitations, equation (5.9) shows that an increase in the effective dielectric constant of the suspension ε_r, will increase the capacitance, causing the magnitude of the measured impedance |Z| to decrease. In chapter 4, we explained how an increase in the mitochondrial membrane potential $\Delta\psi_m$ can exhibit an increase in the relative dielectric constant. Therefore, the change in $\Delta\psi_m$ can be studied by observing the response of the impedance of mitochondrial suspensions.

5.5 Impedance measurements

The technique of impedance measurements of biological suspensions is an important component to obtain stable and reliable measurements. Typical microscopic scale measurements of biological mediums allow characterization of cell and mitochondrial suspensions that require impedance measuring methods that must be sensitive to infinitesimal changes. Bioimpedance measuring techniques accommodate such sensitive devices that include electrodes to obtain subtle electronic signals [95].

Electrodes are unique components that can measure impedance of various forms of medium, such as solids or aqueous solutions. Two current-carrying electrodes are involved in passing an electric current through a medium; a source and a sink. The source and sink of an electronic circuit make up the path for the applied dc or ac signal through the medium 28]. For frequency-dependent electric signals, an ac signal is generated, and a current is passed across the two electrodes, while the potential change across the medium is measured by another two electrodes. Bioimpedance measurements, typically require four electrodes for measurement purposes: two current-carrying electrodes, and two voltage-sensitive electrodes. Figure 5.4 shows a four-electrode impedance measurement setup of a medium. The measured impedance of this medium is given by,

$$Z = \frac{\Delta V}{\Delta I}, \tag{5.13}$$

where, ΔV is the potential difference between the voltage-sensitive electrodes, and I is the current applied across the current-carrying electrodes [96, 97].

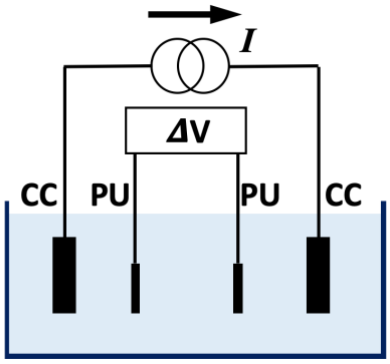

Figure 5.4: Four-electrode impedance measurement of a medium. The outer electrodes are current-carrying electrodes (CC), while the inner electrodes are voltage pick-up electrodes (PU). Image adapted from Grimnes *et al.* [28].

A metal electrode with electrons as charge-carriers, that comes in contact with an electrolyte with charge-carrier ions, will form an electrical double-layer at the interface. The electrical double-layer is a charge-depleted region where electron to ion charge transfer takes place. The double-layer is also called the polarizability of the electrode material, and its presence affects the accuracy of the measured impedance. The effect of the double-layer can be significantly reduced by separating the voltage path from the current path. This can be done by using four-terminal impedance measuring techniques, where the electrical double-layer formed at the current-carrying electrodes does not affect the measured potential difference. Figure 5.5 shows the schematic of the four-terminal configuration.

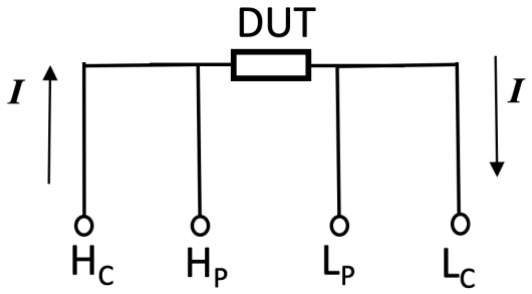

Figure 5.5: Four-terminal configuration. H_C and L_C are the high and low current paths, and H_P and L_P are the high and low voltage paths. DUT is the device-under-test and *I* is the current. Image adapted from *Impedance Measurement Handbook* [88].

The purpose of the four-terminal measurement technique is to reduce the double-layer interface impedance to allow accurate measurement of the impedance of the medium [95]. The probe designed in this study was designed for the purpose of measuring four-electrode impedances to avoid the polarization effect (Figure 5.6).

Figure 5.6: Design of probe for impedance measurement in four-terminal configuration. Designed by Karlapudi *et al.* [98].

The four-terminal measurement can be set to measure impedance in 2-terminal, 3-terminal, or 4-terminal configurations. The simplest technique is two-terminal configuration that combines both voltage path and current path together. However, this measurement technique contains error sources that dominates the impedance measurements of the medium with electrical double-layer interface effects at low frequencies [96].

The two-terminal configuration is shown in Figure 5.7. Here, the current path is the same as the voltage path, and adds polarization effect of double-layer interface to the measurements. For the purpose of our study, measurements were taken in two-terminal measurements due to instrumental setbacks.

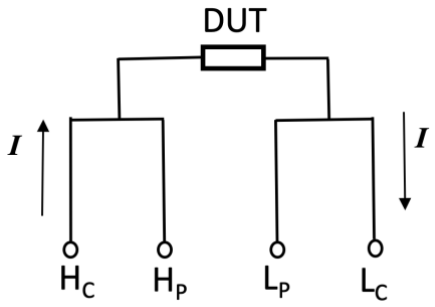

Figure 5.7: Two-terminal configuration. H_C and L_C are the current paths, and H_P and L_P are the voltage paths. Image adapted from *Impedance Measurement Handbook* [88].

Chapter 6: Experimental Methods and Results

6.1 Design and Fabrication of the Device and Test Leads

Impedance studies of mitochondrial suspensions required a device that could measure impedance of infinitesimal conductive solutions. A probe for the measurement of impedances of various dielectric suspensions was designed and fabricated in this study. The probe was built using a printed circuit board (PCB) with gold electrode arrays on one end (Figure 5.6). The gold electrode arrays which extend by electronic strips along a 100 mm long PCB, are then soldered onto dupont connector pins that are crimped with wires. As shown in Figure 6.1, the PCB with electronic pathways are covered with a tubing made of *Peek polymer*, and hot glue sealed on either end, allowing 4 mm of the tip of the with electrodes to remain uncovered.

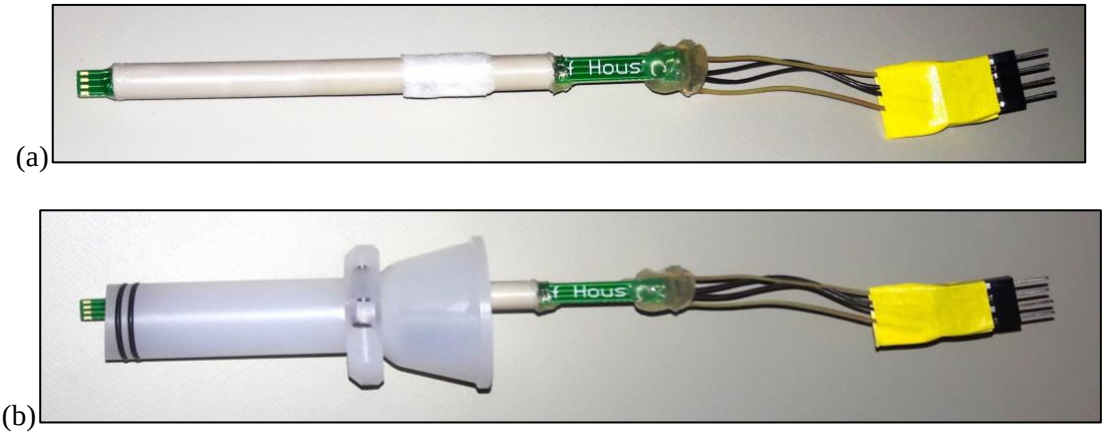

Figure 6.1: The designed and fabricated probe to measure impedance of various mediums: (a) the PCB covered with tubing and soldered to wires and (b) the completed probe placed inside the PVDF stopper of the Oroboros respirometer.

The probe was designed to be compatible with the *Oroboros Oxygraph O2k* high-resolution respirometer, providing a convenient method of measuring the impedance of mitochondrial suspensions, while simultaneously measuring the oxygen consumption. The diameter of the probe was selected to match the 6 mm port of the white PVDF stopper, a standard part of the respirometer. The inner diameter (16 mm) and height (10 mm) of the respirometer chamber provides sufficient space for inserting the probe through the stopper, allowing the tip of the probe to be immersed in the 2.2 ml volume of the chamber, without obstructing the rotating motion of the magnetic stirrer. (Figure 6.2)

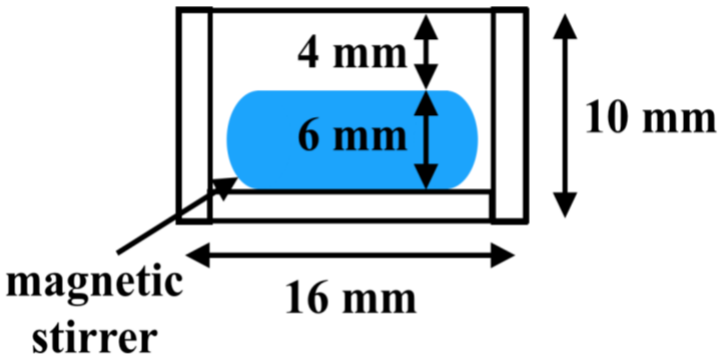

Figure 6.2: Schematic of the chamber in the respirometer, where the measured medium is placed. The chamber has an inner diameter of 16 mm and a height of 10 mm, and a magnetic stirrer with a height of 6 mm placed inside at all times.

The probe was then connected to the Keysight Technologies E4990A Impedance Analyzer (frequency range of 20 Hz to 50 MHz) shown in Figure 6.3, using the self-fabricated test leads. The test leads were constructed in two parts (Figure 6.4). The first part of the test leads were four coaxial cables connected to BNC connectors, which were then connected to the four terminals on the impedance analyzer. The second part of the test leads was a 2-terminal fixture, that combined the H_{cur} and H_{pot} terminals together, and the L_{cur} and L_{pot} terminals together, respectively, allowing the two terminals of the device-under-test (DUT) to be connected. The 2-terminal fixture then connects to two

electrode pathways on the probe, allowing it to measure impedance in 2-terminal mode using two electrodes.

Figure 6.3: Keysight E4990A Impedance Analyzer.

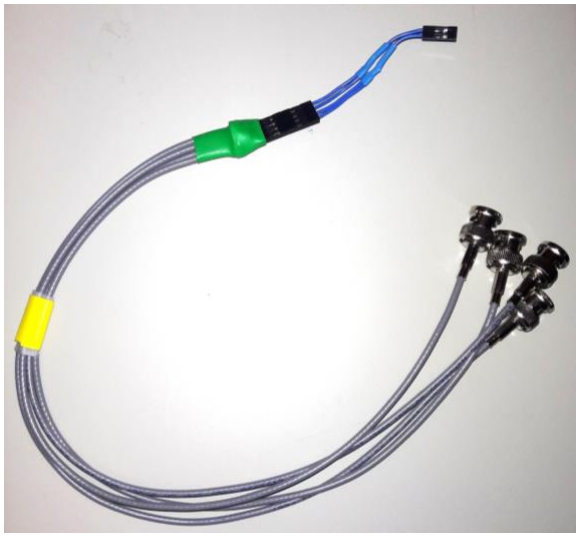

Figure 6.4: The test leads designed for measurement in 2-terminal configuration. The two-part test leads include 4 coaxial cables, connected to a 2-terminal fixture (blue part).

6.2 Test Cable and Fixture Calibration

Impedance measurements were performed using a E4990A Keysight Technologies impedance analyzer, with a measurement frequency range of 20 Hz up to 50 MHz. Calibration was important for correction of loses in test leads and fixtures that were used to measure impedance. The self-fabricated test leads and fixture were tested for accuracy by comparing calibration with standard test leads and fixtures that normalized with the instrument. To test the losses of the self-fabricated cables, impedance measurements for standard electronic components were recorded, and used to validate the stability of the impedance measuring method of the device.

Keysight Technologies offers a range of test measurement accessories that are suitable for many applications. The 16334A tweezer contact test fixture was used to compare and justify the calibration of the self-fabricated test leads used in this study. Figure 6.5 shows the 4-terminal pair type fixture which is equipped with a tweezer type probe. The fixture allows a frequency range of 5 Hz to 15 MHz.

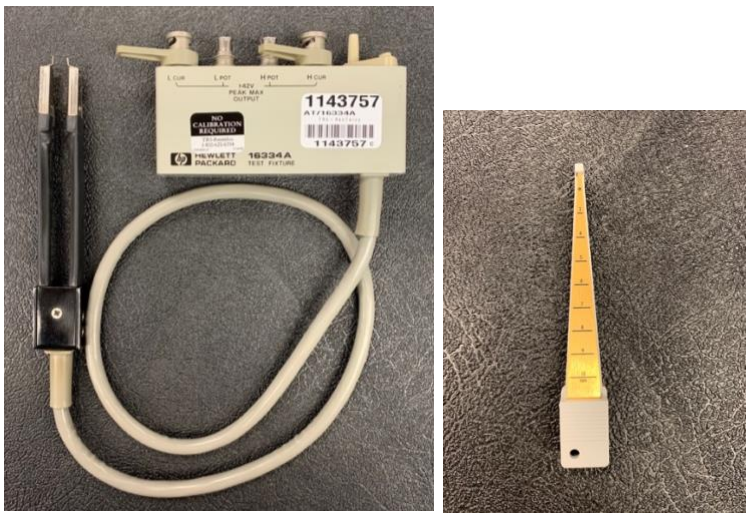

(a) (b)

Figure 6.5: The 16334A tweezer contact fixture and components: (a) the tweezer type fixture, and (b) the compensation block used to calibrate the fixture.

Calibrating and compensating verifies its accuracy by comparing the instrument's impedance measurements with standard electrical components, by connecting at the calibration plane and adjusting the instrument setup (through computation/data storage) so that it measures to a specific accuracy. The calibration plane indicates the electrical reference plane at which the standard devices are connected and measured. Calibration and compensation improves the effective measurement accuracy when test fixtures, test leads, or additional measurement accessory are used with the instrument. The most common compensation technique used to test the accuracy of an instrument is the Open/Short compensation. Open compensation measures the stray capacitance between the test fixture terminals and compensates the calibration plane accordingly, while the short measurement is performed by connecting a shorting device to the terminals to achieve the same.

Open and short calibration and compensation for both 16334A standard test fixture, and the self-fabricated test cable and fixture were performed on the Keysight impedance analyzer with appropriate settings for each adapter. The data for open and short configurations for each test fixture can be observed in Figures 6.6 and 6.7 below. Figure 6.6 (a) and 6.7 (a) show open-circuit configuration of the self-fabricated test cable and the standard fixture after calibration was performed. Here the impedance has very high values since the capacitance between the terminals is very small. Figure 6.6 (b) and 6.7 (b) shows short configuration where the terminals are in contact with each other. Here, the impedance values were equivalent to zero after calibration was performed. Open and short calibration measurement data for both fixtures showed correlation between data values, concluding that the self-fabricated cable could be calibrated accurately, and that connections between test leads were secure.

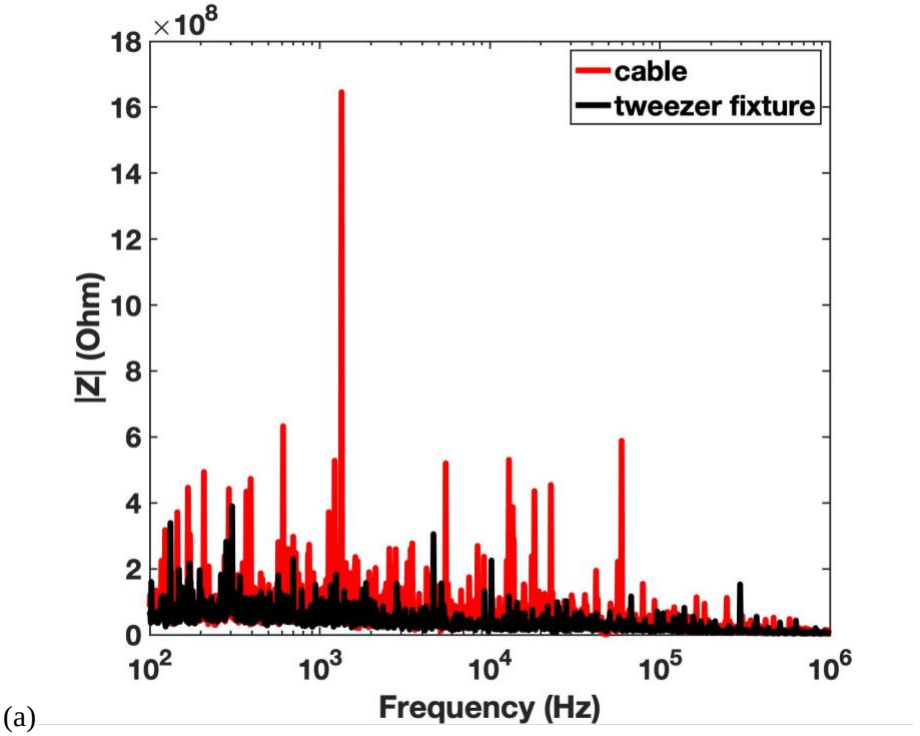

(a)

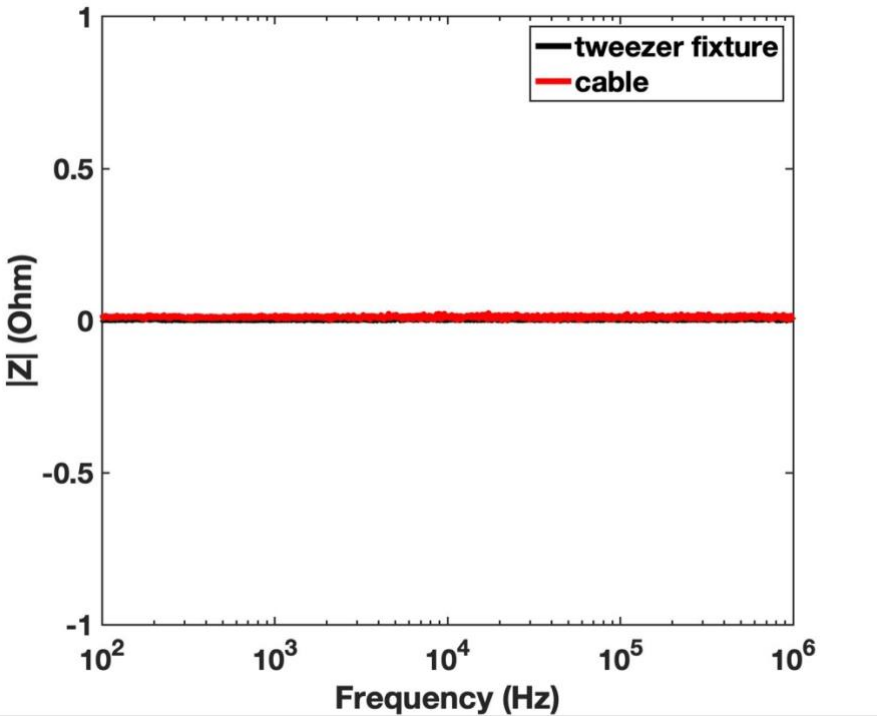

(b)

Figure 6.6: Bode plots showing calibration between the self-fabricated and standard fixtures: (a) open calibration and (b) short calibration. The standard tweezer fixture appears to reduce noise levels during the open calibration.

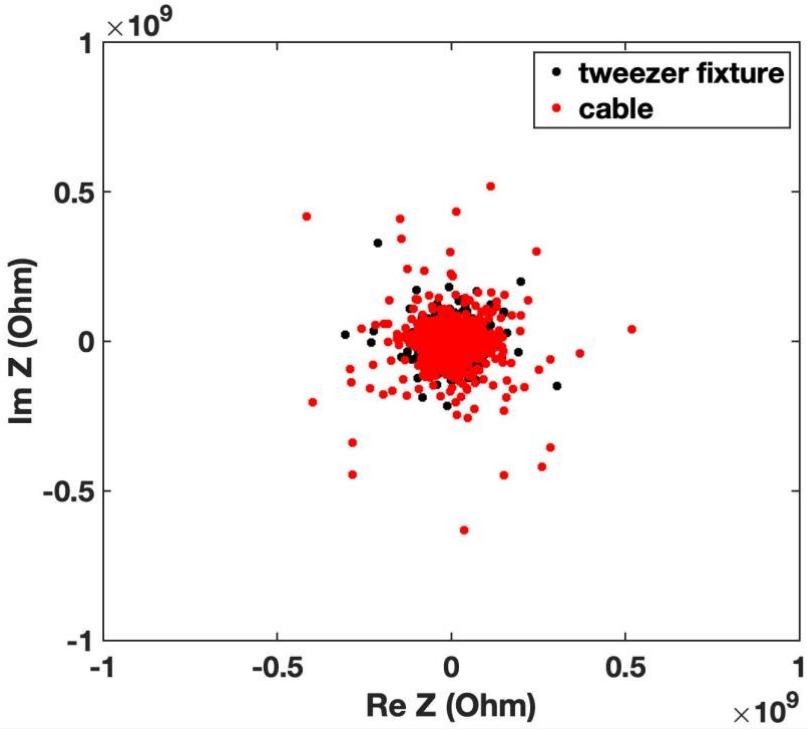

(a)

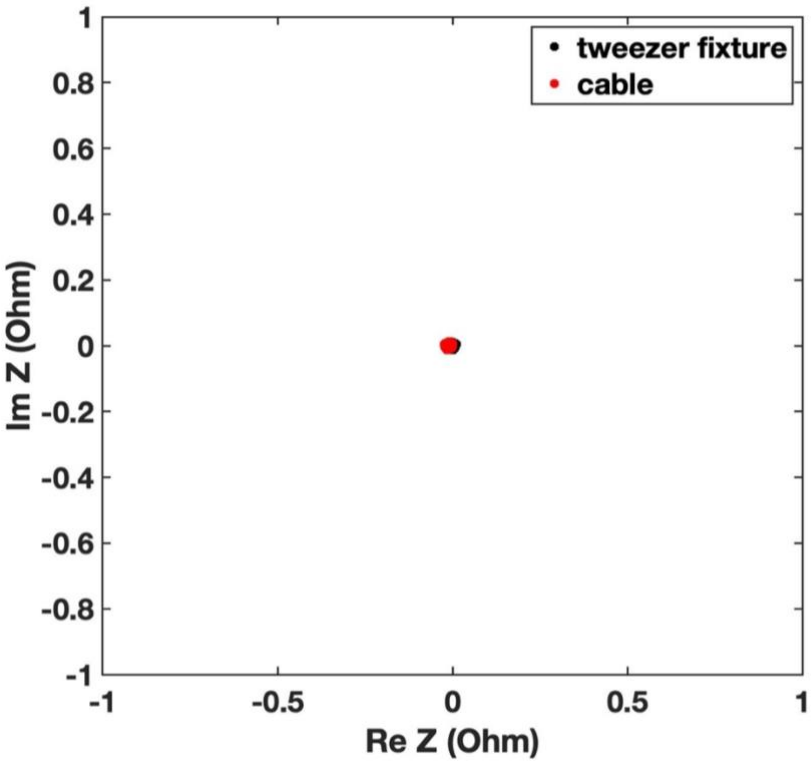

(b)

Figure 6.7: Nyquist plots showing calibration between the self-fabricated and standard fixtures: (a) open calibration and (b) short calibration.

Next, experimental data were obtained for a range of resistors, capacitors, and RC circuit configurations, and compared with theoretical data. The standard tweezer contact fixture was used to take measurements for more accuracy.

In section 5.4, we discussed the frequency response of real-world electronic components. A resistor has a frequency dependent response based on its resistance value. An ideal value of a resistor has a constant impedance modulus value, $|Z| = R$, where, R is the resistance of the resistor. As discussed in the above-mentioned section, an ideal value of a resistor is a theoretical value, that does not consider the parasitics and manufacturing errors. Figure 6.8 below shows correlation between theoretical calculations and measured values for a range of resistors, which justifies the accuracy of the experimental data.

A capacitor has a capacitive reactance,

$$X_C = \frac{1}{\omega C} = \frac{1}{2\pi f C}, \tag{6.1}$$

where, f is the applied frequency, and C is the capacitance. The impedance modulus for a capacitor has a high value at low frequency, and decreases for higher frequencies. Figure 6.9 shows theoretical and experimental data values for a range of different capacitors that show correlation.

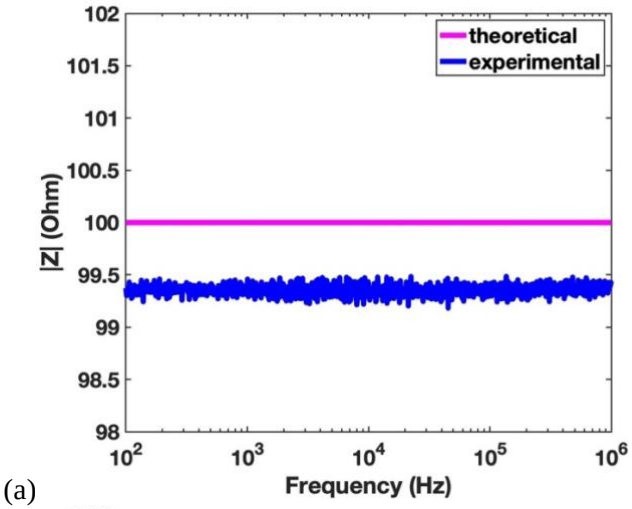

(a)

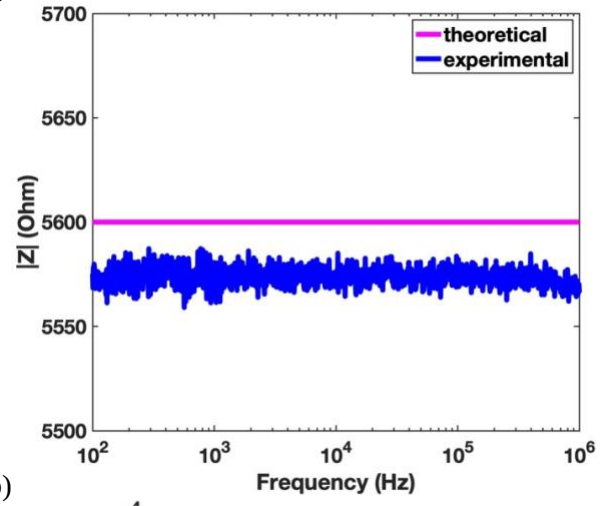

(b)

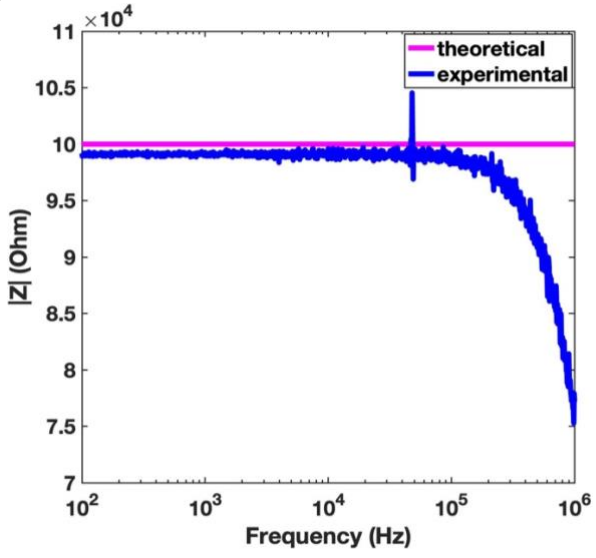

(c)

Figure 6.8: Theoretical and experimental Bode plots for $|Z| = R$ (ideal case) for various values of resistors: (a) $R = 100\ \Omega$, (b) $R = 5.6\ k\Omega$, and (c) $R = 100\ k\Omega$.

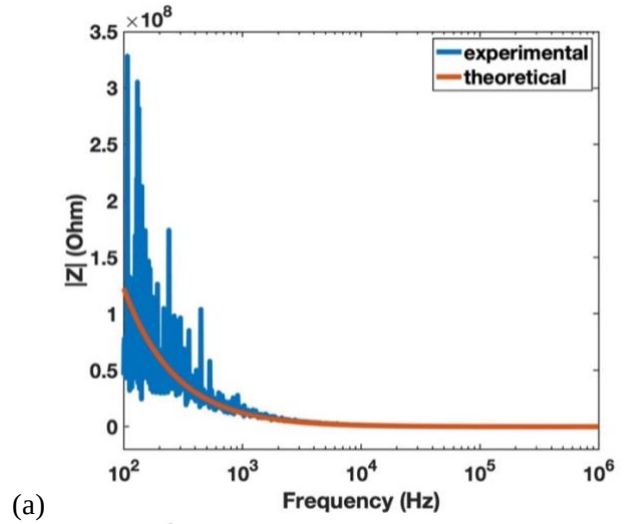

(a)

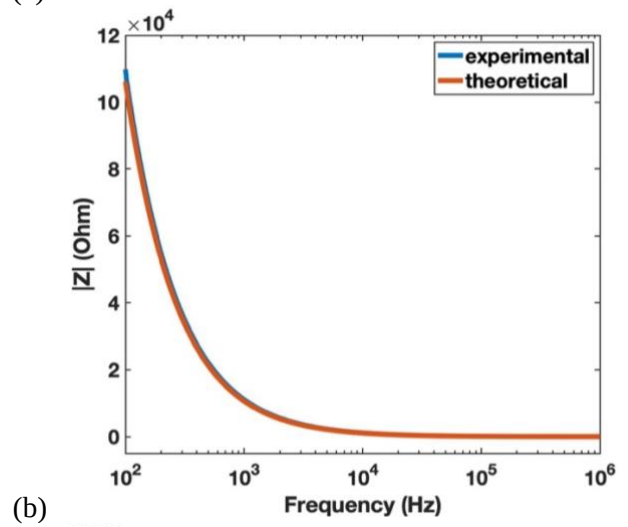

(b)

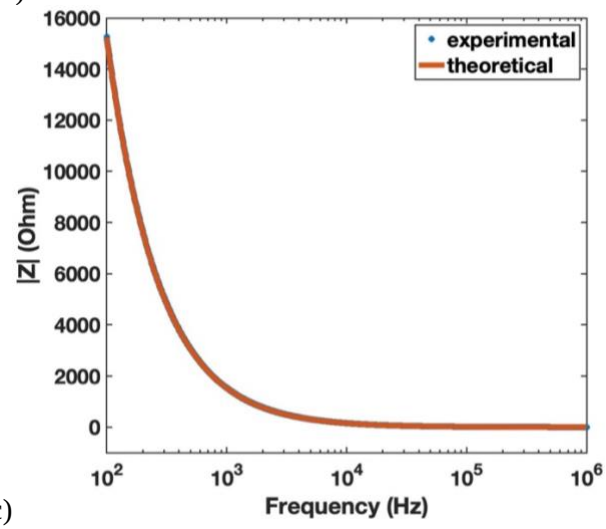

(c)

Figure 6.9: Theoretical and experimental Bode plots for $|Z| = 1/\omega C$ (ideal case) for various values of capacitors: (a) $C = 13.0\ pF$, (b) $C = 15.0\ nF$, and (c) $C = 104.5\ nF$.

For a series RC circuit, the impedance is derived as,

$$Z_S = \sqrt{\left(R^2 + {}^{1}/_{(\omega C)^2}\right)}, \tag{6.2}$$

where, R is the resistance (Figure 6.10). As the frequency increases, the effective impedance of the resistance becomes more prominent, while the capacitive reactance decreases for both theoretical and experimental data values, which can be seen in Figures 6.11 and 6.12. The low frequency noise for small capacitances may result, in part from the extremely tiny values of ωC when both ω and C are small.

Figure 6.10: Schematic for a series RC circuit.

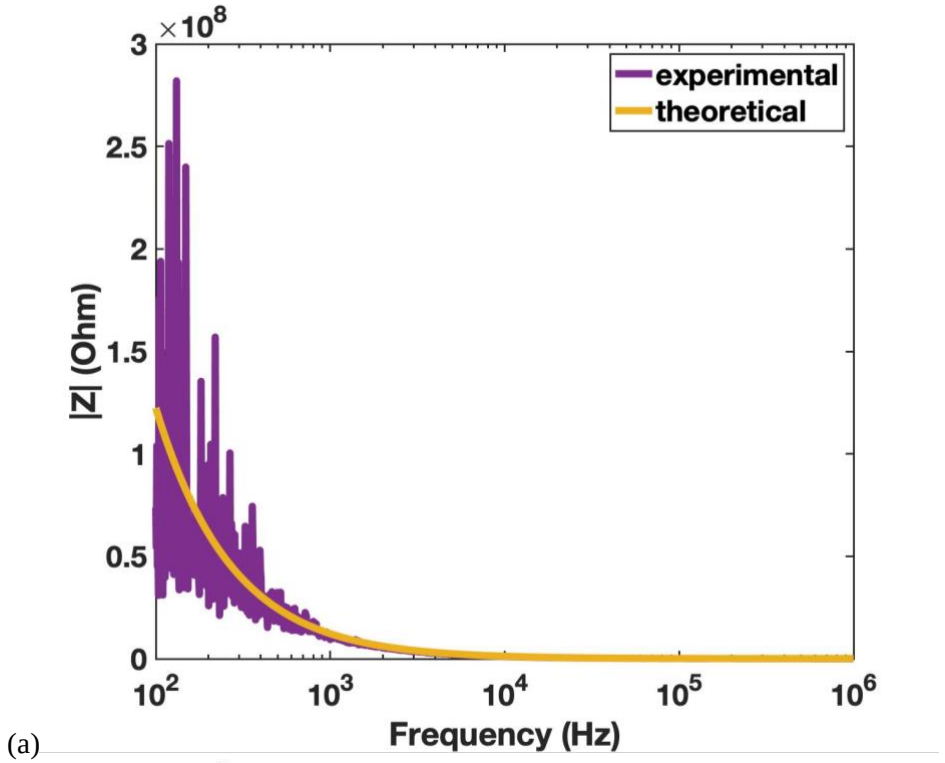

(a)

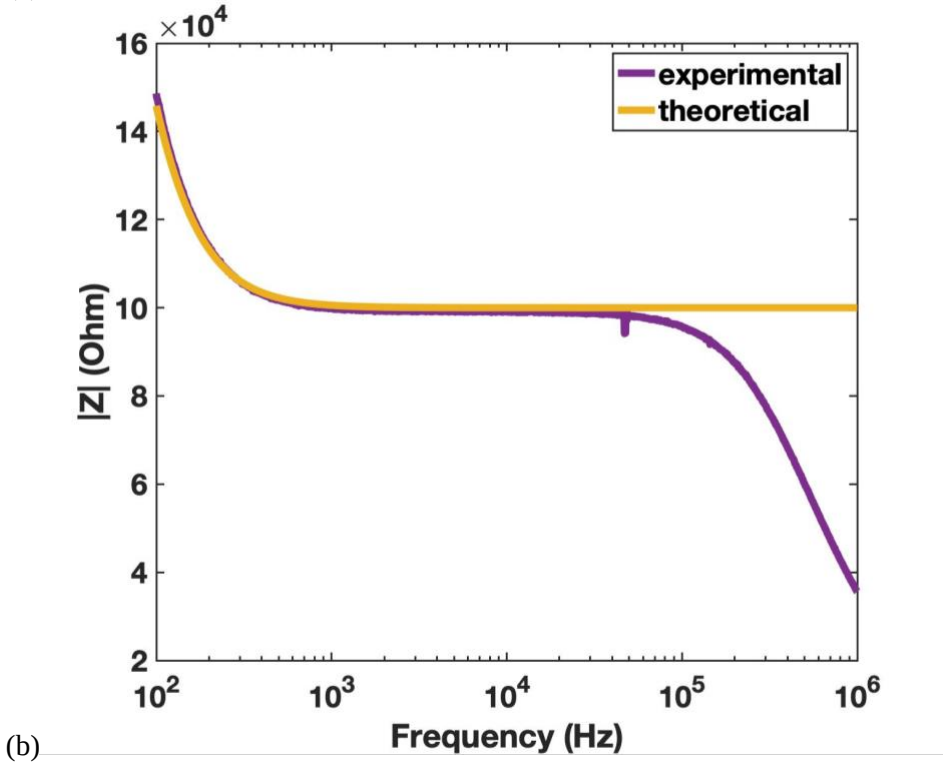

(b)

Figure 6.11: Theoretical and experimental Bode plots for |Z| for series RC circuits with $R = 100\ k\Omega$: (a) $C = 13.0\ pF$ and (b) $C = 15.0\ nF$.

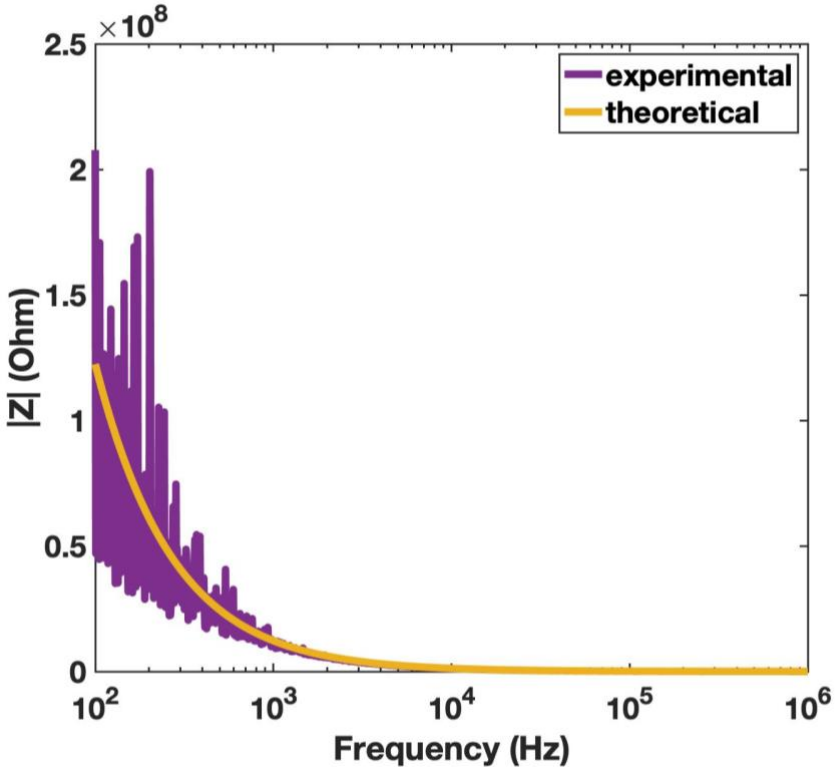

(a)

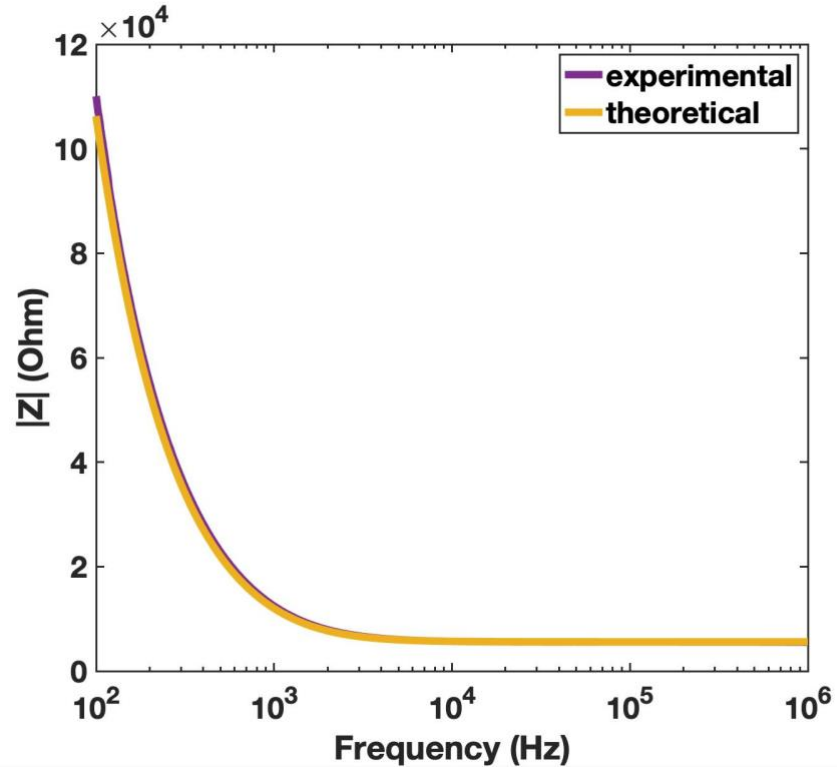

(b)

Figure 6.12: Theoretical and experimental Bode plots for |Z| for series RC circuits with $R = 5.6\ k\Omega$: (a) $C = 13.0\ pF$, and (b) $C = 15.0\ nF$.

For a parallel RC circuit, the impedance is derived as,

$$Z_P = {(R/\omega C)}\Big/{\sqrt{\left(R^2 + {1}/{(\omega C)^2}\right)}}, \tag{6.3}$$

where, R is the resistance (Figure 6.13). For small capacitances in parallel, the impedance approaches the resistive component at low frequencies and decreases with increasing frequency. However, for high capacitances in parallel, the impedance starts decreasing even at lower frequencies. This can be seen for both theoretical and experimental data shown in Figures 6.14 and 6.15.

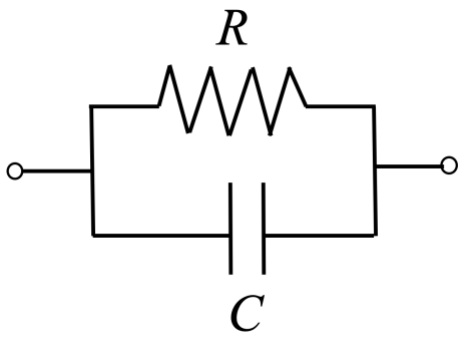

Figure 6.13: Schematic for a parallel RC circuit.

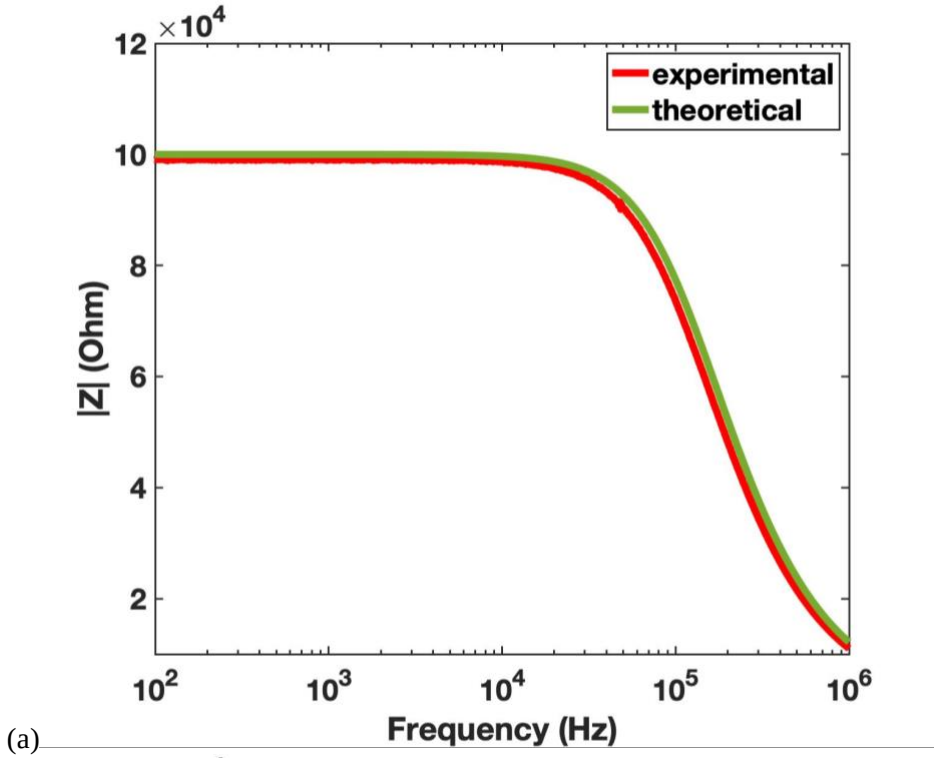

(a)

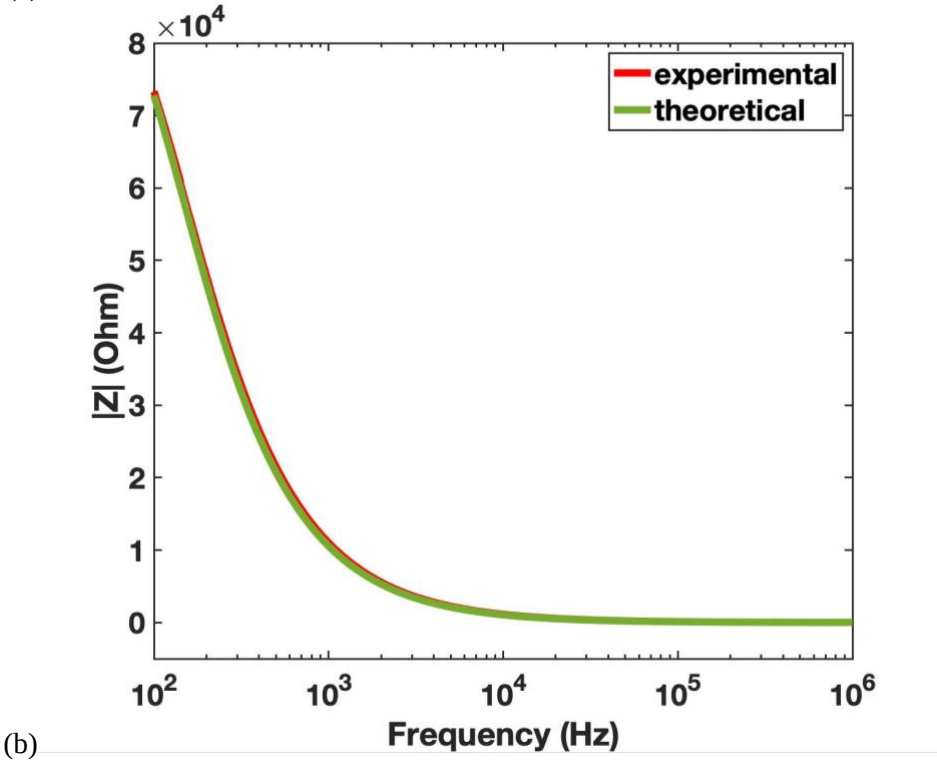

(b)

Figure 6.14: Theoretical and experimental Bode plots for |Z| for parallel RC circuits with $R = 100\ k\Omega$: (a) $C = 13.0\ pF$ and (b) $C = 15.0\ nF$.

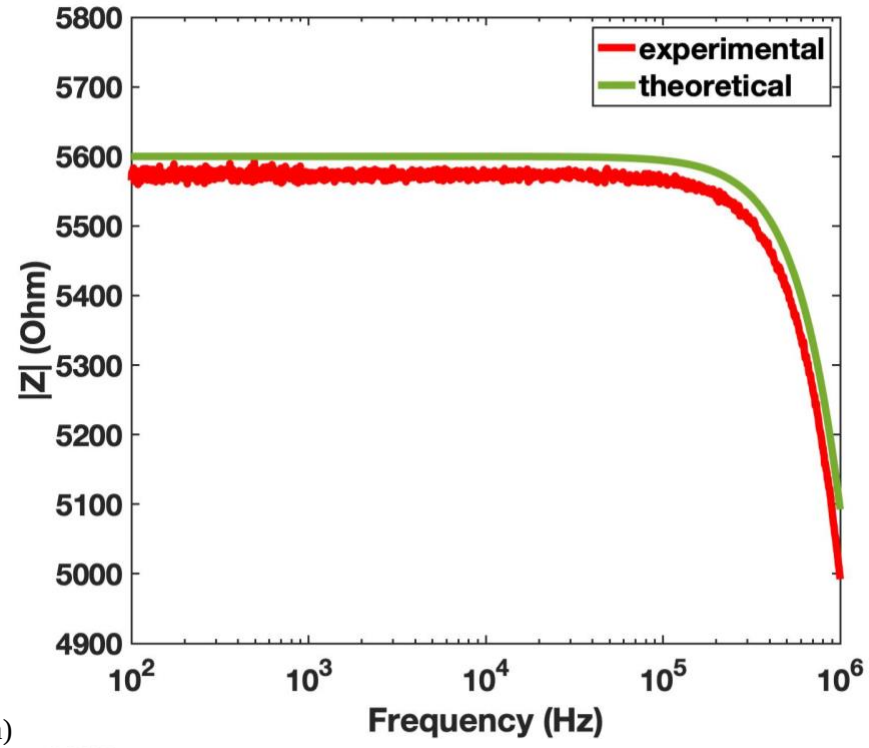

(a)

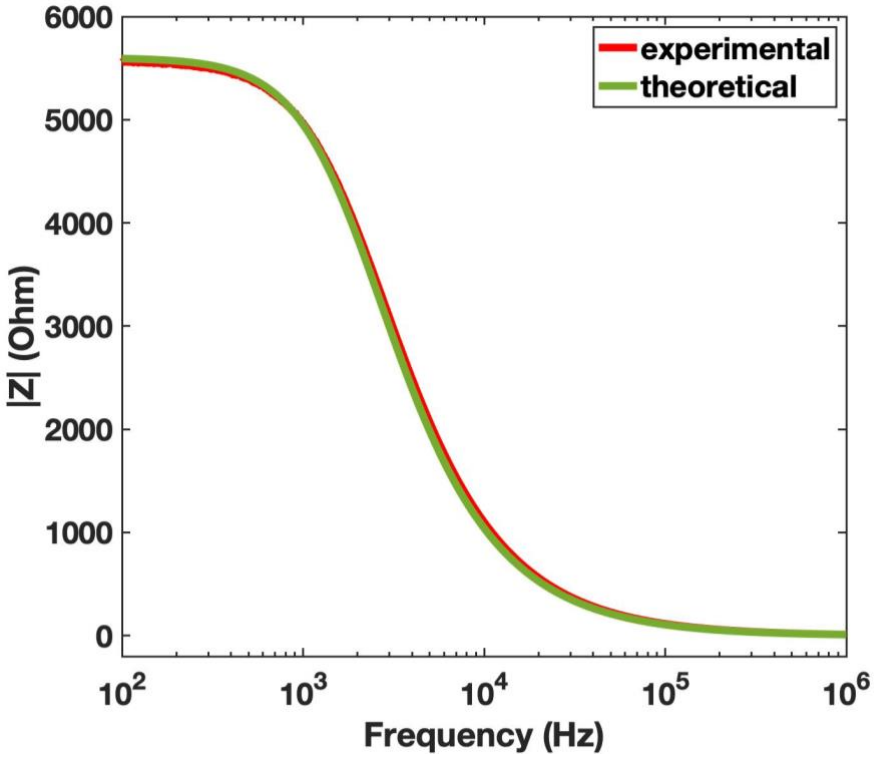

(b)

Figure 6.15: Theoretical and experimental Bode plots for |Z| for parallel RC circuits with $R = 5.6\ k\Omega$: (a) $C = 13.0\ pF$, and (b) $C = 15.0\ nF$.

6.3 Calibration of the Probe using Dielectric Solutions

Before measurements were acquired for mitochondrial suspensions, the designed impedance measuring probe was tested on dielectric solutions with known dielectric permittivity and conductivity values.

For the accuracy and consistency of measurements and analysis, micro-centrifuge tubes were used to perform the experiment. A volume of 500 µl of each dielectric solution was placed in the micro-centrifuge tube at a temperature of 25 ^{0}C, and the probe was placed in the solution as shown in Figure 6.16.

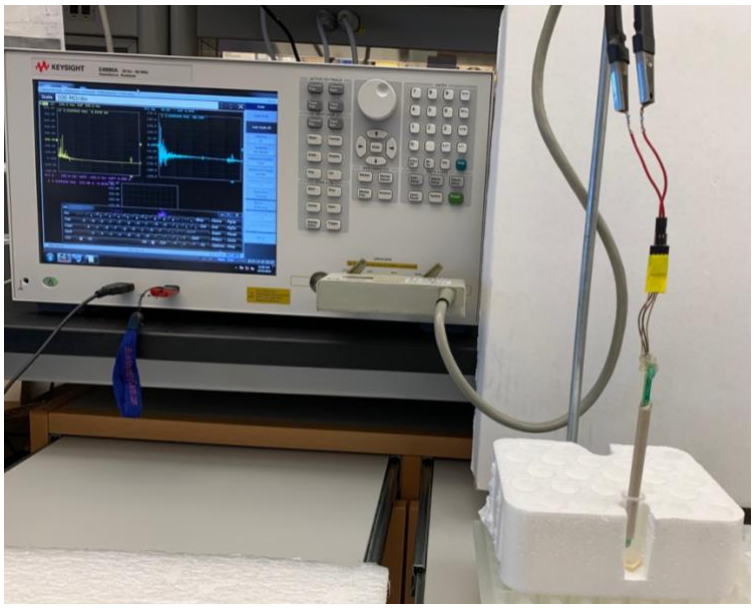

Figure 6.16: Experimental setup using micro centrifuge tubes.

Complex impedance of pure deionized water (DI water) with a resistivity of 18.0 MΩcm ($\sigma = 5.56e^{-6}$ S/m) was measured. The obtained data is shown in the Figures 6.17 and 6.18. The high resistivity of DI water depicts a high impedance response at low frequency. The Nyquist plot for the

impedance data obtained for DI water is shown in Figure 6.18. The Nyquist plot is a data plot between the imaginary part of the complex impedance, and the real part, where each point is characteristic of one frequency of measurement. The low frequency data are depicted on the right side of the plot with higher value of impedance, whilst the high frequency data are depicted on the left side with decreasing impedance. The Nyquist plot is portrayed as a semi-circle for truly complex impedance data, due to the second order variation. Typical frequency spectra data in Figure 6.17 for impedance magnitude and phase shows the dependency of resistive pathways at low frequencies and the capacitive pathways at higher frequencies.

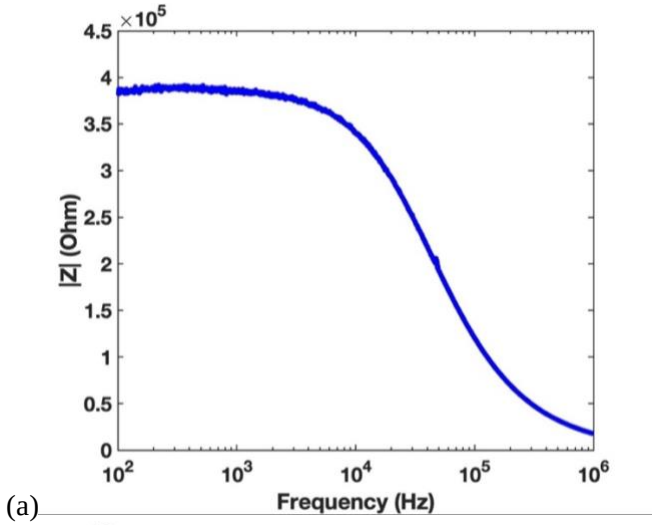

Figure 6.17: Bode plots obtained for impedance and phase measurements of DI water at 25 ^{0}C: (a) impedance magnitude vs frequency and (b) phase vs frequency.

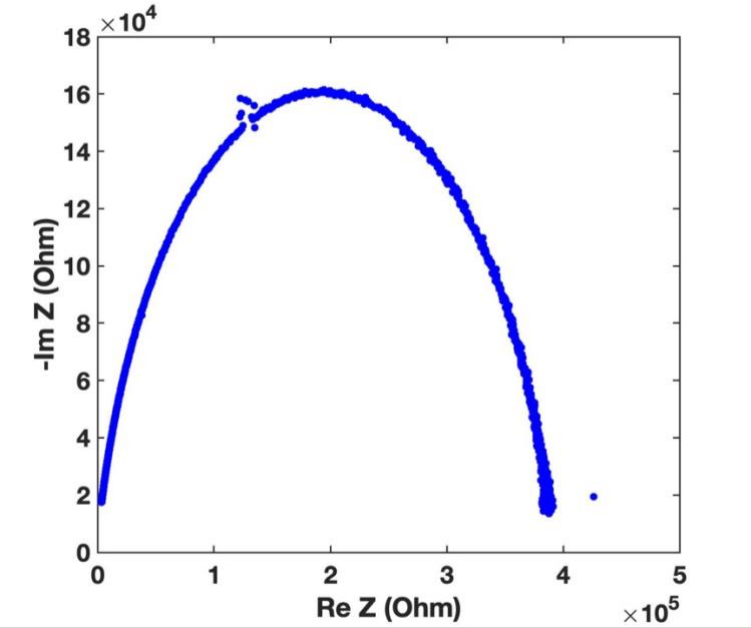

Figure 6.18: Nyquist plots obtained for impedance measurements of DI water at 25 ^{0}C.

Impedance measurements were also performed, and impedance magnitude and phase data were observed for absolute ethyl alcohol (pure ethanol with MW=46.07 g/mol), methanol, isopropyl alcohol and tap water (Figure 6.19 and 6.20). Alcohols usually have very low conductivity. This can be observed by the high impedance values alcohols exhibit at low frequency, in comparison to tap water, which has high concentrations of ions such as sodium, potassium, and is able to conduct current much easily. Methanol, however, is comprised of polar molecules like water, and thus has a relatively high conductivity as compared to the other alcohols. Margo *et al.* [96] and Ayliffe *et al.* [99] show impedance and phase responses for various ionic solutions that are comparable with the experimental data plots shown below.

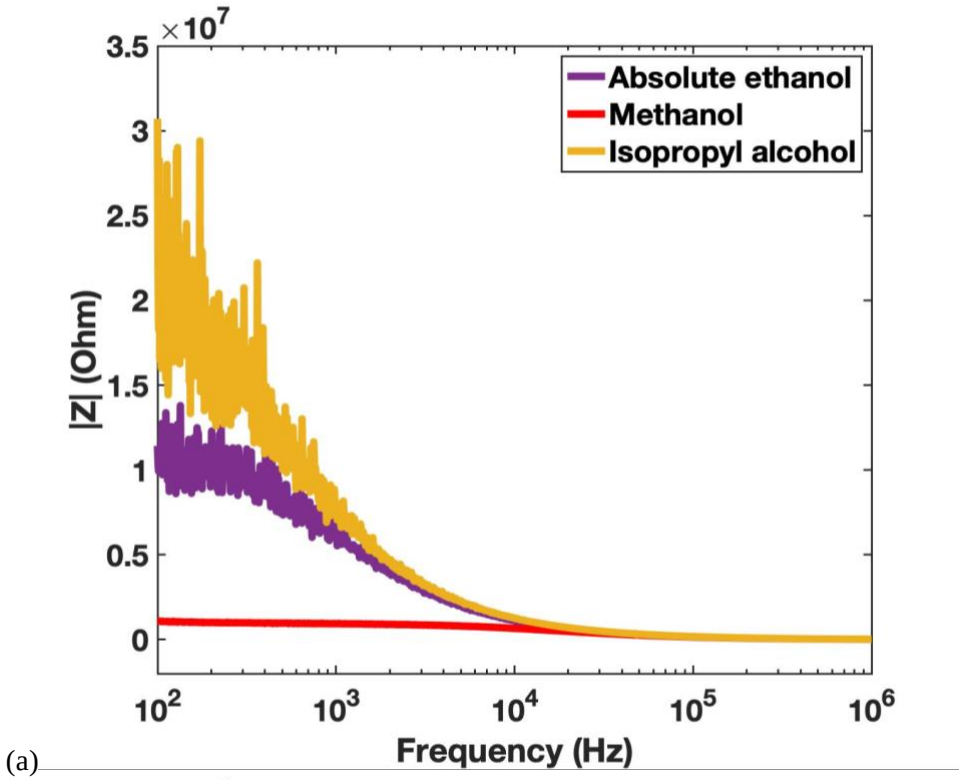

(a)

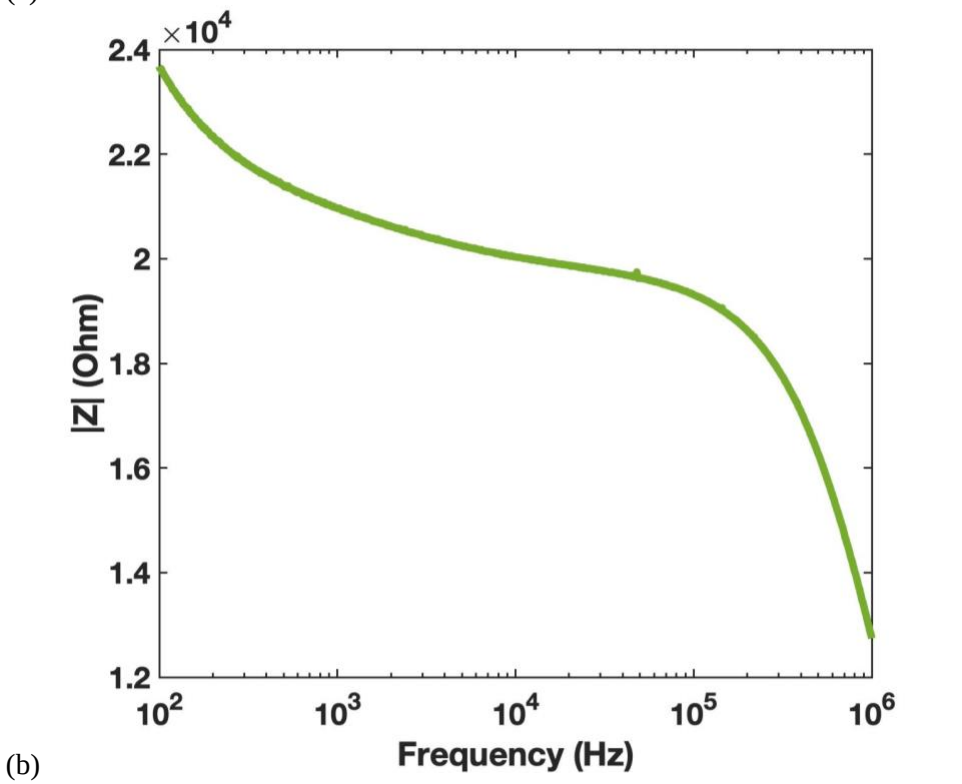

(b)

Figure 6.19: Experimental data plots for |Z| obtained for various dielectric solutions at 25 ^{0}C: (a) for absolute ethyl alcohol, methanol, and isopropyl alcohol, and (b) for tap water.

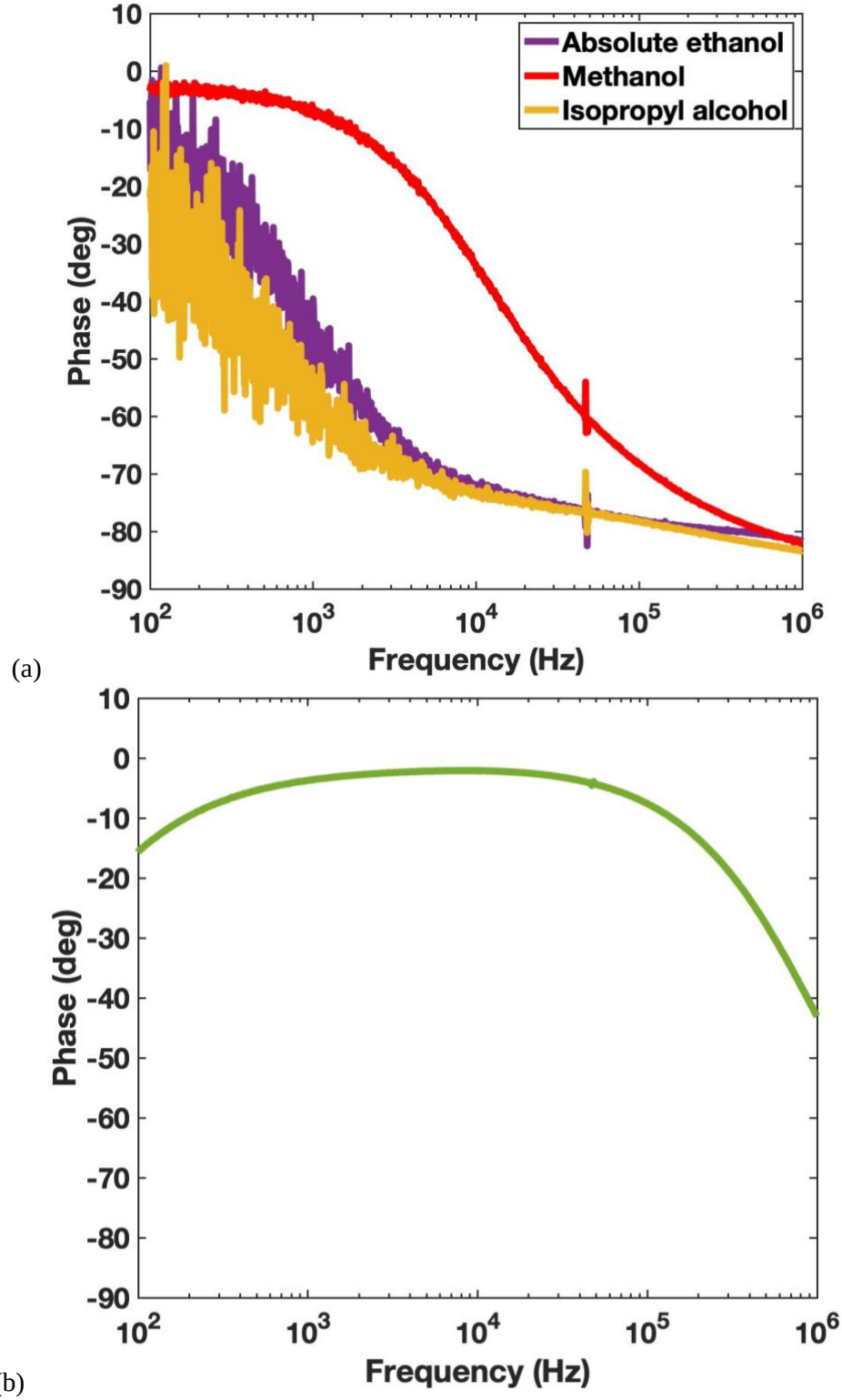

(a)

(b)

Figure 6.20: Experimental data plots for phase obtained for various dielectric solutions at 25 ^{0}C: (a) for absolute ethyl alcohol, methanol, and isopropyl alcohol, and (b) for tap water.

6.4 Correcting the Polarization Impedance Effect

The effect of the ionic charges that accumulate near the interface between the solution and the metal electrodes is the electrical double-layer effect. The electrical double-layer effect on measured impedance causes a polarization effect, where a polarization impedance Z_P exists in series with the intrinsic impedance of the sample, Z_S. Therefore, the measured impedance becomes the sum of the intrinsic impedance and the polarization impedance as,

$$Z_m = Z_S + Z_P. \tag{6.4}$$

The measured impedance of the medium is given by Z_m. The ideal impedance that gives the intrinsic impedance of the solution Z_S is given by Equation (6.5) below [3, 79, 80]. Assuming that the polarization effect is absent in the high-frequency range, the experimental impedance data were fitted with parameters of dielectric permittivity and conductivity for various dielectric solutions. The intrinsic impedance of the solution is given by,

$$Z_S = \frac{\alpha}{\sigma + j\omega\varepsilon}, \tag{6.5}$$

where α is a geometrical constant, the electrical conductivity σ and dielectric permittivity ε are fitting parameters, and $\omega = 2\pi f$ is the frequency [3]. Equation 6.5 can be arranged to extract the real and imaginary components,

$$Re\,(Z_S) = \frac{\alpha\sigma}{\sigma^2 + \omega^2\varepsilon^2}, \tag{6.6}$$

$$Im\,(Z_S) = \frac{-\alpha\omega\sigma}{\sigma^2 + \omega^2\varepsilon^2}. \tag{6.7}$$

Here, the geometrical constant α depends on the distance between the electrodes and the area of the electrodes. Since α was not known for the electrode setup in this experiment, known values for relative dielectric permittivity for absolute ethanol, methanol, and isopropyl alcohol, and imaginary parts of

experimental impedance data were used to calculate α. The relative dielectric permittivity for these solutions were taken from literature as ε_r = 25.3, 33.0, and 18.2, respectively (relative to vacuum) [100]. The value of α was determined as 28.55 1/m.

Figures 6.21, 6.22, and 6.23 show the experimental data fitted at high frequency using equation (6.7) for known dielectric solutions. These plots show that data can be fitted for frequencies approximately 100 kHz and higher, where the appropriate ε and σ values agree with the data, while the frequencies below approximately 100 kHz, the fitting deviates quite significantly. This anomalous behavior of ε at low frequencies is justified by the effect of polarization.

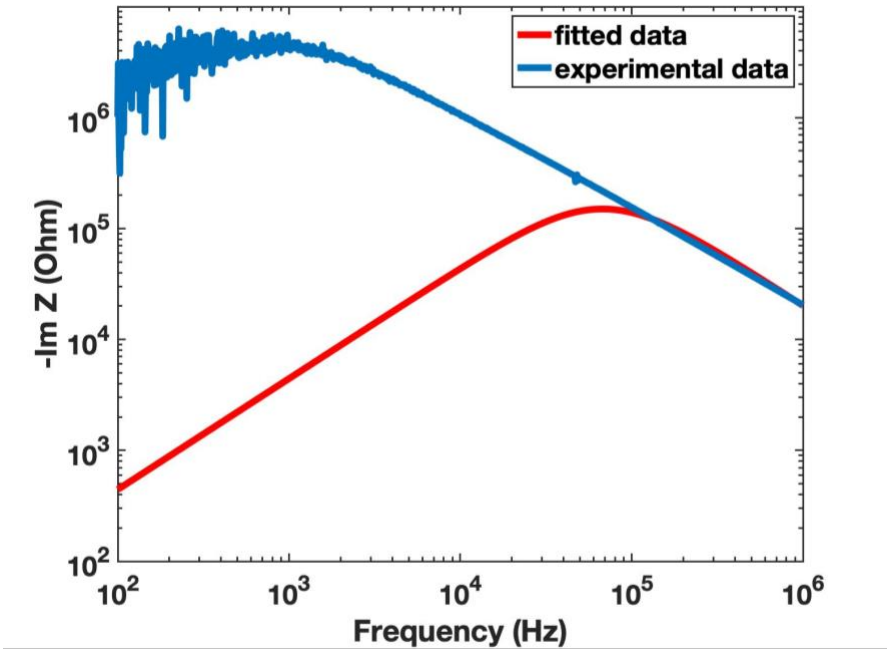

Figure 6.21: Impedance measurement data for absolute ethanol fitted to equation (6.7) with $\varepsilon_r = 25.3$ and $\sigma = 9.52e^{-5}\ S/m$ [100].

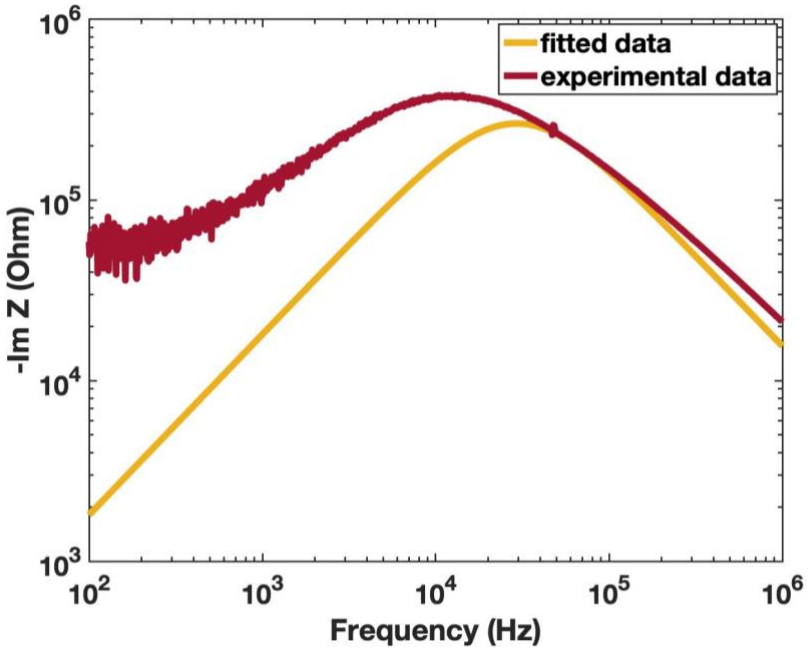

Figure 6.22: Impedance measurement data for methanol fitted to equation (6.7) with $\varepsilon_r = 33.0$ and $\sigma = 5.39e^{-5}\ S/m$ [100].

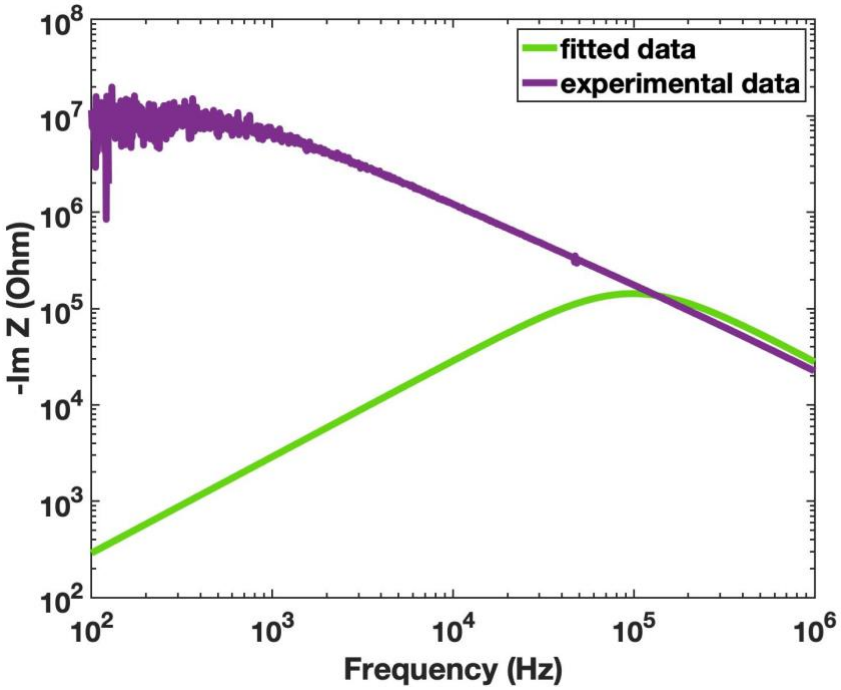

Figure 6.23: Impedance measurement data for absolute ethanol fitted to equation (6.7) with $\varepsilon_r = 18.2$ and $\sigma = 9.99e^{-5}\ S/m$ [100].

For the determined value of α, and fitting parameters ε and σ, impedance measurement data obtained for the respiration buffer solution were then used to calculate the real and imaginary components of the polarization impedance (Figure 6.24). Based on equation (6.4), the polarization error in impedance for the respiration buffer can be determined by subtracting the fitted data values from the measured experimental data values. Z_P determined from the impedance data for the respiration buffer were then used to calculate the intrinsic impedance values obtained in the experiments performed with isolated mitochondria and various substrates, assuming Z_P is the only polarization error affecting impedance measurements.

Using the data obtained in the previous calculations, the intrinsic ε and σ were calculated as shown below. The intrinsic conductivity is given by,

$$\sigma = Re\left(\frac{\alpha}{Z_S}\right), \tag{6.8}$$

And the intrinsic dielectric permittivity is given by,

$$\varepsilon = Im\left(\frac{\alpha}{\omega\, Z_S}\right). \tag{6.8}$$

These equations can be simplified further as,

$$\sigma = \frac{\alpha \cos\theta}{|Z_S|} = \frac{\alpha\, Re\,(Z_S)}{|Z_S|^2}, \tag{6.10}$$

and,

$$\varepsilon = \frac{-\alpha \sin\theta}{\omega\, |Z_S|} = \frac{-\alpha\, Im\,(Z_S)}{\omega\, |Z_S|^2}, \tag{6.11}$$

where, $\varepsilon = \varepsilon_r \varepsilon_0$ with ε_r as relative dielectric permittivity, and $\varepsilon_0 = 8.854e^{-12}\ F/m$.

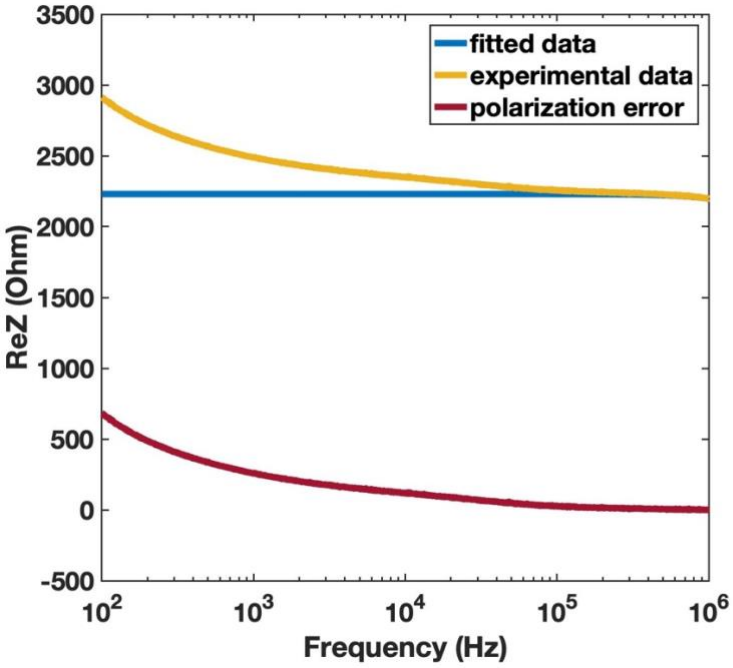

(a)

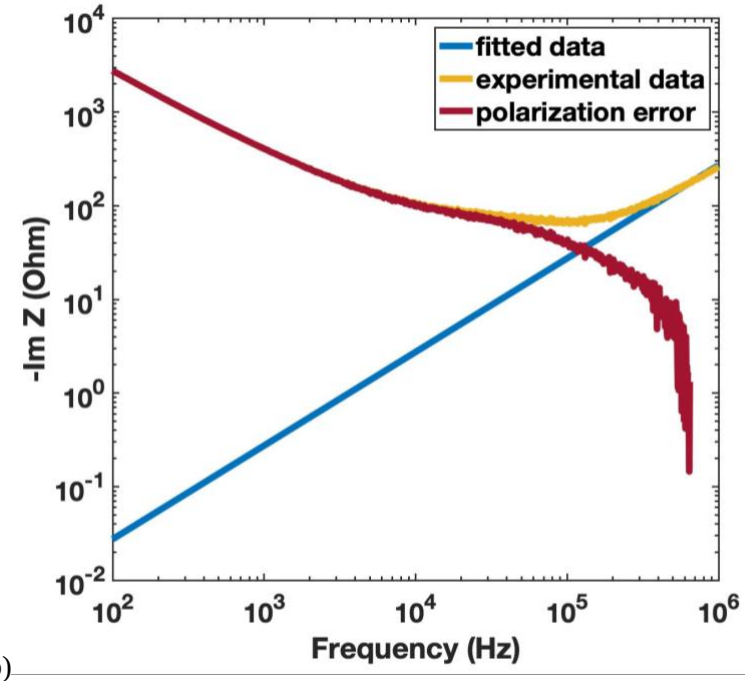

(b)

Figure 6.24: Impedance measurement data for the respiration buffer fitted to equations (6.6) and (6.7) at high frequencies. Here, $\alpha = 28.55\ 1/m$ was used to obtain Z_P. The difference between experimental data (yellow line), and fitted data (blue line) is the polarization error (maroon line).

Using the polarization corrected data for the respiration buffer, the conductivity and dielectric permittivity responses to frequency were calculated and plotted with respect to frequency as shown in Figure 6.25. The comparison between measured data before the polarization effect was extracted out, and the polarization corrected data is shown. The conductivity and dielectric permittivity responses calculated here show agreement to data obtained by Bot *et al.* [3, 79].

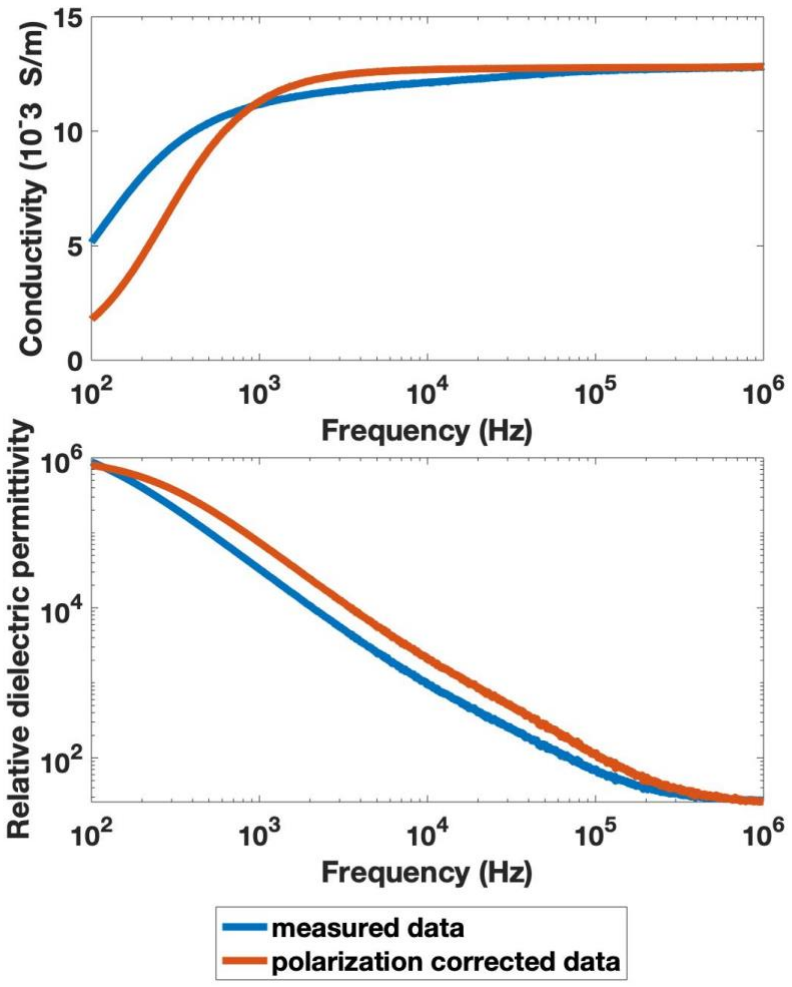

Figure 6.25: Dispersion curves for the respiration buffer. The frequency dependence of conductivity (top) and relative dielectric permittivity (bottom) are shown for measured values and polarization corrected data values.

6.5 Experiment with Isolated Mitochondria

All experiments were conducted on mitochondria extracted from mice heart/liver according to the approved IACUC protocol. The procedures used were in agreement with the institutional guidelines, and in compliance with the approvals of the Guide for Care and Use of Laboratory Animals. In the present study, we performed impedance measurements on freshly pelleted mice cardiac and liver mitochondria in the respiration buffer solution, extracted by following the isolation procedure mentioned below.

Isolation of mouse heart/liver mitochondria (procedure followed in Bioenergetics lab at Houston Methodist Research Institute)

1. The mouse was isofluoraned for 15 s and heart/liver was extracted, weighed, and placed in a glass tube on ice, and washed 4 times with Buffer A and minced on ice.
2. The minced organ was placed in Buffer A aliquots on ice and then transported quickly to the lab for further processing.
3. In the laboratory, the micro-centrifuge tube was pre-refrigerated to 4 ºC. All buffers, dissection gear, homogenization tools were kept at 4 ºC and all centrifuge spins were done at this temperature.
4. An ice bucket was gathered and filled with ice. The organ, Buffer A, Buffer B, and Buffer E were placed on ice.
5. Micro-centrifuge tubes of 1.5 ml were pre-labeled with the following per sample:
    a. "SSM" (2 tubes) b. "IFM" (2 tubes)
6. Using forceps, the sample was transported from Buffer A and pat dry on a paper towel.

7. Using a razor, the sample was chopped for 1.5 minutes, and transported to a new 1.5 ml tube labeled “IFM”.
8. Making sure to mix Buffer A well before use, 200 µl of Buffer A was added to the chopped-up sample and the sample was homogenized on ice for 2 minutes.
9. Approximately 500 µl - 1 ml of Buffer B was added to the sample and was centrifuged for 10 minutes at 800 rpm.
10. The supernatant was then transferred to a new 1.5 ml tube labeled “SSM”. This sample should be cloudy and any excess supernatant was removed from the pellet.
11. Buffer B was then added to the sample and centrifuged for 5-10 minutes at 12,000 rpm.
12. While the supernatant sample was spinning, the “IFM” pellet was weighed and the weight was recorded.
13. The weight was then multiplied by 500 (*divided by 1000 if the weight is in mg). This is the amount of Trypsin2 solution needed to be added to the pellet sample. (Trypsin a 10 mg/ml solution of Buffer A)
14. The pipette tip was used to add Trypsin and mixed well with the pellet.
15. The Trypsin-pellet mixture was allowed to sit on ice for 10 minutes. (*After 5 minutes, the homogenizer was used for 30 seconds to mix the solution even further and then let sit for the remaining 5 minutes)
16. While the “IFM” sample was sitting on ice in Trypsin, the supernatant was removed from the “SSM” sample and the pellet was re-suspended in Buffer A.
17. The “SSM” sample was centrifuged for 5-10 minutes at 12,000 rpm.
18. Followed by the incubation on ice, the “IFM” sample was topped with approximately 500 µl - 1 ml of Buffer B and the sample was centrifuged for 10 minutes at 800 rpm.

19. The supernatant of the “SSM” sample was trashed and the pellet was re-suspended in 30-50 µl of Buffer B. (Buffer B was used in place of Buffer E to accommodate electrical impedance measurements with Buffer B as a control)
20. The “SSM” sample was set aside ready to be used with the respirometry equipment.
21. The supernatant was then transferred from the “IFM” sample to a new, similarly labelled 1.5 ml tube. This sample should be cloudy.
22. The supernatant sample was topped with Buffer B and centrifuged for 5-10 minutes at 12,000 rpm and the pellet was then re-homogenized and steps 22-26 were repeated.
23. The supernatant was removed from the “IFM” sample, and the pellets were re-suspended in Buffer A. *At this stage, the two “IFM” samples can be combined into one tube.
24. The “IFM” sample was centrifuged for 5-10 minutes at 12,000 rpm.
25. The supernatant of the “IFM” sample was trashed, and the pellet was re-suspended in Buffer B, (Buffer B was used in place of Buffer E to accommodate electrical impedance measurements with Buffer B as a control).
26. The “IFM” sample was set aside ready to be used with the respirometry equipment.

The buffers used were:

1. Buffer A: 40.08 g of 220 mM mannitol (MW=182.17 g) + 23.96 g of 70 mM sucrose (MW=342.30 g) + 1.05 g of 5 mM Mops (MW=209.30 g) in 1 L of water.
2. Buffer B: 0.076 g of 2 mM EGTA (MW=380.4 g) + 4 ml of 5% FAF BSA for 0.2% BSA in 100 ml of Buffer A solution.
3. Buffer E: 0.019 g of 0.5 mM EGTA (MW=380.4 g) in 100 ml of Buffer A solution.

Figure 6.26: A sample of isolated mitochondria.

The mitochondria experiments were performed several times with different concentrations of mouse heart or liver mitochondria. The experiments were performed using two methods. One was using the Oroboros Oxygraph O_2k respirometer, and another using micro-centrifuge tubes. The experiments performed using the respirometer allowed measurement of impedance and oxygen consumption at the same time, while the experiments performed using micro-centrifuge tubes allowed measurement of impedance only, however with higher concentration of isolated mitochondria in suspension.

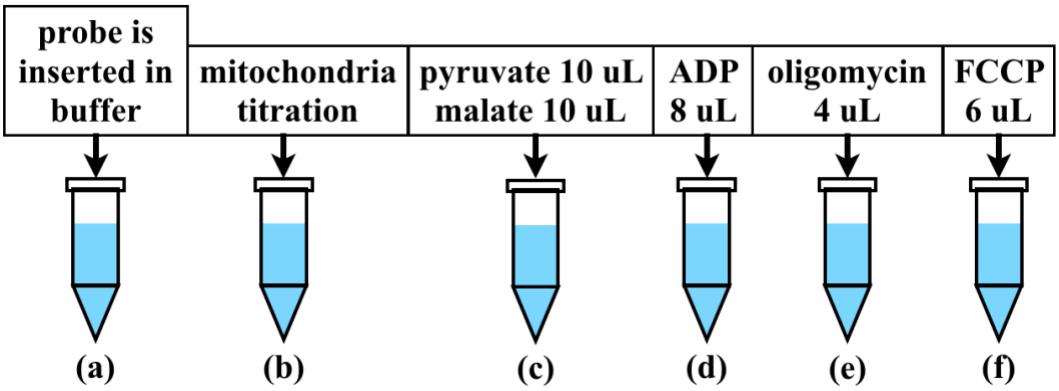

Figure 6.27: Experiment with isolated mitochondria performed in micro-centrifuge tubes: (a) the probe was inserted in a volume of respiration buffer, (b) isolated mitochondria was added, (c) pyruvate and malate, 10 µl each was added, (d) ADP 8 µl was added, (e) oligomycin 4 µl was added, and (f) FCCP 6 µl was added. After titration of mitochondria or each substrate, 150 s time was given before the next substrate was added. Impedance vs frequency data was obtained for 6 runs within this time period.

The mitochondria experiment was carried out in 1.5 ml micro-centrifuge tubes of length 40 mm and outer length 11 mm. Freshly prepared mouse liver mitochondria were obtained according to the procedure, and the concentration was determined to be 61 μg/μl by the spectrophotometer based Biuret method. The mitochondrial isolation had to be performed quickly, and the extracted isolated mitochondria has to be stored in ice, to be used within 3 to 4 hours. After isolation, biological assays were performed to determine the concentration of mitochondria, which allowed us to determine the yield. Approximately 15.25 mg of isolated mitochondria were extracted from the mouse liver.

Initially before each measurement, the respiration buffer was added to each tube. For the purpose of this set of experiments, volumes of 500 μl, 200 μl, and 100 μl were used with different quantities of isolated mitochondria added, to achieve various concentrations of isolated mitochondria in respiration buffer. The probe was then connected to the impedance analyzer, and was placed in the tube that contains the respiration buffer. Afterwards, isolated mitochondria were added to the respiration buffer. Next, various substrates were added to the mitochondrial suspension in the quantities and the order explained below. For control experiments, the volume of isolated mitochondria added were either replaced by a similar volume in the respiration buffer, or by adding no amount of isolated mitochondria.

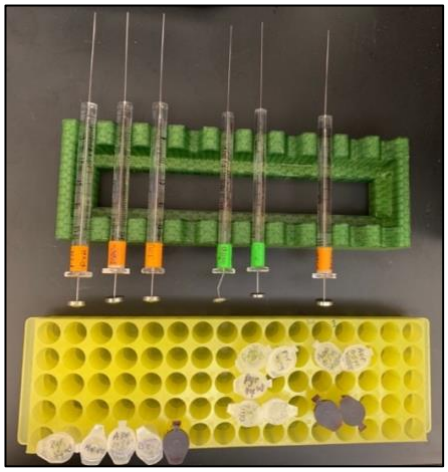

Figure 6.28: Preparations of titrations of substrates followed in the protocol. Prepared titrations of isolated mitochondria, pyruvate, malate, ADP, oligomycin, and FCCP are shown here.

According to the protocol used in the lab, pyruvate and malate were added to the mitochondrial suspension in aliquots of 10 μl each, followed by 8 μl aliquots of ADP with a concentration of 0.5 mM. Next, 4 μl aliquots of oligomycin were added, followed by 6 μl aliquots of FCCP.

The frequency range of measurement was set from 100 Hz to 1 MHz, with an applied current of 200 μA, and data was recorded 6 times within approximately 150 s after each addition of substrates, to allow time for changes in impedance to be observed. The experiment was performed at 25 ^{0}C. The probe was cleaned with deionized water, 70% ethanol, and deionized water between each consecutive measurement.

Figures 6.29 and 6.30 show the impedance magnitude and phase data recorded for suspensions with and without mitochondria. In these and subsequent figure, “mito” = “isolated mitochondria”, “pyrmal” = “pyruvate + malate,” and “oligo” = “oligomycin.” The frequency response data for both |Z| and θ are consistent with expected properties of capacitive membranes, where the measure impedance magnitude decreases with increasing frequency. The curves in each plot show frequency response data when isolated mitochondria and each substrate was added to the suspension, showing also capacitive properties due to the dielectric properties that can be observed even without isolated mitochondria present.

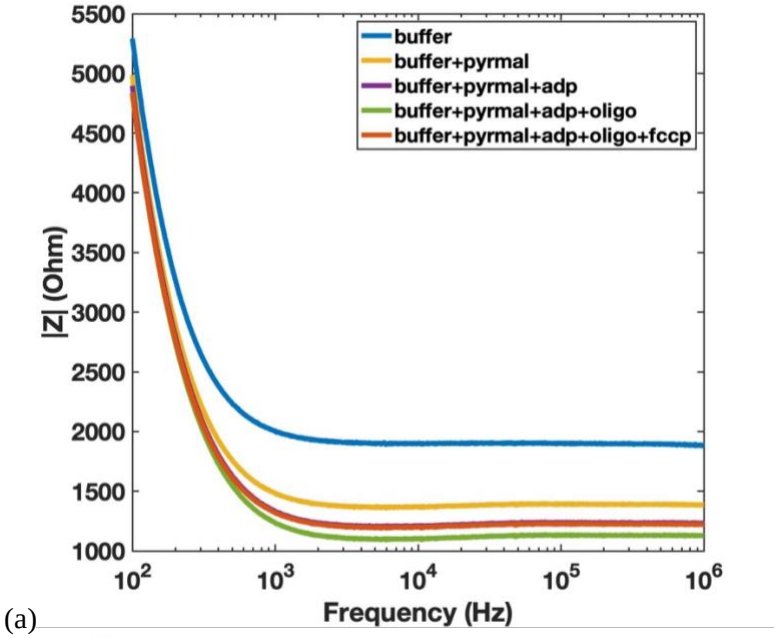

(a)

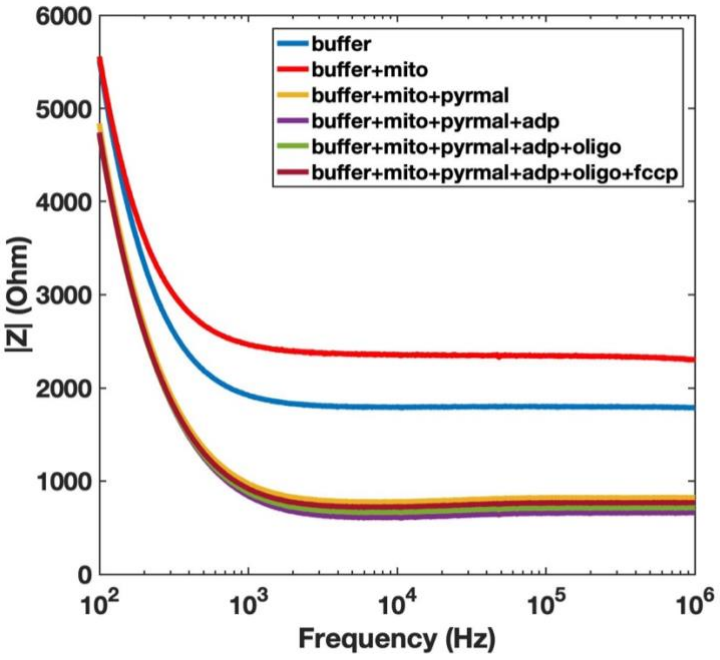

(b)

Figure 6.29: |Z| data for suspensions with and without mitochondria, when various substrates were added: (a) without mitochondria and (b) with mitochondria. In these and subsequent figure, “mito” = “isolated mitochondria”, “pyrmal” = “pyruvate + malate,” and “oligo” = “oligomycin.”

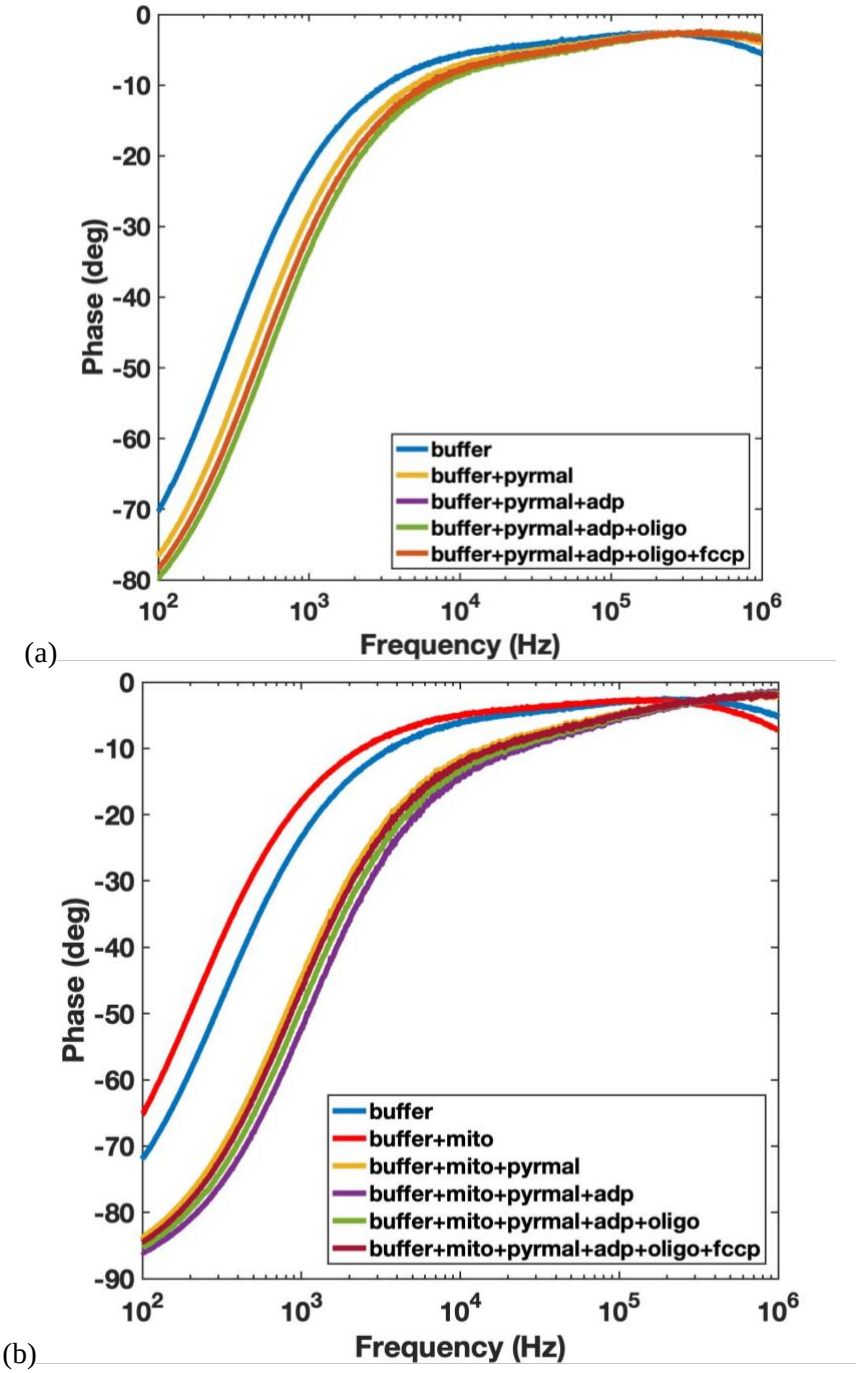

Figure 6.30: Phase data for suspensions with and without mitochondria, when various substrates were added: (a) without mitochondria and (b) with mitochondria.

As seen in Figure 6.31 below, the relative dielectric permittivity for a suspension of isolated mitochondria and yeast cells in DI water show dispersion in the observed frequency range that can be comparable with β dispersion clearly. Asami *et al.* [78] show experimental data for ε_r and σ for mitoplasts suspended in medium that show similarities to experimental data obtained for isolated mitochondria in this study. The dielectric dispersion curves of cell suspensions are sensitive to the conductivity of the suspension medium. The conductivity of the respiration buffer for isolated mitochondria is more conductive than DI water, and exhibits higher dielectric constant in the frequency region as well.

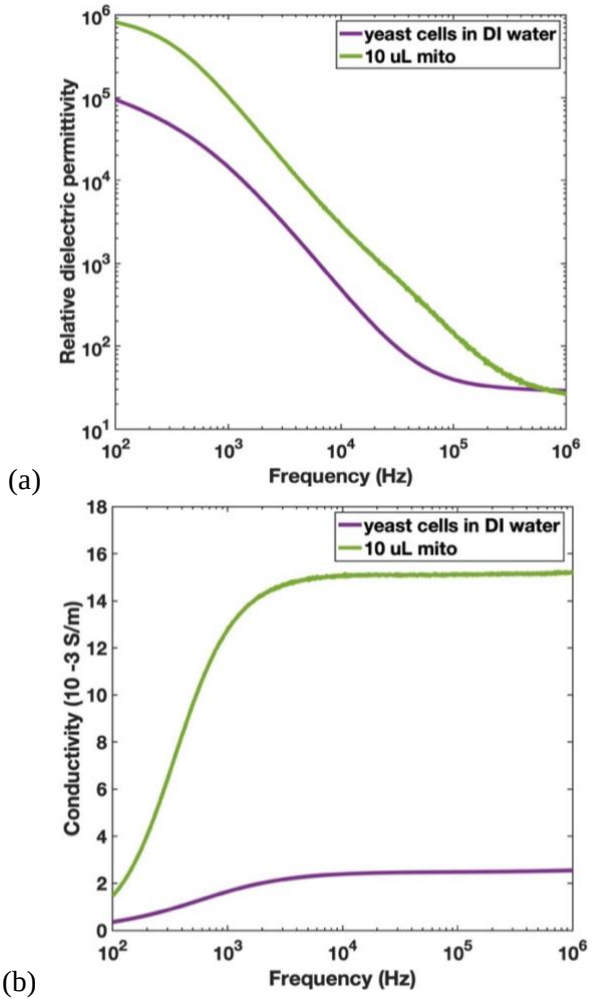

Figure 6.31: Experimental dispersion curves for comparison of suspensions of isolated mitochondria and yeast cells suspended in DI water: (a) ε_r and (b) σ.

Figure 6.32 shows ε_r values for different volume fractions of mitochondrial suspensions in respiration buffer. For higher volume fraction, the concentration of isolated mitochondria in suspension increases, and can be seen to decrease the dielectric constant.

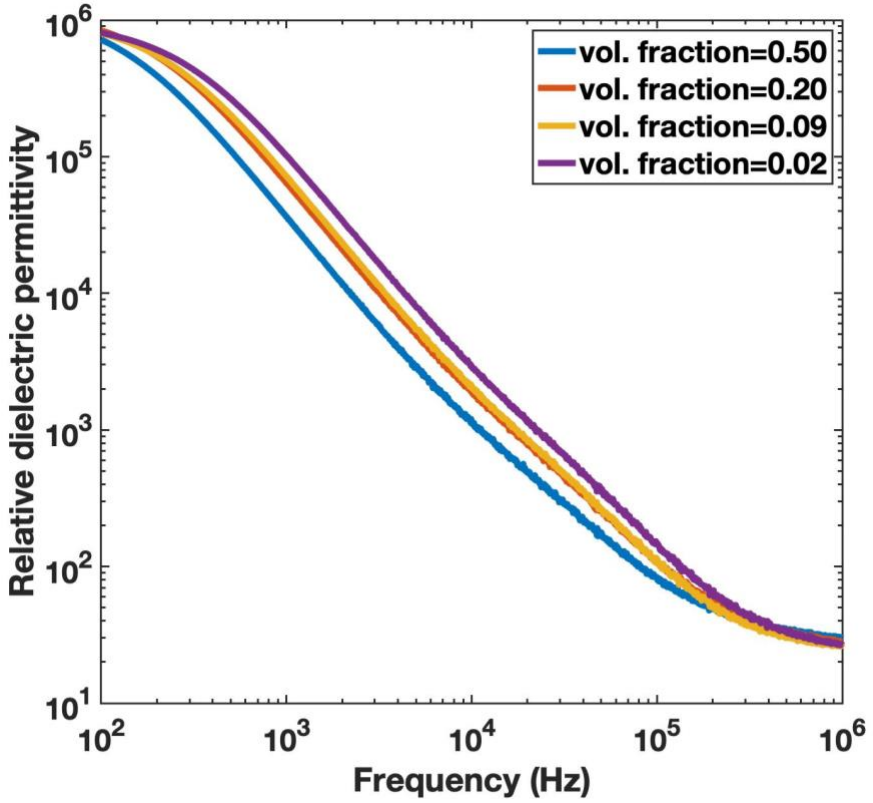

Figure 6.32: Experimental dispersion curves for various volume fractions of isolated mitochondrial suspensions.

Another mitochondria experiment was carried out in the chamber of the respirometer. Before starting the experiment, 2.2 ml of the respiration buffer was added to the chamber. The stopper was placed along with the probe, while suction pumping the additional buffer solution. This was done to ensure that no air bubbles were retained in the chamber filled with buffer solution. The probe was placed in the stopper as shown in Figure 6.33 (a), such that the substrates were added by the micro syringes as close to the electrodes as possible to maximize the effectiveness for the probe. Freshly prepared mouse heart mitochondria were obtained according to the isolation procedure and the

concentration was determined to be 43.9 μg/μl by the spectrophotometer based Biuret method. We extracted approximately 13,170 mg of isolated mitochondria from the mouse liver. The experiment was performed in the same order of adding isolated mitochondria and substrates as before.

(a)

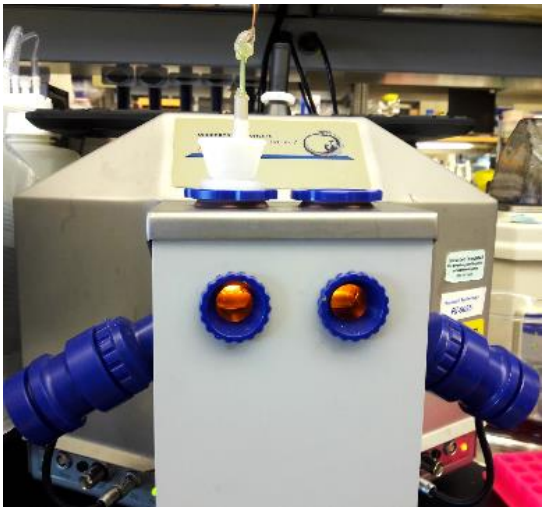

(b)

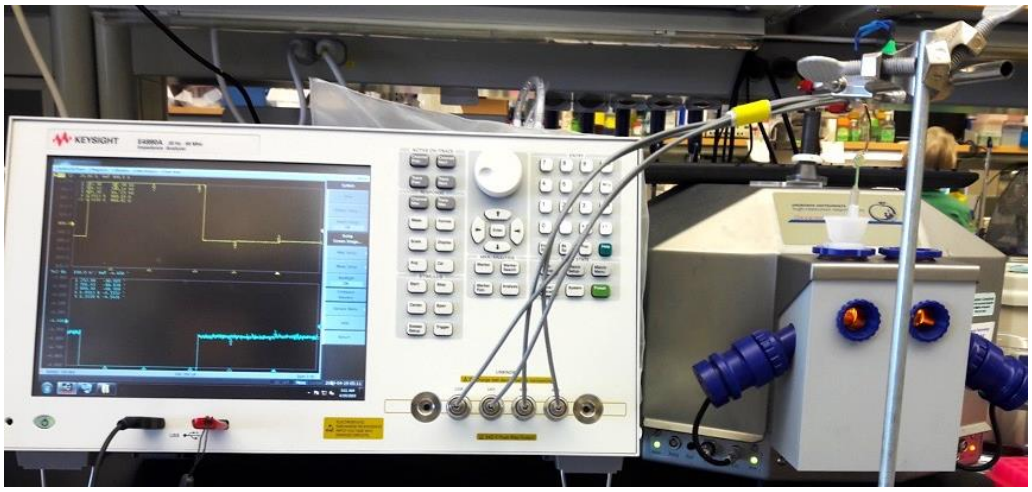

Figure 6.33: Experimental setup for measurements of impedance performed in parallel with oxygen consumption measurements using the respirometer: (a) the probe placed in the stopper was then placed inside the chamber of the respirometer, and (b) the probe was then connected to the analyzer via the self-fabricated cable.

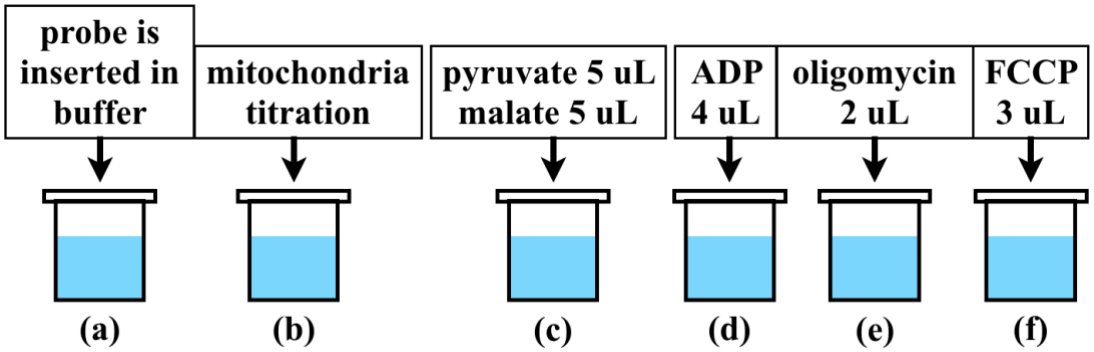

Figure 6.34: Experiment with isolated mitochondria performed in the chamber of the respirometer: (a) the probe was inserted in a volume of respiration buffer, (b) isolated mitochondria was added, (c) pyruvate and malate, 5 µl each was added, (d) ADP 4 µl was added, (e) oligomycin 2 µl was added, and (f) FCCP 3 µl was added. After titration of mitochondria or each substrate, 200 s time was given before the next substrate was added. Impedance data was recorded at a frequency of 100 kHz.

The impedance analyzer was moved next to the respirometer, the probe placed inside the stopper in the chamber with the respiration buffer, and the cable was connected to the probe (Figure 6.33 (b)). The DatLab program was started running and impedance measurements were also started. For the purpose of this set of experiments, a volume of 2.2 ml respiration buffer was used, and different quantities of isolated mitochondria were added, to achieve various concentrations of isolated mitochondria in respiration buffer. Next, various substrates were added to the mitochondrial suspension in the quantities and the order explained below. For control experiments, no isolated mitochondria was added and experiments were repeated in the same order of substrate addition.

According to the protocol used in the lab, pyruvate and malate were added to the mitochondrial suspension in aliquots of 5 µl each, followed by 4 µl aliquots of ADP with a concentration of 0.5 mM. Next, 2 µl aliquots of oligomycin were added, followed by 3 µl aliquots of FCCP.

The frequency of measurement was set to 100 kHz, with an applied current of 200 µA. The sweep time was set to 1200 s during which substrates were added in time periods of 200 s, and data was recorded after the protocol was completed. The chamber in the respirometer was maintained at a

temperature of 37 ^{0}C at all times, and the experiment was done under oxygen restrictive conditions. Between each consecutive experiment, the chamber was cleaned with 3 cycles of deionized water, let sit with one cycle of ethanol for 5 minutes, and then cleaned again with 3 cycles of deionized water.

The magnitude in impedance and phase were recorded as various substrates were added to suspensions of no mitochondria, 5 µl mitochondria, and 20 µl mitochondria. The observed impedance magnitude data is shown in Figure 6.35. The time between each addition of substrate is 200 s. The observed changes in impedance can be compared with the corresponding oxygraphs shown in Figure 6.36.

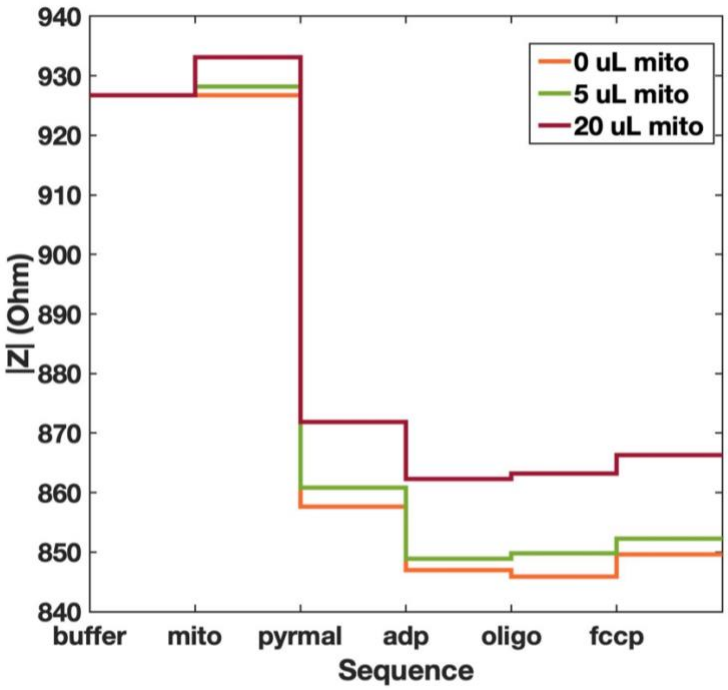

Figure 6.35: Step plot for impedance magnitude data for the mitochondrial suspension for a respiration buffer volume of 2.2 ml at a frequency of 100 kHz. Data for 0 µl, 5 µl, and 20 µl mitochondria added is shown. Here, the x axis represents each component added to the suspensions: buffer = respiration buffer, mito = isolated mitochondria, pyrmal = pyruvate and malate, adp = ADP, oligo = oligomycin, and fccp = FCCP.

The oxygraphs in Figure 6.36, show the change in oxygen flux as mitochondria, or each substrate is added to the suspension. Figure 6.36 (a) has no mitochondria in the suspension, which explains the constant oxygen concentration and zero change in the oxygen flux. Figure 6.36 (b) and (c)

shows the changes in oxygen flux for each concentration of added 5 μl and 20 μl mitochondria in the suspension. These changes in oxygen flux can be used to understand the expected change in impedance in Figure 6.35. When substrates pyruvate and malate were added to the suspension, these molecules break down to provide the required NADH to complex I to initiate the electron transport chain. Since this should initiate the process of H^+ translocation across the inner membrane to the intermembrane space, the membrane potential increases as explained in section 2.2.

As explained in section 4.2 and 5.4, the increase in the membrane potential is expected to correlate with a decrease in |Z| based on the electrical model considered for the mitochondrial suspension. Thus, the measured impedance should decrease, which can be seen when pyruvate and malate was added in Figure 6.35. The addition of substrate ADP can be seen to increase the oxygen flux exponentially, by providing the necessary ADP for the synthesis of ATP at complex V. However, ADP is expected to reduce the membrane potential, since it is required by complex V to drive ATP synthesis. The expected increase in |Z| cannot be seen in Figure 6.35. The charged and polar properties of ADP and ATP may play important roles in their observed behavior. After respiration comes to a steady state, the addition of oligomycin is seen to decrease the oxygen flux significantly, which is consistent with its property as a mitochondrial inhibitor and decreasing the oxygen consumption rate. However, the increase in membrane potential in the presence of oligomycin should decrease the |Z|, which is also not consistently seen in Figure 6.35 in the impedance data. The final addition of uncoupler FCCP is shown to increase the oxygen flux as the mitochondrial membrane is uncoupled and maximal respiration rate is ensured. The uncoupling of the inner membrane causes the membrane potential to decrease significantly, expecting the |Z| to increase. This change can be seen in Figure 6.35, however, not a significant increase due to the very low concentrations of substrates in the mitochondrial suspension with a respiration buffer volume of 2.2 ml.

(a)

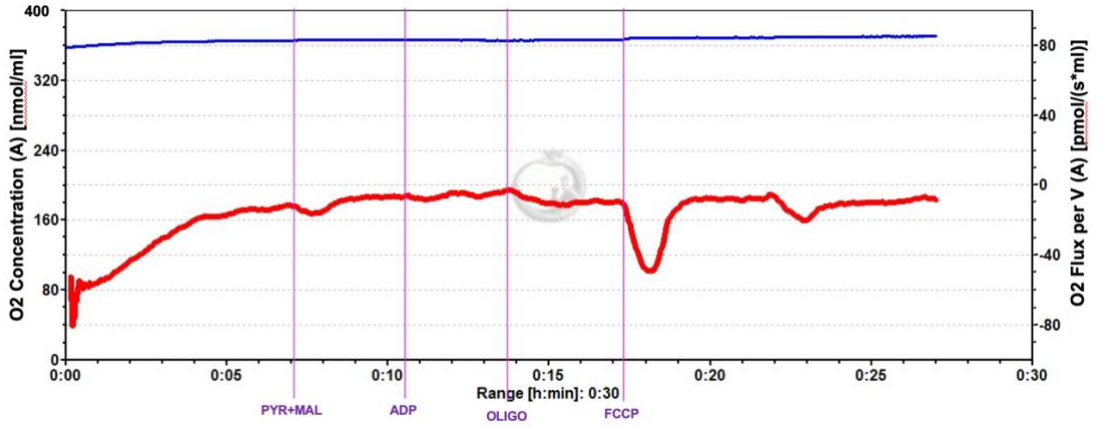

(b)

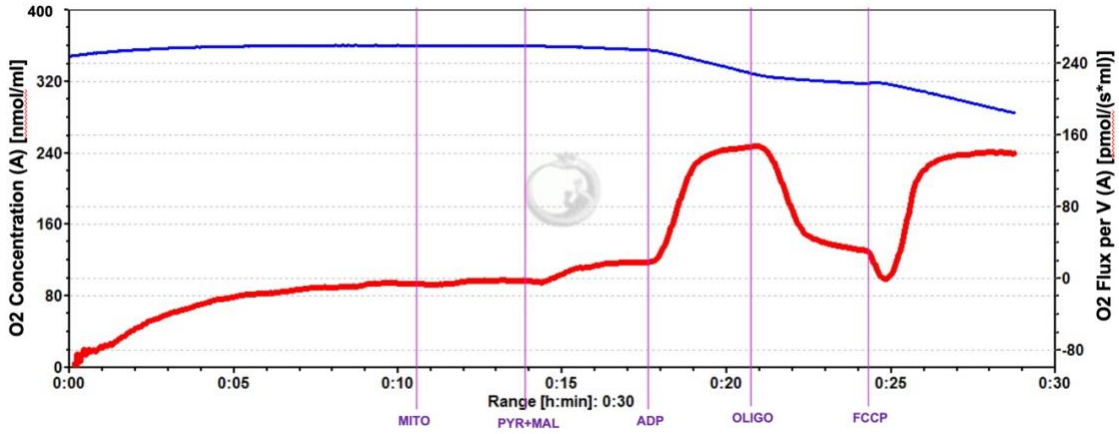

(c)

Figure 6.36: The oxygraphs correlating with impedance data: (a) no isolated mitochondria, (b) 5 µl isolated mitochondria, and (c) 20 µl isolated mitochondria. The oxygen flux per volume (red line), and the oxygen concentration in the chamber (blue line) is shown.

Chapter 7: Experimental Data Analysis

7.1 Relative Dielectric Permittivity Analysis

According to our hypothesis, a change in the mitochondrial membrane potential is directly proportional to the change in the effective relative dielectric constant for the biological medium being measured. The measured impedance data for different concentrations in mitochondria with various substrates were analyzed by calculating the dielectric permittivity and conductivity values. We chose a frequency of 100 kHz to study the changes in effective dielectric permittivity and conductivity being measured.

As discussed in chapter 3, cell respiratory control is the most convenient measure of mitochondrial function. In manipulating mitochondrial function by adding substrates to the suspension medium of isolated mitochondria, respiratory control and coupling of mitochondrial membrane potential to the electron transport chain, can be studied extensively in a single experiment. Electron donor substrates of pyruvate and malate, substrate ADP, mitochondrial inhibitor oligomycin, and mitochondrial uncoupler FCCP were used as substrates that change mitochondrial function and to correlate with changes in impedance spectroscopy. Sequential addition of such substrates that trigger different protein complexes to be activated or inhibited can be determined by observing respiration rates. The direction of the membrane potential change indicates whether the change in respiration causes an upstream of $\Delta\psi_m$ or a downstream of $\Delta\psi_m$.

Substrates pyruvate and malate initiate state 2 respiration in isolated mitochondria and increase the oxygen consumption rate, giving way for the electron transport to be activated and proton concentration gradient and membrane potential to accumulate. This increase in the $\Delta\psi_m$ essentially

means the effective dielectric constant should increase, assuming the change in dielectric constant is not dependent on any other component or reaction taking place within the mitochondrial suspension.

The addition of substrate ADP will allow the ATP synthase to function and generate ATP as state 3 respiration, while the $\Delta\psi_m$ drops and electron transport accelerates. According to our hypothesis, the drop in $\Delta\psi_m$ should cause a drop in the effective dielectric constant, while also increasing the oxygen consumption rate due to the accelerated electron transport. However, the expected drop (from reduced $\Delta\psi_m$) is likely compared by an increase due to the fact that ADP and ATP are charged polar molecules.

State 3 respiration is then terminated by the addition of the ATP synthase inhibitor oligomycin, achieving a 'state 4o' respiration rate where the ATP synthase is inhibited, bringing the ATP generation to a halt. The ATP synthase inhibition causes a hyperpolarization of the $\Delta\psi_m$, causing a failure of glycolysis due to the reaction that requires ATP, and progressively decreases the oxygen consumption rate. However, based on our hypothesis, the effective dielectric constant should increase due to the hyperpolarization of the membrane potential.

Titration of a protonophore FCCP brings the respiration rate to state 4, the maximum respiration rate where protons leak across the mitochondrial membrane, causing depolarization and uncoupling of the membrane potential. This decrease in the membrane potential should be consistent with a decrease in the effective dielectric constant.

The experimental data obtained in this study showed correlation in $\Delta\psi_m$ with obtained ε_r values for substrate addition of pyruvate and malate, and FCCP. However, the correlations were not observed for substrates ADP and oligomycin. This will be explored further in this chapter.

Figure 7.1 shows changes in dielectric constant values for the experiment performed in micro-centrifuge tubes with various aliquots of isolated mitochondria added to a volume of 100 µl respiration buffer and various substrates added afterwards (Figure 6.27). Here, experimental results of three concentrations of mitochondria are shown for no mitochondria, 10 µl mitochondria, and 100 µl

mitochondria added to 100 µl of respiration buffer. The changes in dielectric constant between the suspensions with no mitochondria and 10 µl mitochondria showed an elevation between the observed changes. The expected increase in ε_r when pyruvate and malate was added was consistent with an increase in $\Delta\psi_m$. However, the expected decrease in $\Delta\psi_m$ when ADP was added, was not observed since the ε_r was increased by the addition of ADP. The titration of oligomycin with no mitochondria showed a decrease in ε_r, yet showed a smaller decrease when 10 µl mitochondria is present in the suspension. This observation may allow us to assume that oligomycin exhibits an increase in ε_r when mitochondria is present in the suspension, which correlates with our hypothesis that $\Delta\psi_m$ increases with an addition of oligomycin. However, this cannot be confirmed, since it shows a drop in ε_r from its value in the presence of ADP, when the expected change is an increase in ε_r. Finally, FCCP showed a significant drop in ε_r in the suspension with 10 µl mitochondria in comparison to the suspension with no mitochondria. Since FCCP is expected to decrease $\Delta\psi_m$ as it depolarizes the membrane, this result correlates with our hypothesis. However, addition of 100 µl mitochondria to 100 µl of respiration buffer (nearly 50% volume concentration) revealed that a high number of mitochondria does not necessarily mean that the expected change in ε_r is elevated. This increase in concentration can negatively affect the changes expected in $\Delta\psi_m$, by also increasing the polarizing effect due to added mitochondria itself, as seen by the decrease in ε_r when only 100 µl mitochondria is added to the respiration buffer. These ε_r changes when each substrate was added to the suspension are shown quantitatively in Table 7.1.

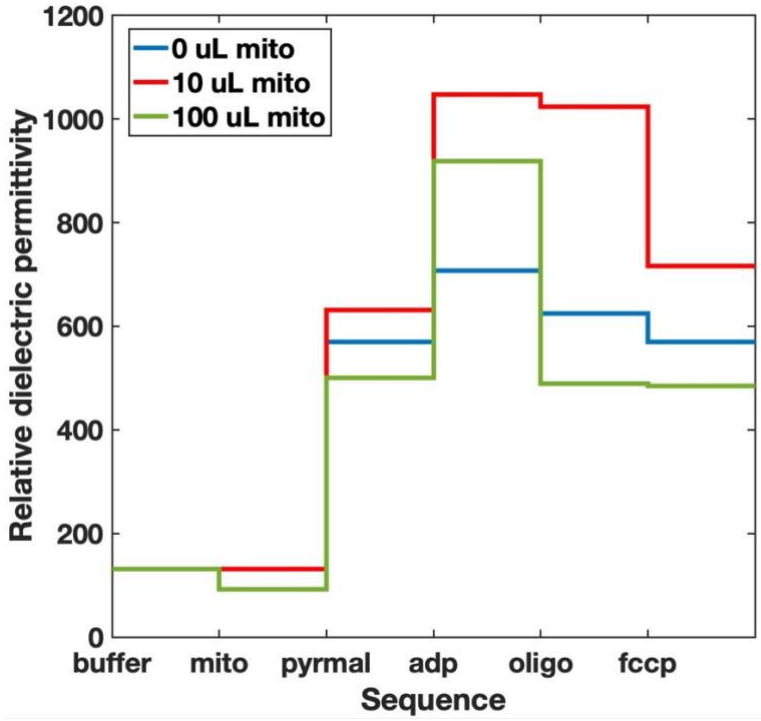

Figure 7.1: Changes in dielectric constant due to addition of different aliquots of isolated mitochondria and various substrates to a respiration buffer volume of 100 µl at 100 kHz frequency. The data show dielectric constants for experiments with 0 µl mitochondria, 10 µl mitochondria, and 100 µl mitochondria added to the buffer medium. Here, the x axis represents each component added to the suspension: buffer = respiration buffer, mito = isolated mitochondria, pyrmal = pyruvate (10 µl) and malate (10 µl), adp = ADP (8 µl), oligo = oligomycin (4 µl), and fccp = FCCP (6 µl).

Table 7.1: Relative dielectric permittivity changes when mitochondria/substrates were added to the respiration buffer volume of 100 µl at 100 kHz frequency
Here, the substrate step represents each component added to the suspensions: buffer = respiration buffer, mito = isolated mitochondria, pyrmal = pyruvate (10 µl) and malate (10 µl), adp = ADP (8 µl), oligo = oligomycin (4 µl), and fccp = FCCP (6 µl).

Substrate step	Relative dielectric permittivity (ε_r) change when mitochondria/substrates are added		
	0 µl mito	10 µl mito	100 µl mito
mito	0.0	- 0.1	- 38.8
pyrmal	+ 439.0	+ 500.2	+ 408.6
adp	+ 137.2	+ 415.9	+ 417.5
oligo	- 83.1	- 23	- 429.5
fccp	- 54.0	- 307.5	- 3.7

Figure 7.2 and 7.3 shows changes in dielectric constant values for two experiments performed with 10 µl isolated mitochondria and 10 µl equivalent volume of buffer (to replace mitochondria volume) added to a volume of 100 µl respiration buffer (Figure 7.2), and 100 µl isolated mitochondria and 100 µl equivalent volume of buffer added to a volume of 100 µl respiration buffer (Figure 7.3). The experiments repeated with an equivalent volume of respiration buffer to replace the volume of mitochondria ensures that the concentrations of the substrates added afterwards were constant between each experiment, proving that the changes in ε_r were not dependent on volume changes in the suspension. The analysis is similar and distinguished in comparison to ε_r changes observed for Figure 7.1. Table 7.2 shows the changes between each equivalent volume of mitochondria or buffer.

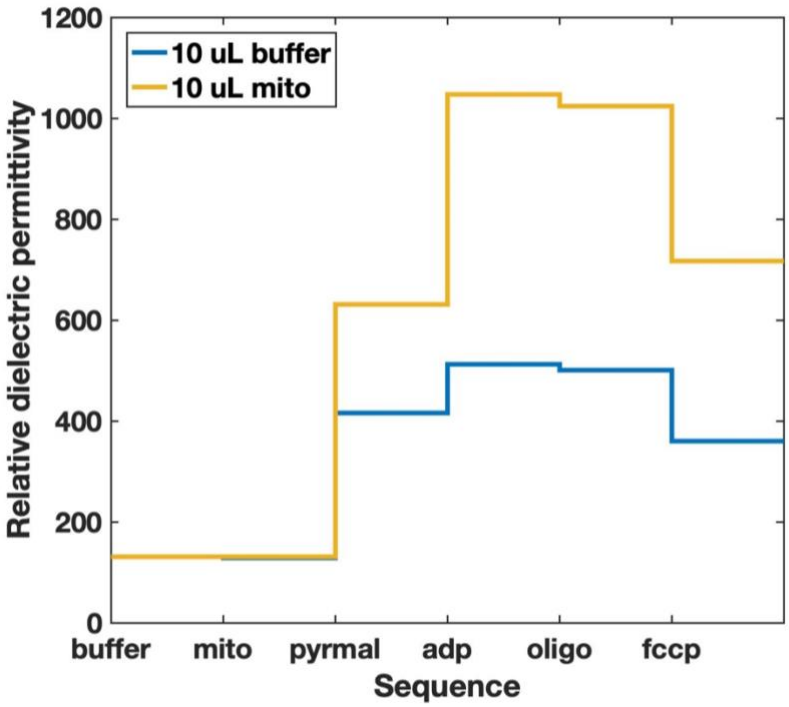

Figure 7.2: Changes in dielectric constant due to addition of 10 µl mitochondria and 10 µl equivalent volume of respiration buffer, with various substrates, to a respiration buffer volume of 100 µl at a frequency of 100 kHz. Here, the x axis represents each component added to the suspensions: buffer = respiration buffer, mito = isolated mitochondria, pyrmal = pyruvate (10 µl) and malate (10 µl), adp = ADP (8 µl), oligo = oligomycin (4 µl), and fccp = FCCP (6 µl).

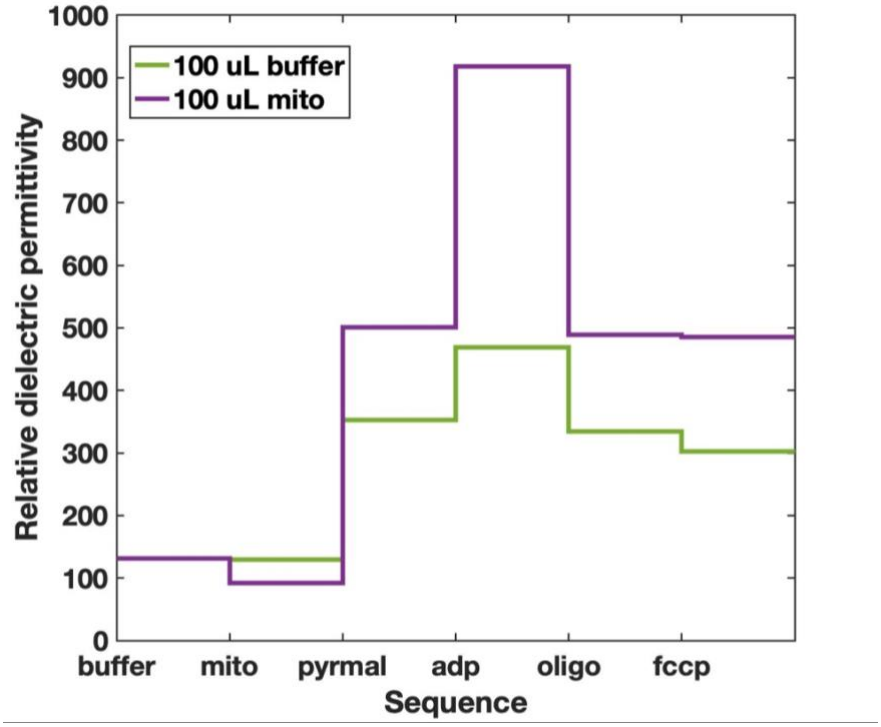

Figure 7.3: Changes in dielectric constant due to addition of 100 µl mitochondria and 100 µl equivalent volume of respiration buffer, with various substrates, to a respiration buffer volume of 100 µl at a frequency of 100 kHz. Here, the x axis represents each component added to the suspensions: buffer = respiration buffer, mito = isolated mitochondria, pyrmal = pyruvate (10 µl) and malate (10 µl), adp = ADP (8 µl), oligo = oligomycin (4 µl), and fccp = FCCP (6 µl).

Table 7.2: Relative dielectric permittivity changes when mitochondria and buffer were added in equivalent volumes to 100 µl respiration buffer at 100 kHz frequency
Here, the substrate step represents each component added to the suspensions: buffer = respiration buffer, mito = isolated mitochondria, pyrmal = pyruvate (10 µl) and malate (10 µl), adp = ADP (8 µl), oligo = oligomycin (4 µl), and fccp = FCCP (6 µl).

Substrate step	Relative dielectric permittivity (ε_r) change when equivalent volume of buffer is added			
	10 µl buffer	10 µl mitochondria	100 µl buffer	100 µl mitochondria
mito/buffer	- 2.3	- 0.1	- 1.9	- 38.8
pyrmal	+ 287.5	+ 500.2	+ 223.9	+ 408.6
adp	+ 95.8	+ 415.9	+ 115.5	+ 417.5
oligo	- 11.8	- 23.0	- 133.8	- 429.5
fccp	- 140.0	- 307.5	- 32.1	- 3.7

As the concentration of isolated mitochondria in the suspension decreases, the change in ε_r becomes less significant. Figure 7.4 shows the changes in dielectric constant for experiments performed for a respiration buffer volume of 500 µl. Since the concentrations of mitochondria and substrates added are much lower in comparison to the previous experiments discussed, changes in ε_r cannot be significantly observed. However, the small changes in ε_r can be comparable with the changes observed for higher concentrations of mitochondria in suspension, and in the presence of various substrates. Table 7.3 gives a quantitative analysis of the changes between each step when mitochondria or substrates were added.

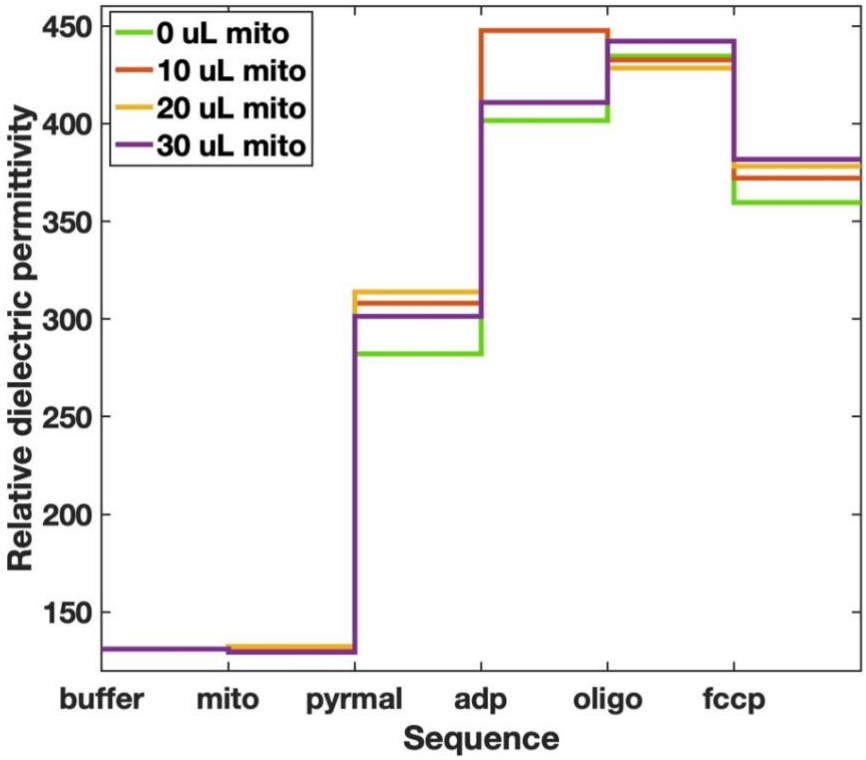

Figure 7.4: Changes in dielectric constant due to addition of mitochondria and various substrates to 500 µl respiration buffer at 100 kHz frequency. The data show dielectric constants for 0 µl mitochondria added, 10 µl mitochondria, 20 µl mitochondria, and 30 µl mitochondria added to the buffer medium. Here, the x axis represents each component added to the suspensions: buffer = respiration buffer, mito = isolated mitochondria, pyrmal = pyruvate (10 µl) and malate (10 µl), adp = ADP (8 µl), oligo = oligomycin (4 µl), and fccp = FCCP (6 µl).

Table 7.3: Relative dielectric permittivity changes when mitochondria/substrates were added to the respiration buffer volume of 500 µl at 100 kHz frequency
Here, the substrate step represents each component added to the suspensions: buffer = respiration buffer, mito = isolated mitochondria, pyrmal = pyruvate (10 µl) and malate (10 µl), adp = ADP (8 µl), oligo = oligomycin (4 µl), and fccp = FCCP (6 µl).

Substrate step	Relative dielectric permittivity (ε_r) change when mitochondria/substrates are added			
	No mitochondria added	10 µl mitochondria	20 µl mitochondria	30 µl mitochondria
mito/buffer	0.0	- 1.0	+ 1.4	- 1.4
pyrmal	+ 151.2	+ 178.2	+ 181.3	+ 171.9
adp	+ 119.4	+ 139.5	+ 97.3	+ 109.3
oligo	+ 33.0	- 15.2	+ 17.3	+ 31.4
fccp	- 75.0	- 60.3	- 50.1	- 60.4

7.2 Effects of Substrates on Mitochondrial Membrane Potential

The substrates used during the protocol for measuring oxygen consumption of isolated mitochondrial suspensions, are components that cause changes in the electron transport within the inner mitochondrial membrane, and change the mechanism of ATP synthesis. Methods of probing these changes in the electron transport chain have been established by studies of oxygen consumption of mitochondrial suspensions. By extensive analysis of impedance changes in correlation with expected membrane potential changes, this method of dielectric spectroscopic analysis may be useful in studies of these complex biological systems. Figure 7.5 compares the changes in ε_r with those of $\Delta\psi_m$ for a detailed explanation of the correlation between these variables.

The respiration rate when substrates pyruvate and malate are added to the suspension, increases as the electron transport chain is activated by the supply of NADH molecules that provide the required high-energy electrons to complex I. This initiates the transfer of high-energy electrons across the inner mitochondrial membrane, with an accumulation of protons in the intermembrane space, and thereby giving rise to a membrane potential. From our hypothesis, the observed change in ε_r when pyruvate and malate are added to the mitochondrial suspension, seemingly correlates with the expected increase in $\Delta\psi_m$.

According to the protocol used in bioenergetics, substrate ADP is titrated in the next step to initiate ATP synthesis. The ATP synthase enzyme, also known as complex V, uses the already established proton concentration gradient and membrane potential across the inner mitochondrial membrane, to drive the synthesis of ATP across its molecular motors. The generation of ATP via ADP and inorganic phosphate (P_i) essentially consumes the membrane potential and decreases it across the inner mitochondrial membrane. However, the mechanism of electron transport and proton pumping also continues to maintain the drop in the membrane potential. This increased rate in electron transport

is apparent from the increase in oxygen flux observed when ADP is added to the suspension. Based on our hypothesis, the drop in the membrane potential should decrease the relative dielectric permittivity observed in the suspension. Figure 7.5 (a) exhibits a significant increase in ε_r when ADP is added. It is plausible that any reduction in ε_r due to reduced $\Delta\psi_m$ is more than compensated by an increase in ε_r caused by ADP's charge and polar characteristics.

A mitochondrial inhibitor, oligomycin is included in the respiration study protocol as a direct measure of the proton leak that takes place in the inner mitochondrial membrane. Oligomycin inhibits the ATP synthase enzyme, by blocking the F_0 subunit proton channel. This causes ATP synthesis to cease, resulting in a slight hyperpolarization of the inner membrane. Figure 7.5 (b) shows how the oxygen flux rate drops increasingly when oligomycin is added, since electron transport rate decelerates. The slight hyperpolarization expected to be caused by oligomycin depends on substrate oxidation upstream of the electron transport chain, and should increase the relative dielectric permittivity according to our hypothesis. However, the drop in ε_r shown in Figure 7.5 (a) can explain a correlating decrease in $\Delta\psi_m$, consistent with reduced glycolytic capacity to allow electron transport to be maintained.

The addition of a protonophore, FCCP ultimately uncouples the mitochondrial membrane. FCCP works by forming a leak of protons across the lipid membrane of the mitochondrial membrane. This causes the membrane to depolarize, bringing the membrane potential down at an increasing rate, and eventually uncoupling the inner mitochondrial membrane. Although FCCP depolarizes the membrane, the oxygen flux is seen to increase as this induces a maximal respiration rate. Consistent with our hypothesis, the expected significant decrease in $\Delta\psi_m$ with FCCP can be correlated with the ε_r decrease seen in Figure 7.5 (a).

(a)

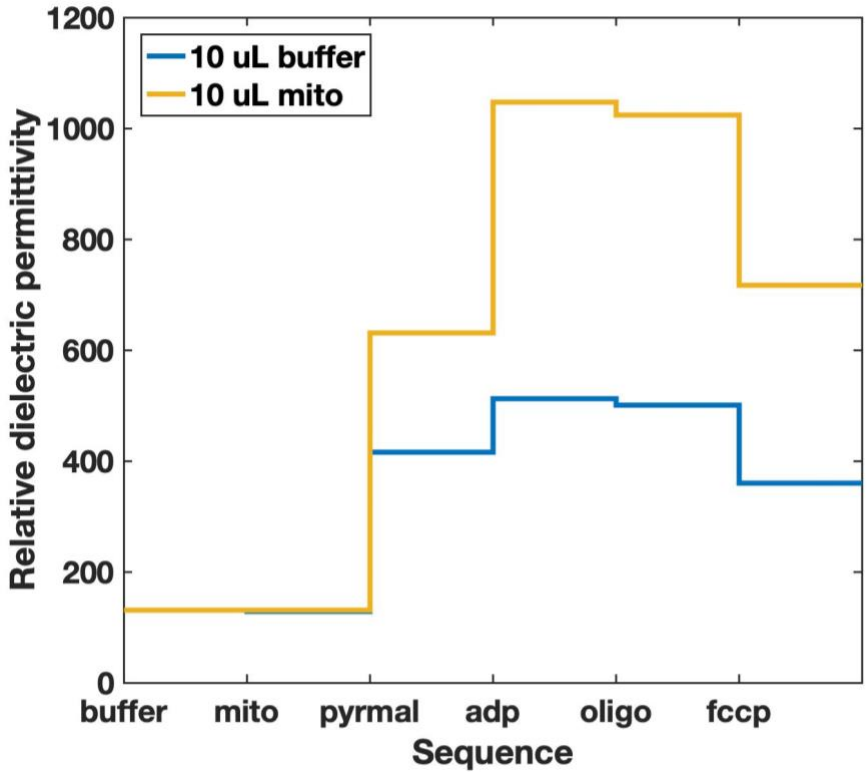

(b)

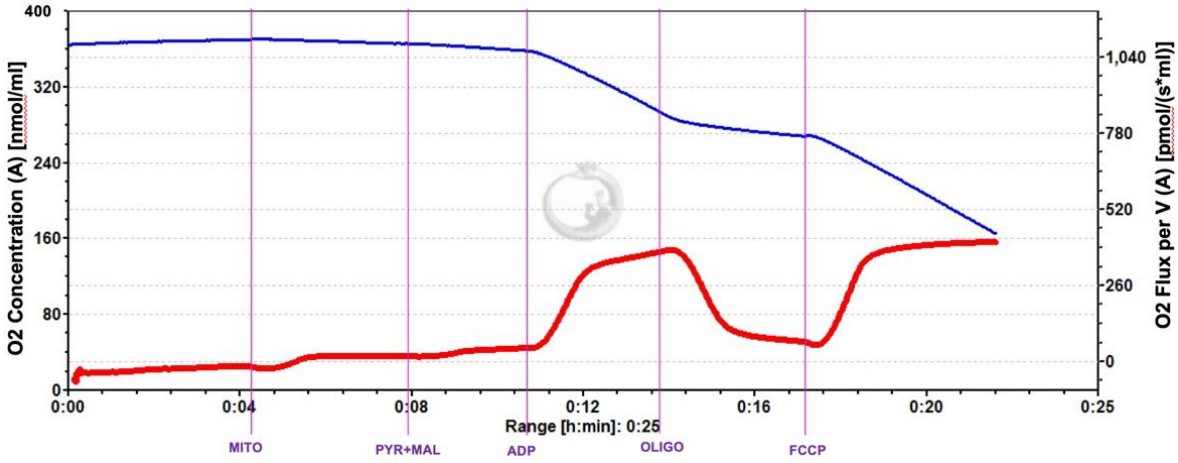

Figure 7.5: Correlation between dielectric constant change and oxygen consumption rate: (a) relative dielectric constant change for 10 µl buffer or 10 µl mitochondria in 100 µl buffer, where the x axis represents each component added to the suspensions: buffer = respiration buffer, mito = isolated mitochondria, pyrmal = pyruvate and malate, adp = ADP, oligo = oligomycin, and fccp = FCCP, and (b) oxygraph for 20 µl mitochondria in 500 µl buffer.

7.3 Admittance Based Analysis

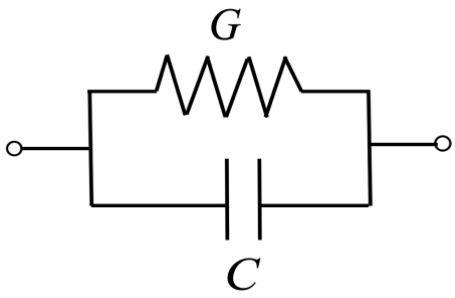

Figure 7.6: Parallel configuration of conductance and capacitance for a mitochondrial suspension.

The mitochondrial suspension that consists of a conductance in parallel with a capacitance provides a simple model of complex admittance (Figure 7.6). The admittance is the inverse of impedance and provides a convenient method of calculating parallel components of a mitochondrial suspension. The admittance of the above circuit is given by,

$$Y = G + j\omega C, \tag{7.1}$$

where, G is the conductance and C is the capacitance. The admittance is also given by,

$$Y = {}^{1}/_{\alpha}\,(\sigma + j\omega\varepsilon), \tag{7.2}$$

where, α=28.55 1/m, σ is the conductivity and ε is the dielectric permittivity of the suspension. From the real and imaginary parts of admittance, the dispersion parameters can be calculated.

$$Re(Y) = \frac{\sigma}{\alpha}, \tag{7.3}$$

$$Im(Y) = \frac{\omega\varepsilon}{\alpha}. \tag{7.4}$$

Therefore, the conductivity and relative dielectric permittivity can be extracted as,

$$\sigma = \alpha\, Re(Y), \tag{7.5}$$

$$\varepsilon_r = \frac{\alpha\, Im(Y)}{\omega\, \varepsilon_0}. \tag{7.6}$$

For a series of substrates added to a mitochondrial suspension, the equivalent circuit can be taken as a parallel combination of the admittance of each component added. Figure 7.7 shows an example of a combination of admittances for the respiration buffer (Y_b), mitochondria (Y_m), and pyruvate and malate (Y_{pm}). The combined admittance for the parallel circuit is given by,

$$Y_{suspension} = Y_b + Y_m + Y_{pm}. \tag{7.7}$$

By calculating $Y_{suspension}$ with different combinations of each component, the individual admittances for mitochondria and pyruvate and malate can be calculated.

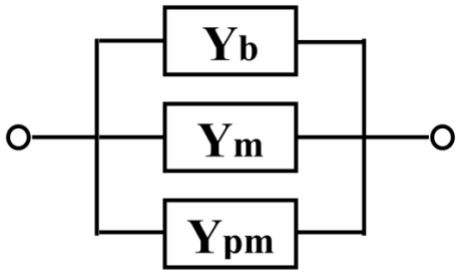

Figure 7.7: Parallel configuration of admittances for a mitochondrial suspension with added substrates pyruvate and malate.

The data plots below were obtained for two sets of experimental data with different mitochondrial volume fractions. The experimental data set with a respiration buffer volume of 100 μl with 10 μl mitochondria added has a mitochondrial volume fraction of 0.09, and the experimental data set with a respiration buffer volume of 200 μl with 100 μl mitochondrial added has a mitochondrial volume fraction of 0.33 were used to obtain admittance data calculations shown below.

In the data plots below, “mito-effective” shows the admittance effect of mitochondria only, without the effect of the respiration buffer, “pyrmal-buffer” represents effective admittance of

pyruvate and malate without the effect of the respiration buffer, and “pyrmal-effective” represents effective influence of pyruvate and malate on mitochondrial function. Here,

$$Y\,[\text{mito-effective}] = Y\,[\text{buffer+mito}] - Y\,[\text{buffer}] \tag{7.8}$$

$$Y\,[\text{pyrmal-buffer}] = Y\,[\text{buffer+pyrmal}] - Y\,[\text{buffer}] \tag{7.9}$$

$$Y\,[\text{pyrmal-effective}] = Y\,[\text{buffer+mito+pyrmal}] - Y\,[\text{buffer+mito}] - Y[\text{pyrmal-buffer}] \tag{7.10}$$

Figures 7.8 and 7.9 show data obtained for real parts of admittance for the addition of substrates pyruvate and malate (pyrmal) to the mitochondrial suspension for volume fraction 0.09 and 0.33, respectively. Figures 7.10 and 7.11 show data obtained for imaginary parts of admittance for the addition of substrates pyruvate and malate (pyrmal) to the mitochondrial suspension for volume fraction 0.09 and 0.33, respectively. The distinction between the curves for effective mitochondria, and effective pyrmal show that substrates pyruvate and malate have an interaction with mitochondria that does not depend on the dielectric properties of the substrates themselves.

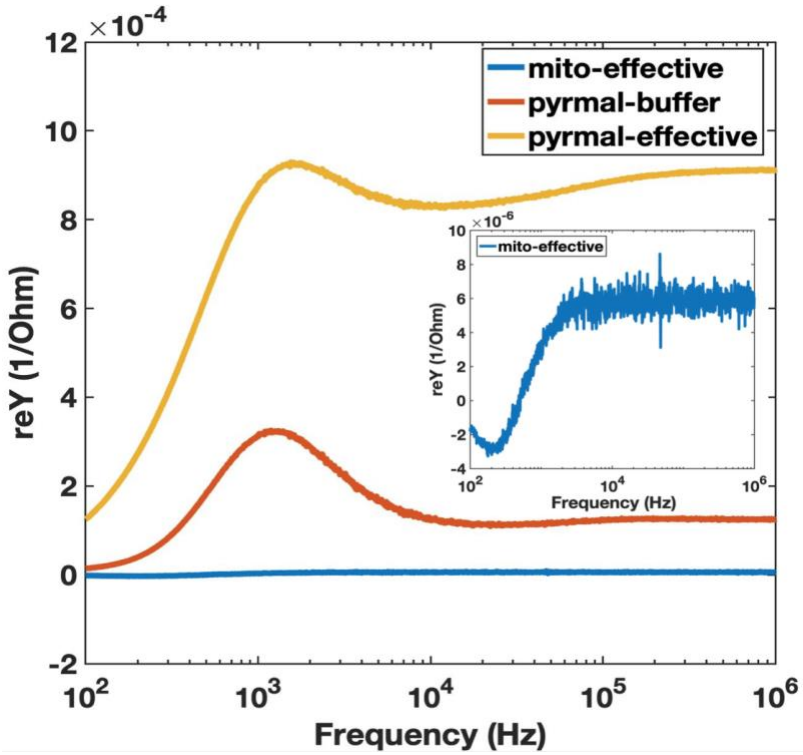

Figure 7.8: Real part of effective admittance for mitochondria, and pyruvate and malate for mitochondrial volume fraction of 0.09.

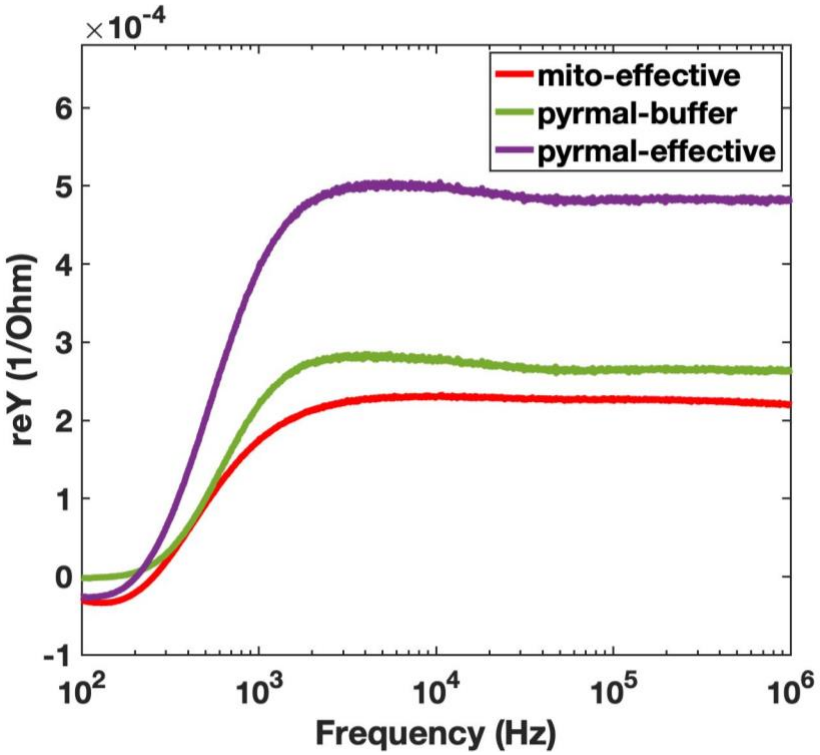

Figure 7.9: Real part of effective admittance for mitochondria, and pyruvate and malate for mitochondrial volume fraction of 0.33.

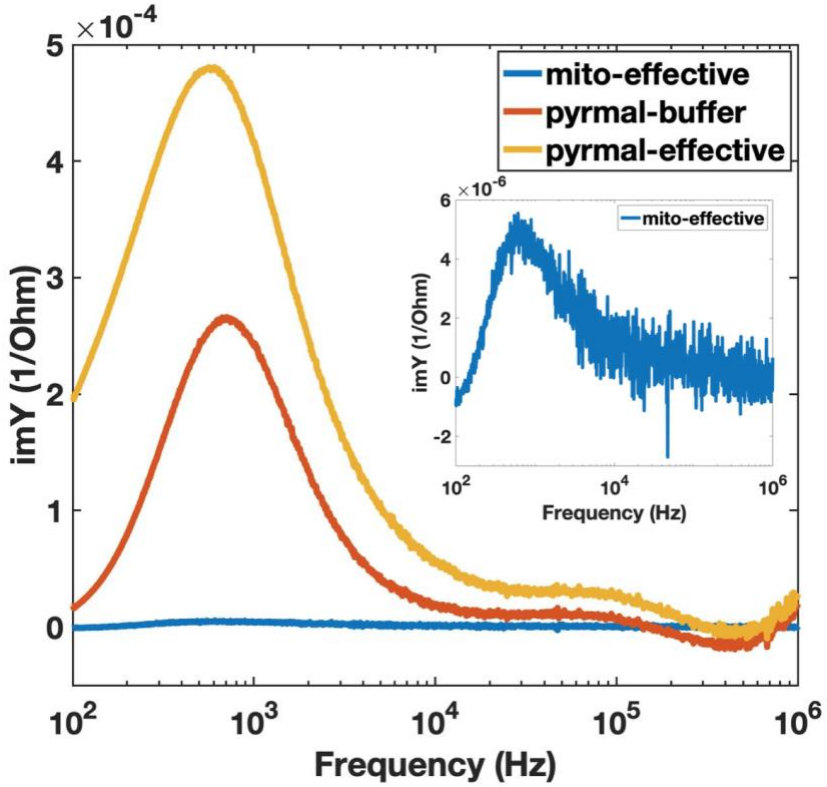

Figure 7.10: Imaginary part of effective admittance for mitochondria, and pyruvate and malate for mitochondrial volume fraction of 0.09.

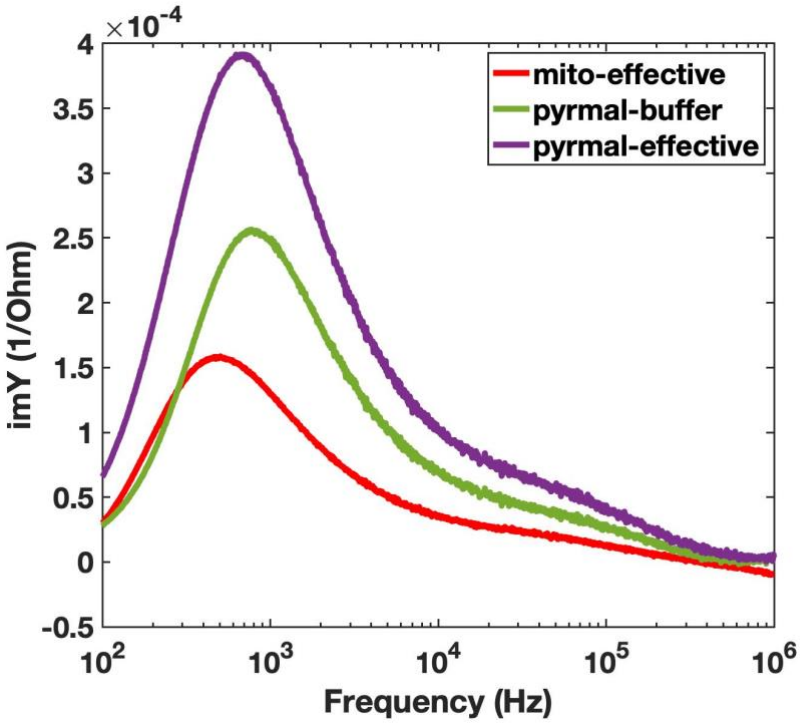

Figure 7.11: Imaginary part of effective admittance for mitochondria, and pyruvate and malate for mitochondrial volume fraction of 0.33.

The responses of relative dielectric permittivity and conductivity for the effective components given by equations (7.8), (7.9), and (7.10), were calculated for the two sets of experimental data, and are displayed below.

Figures 7.12 and 7.13 show data obtained for relative dielectric permittivity for the addition of substrates pyruvate and malate (pyrmal) to the mitochondrial suspension for volume fraction 0.09 and 0.33, respectively. Figures 7.14 and 7.15 show data obtained for conductivity for the addition of substrates pyruvate and malate (pyrmal) to the mitochondrial suspension for volume fraction 0.09 and 0.33, respectively.

The relative dielectric permittivity response for effective pyruvate and malate (pyrmal) shows that ε_r clearly increases in comparison to the effective response of mitochondria. The increase shows that the effective pyrmal component is evidently showing the response for the interaction between mitochondria, and pyruvate and malate, without the effect of the substrates themselves or mitochondria itself affecting. This can be assumed as a clear indication of the membrane potential change caused by mitochondria in the presence of pyruvate and malate.

The conductivity responses seen in Figures 7.14 and 7.15, between the effective component of mitochondria and the effective pyruvate and malate (pyrmal) response also show the clear distinction, and a proportionality at higher frequencies between the two components. The linear response of conductivity at frequencies above 10 kHz for these effective parameters prove that these data show reliable response of mitochondria in the presence of pyruvate and malate substrates.

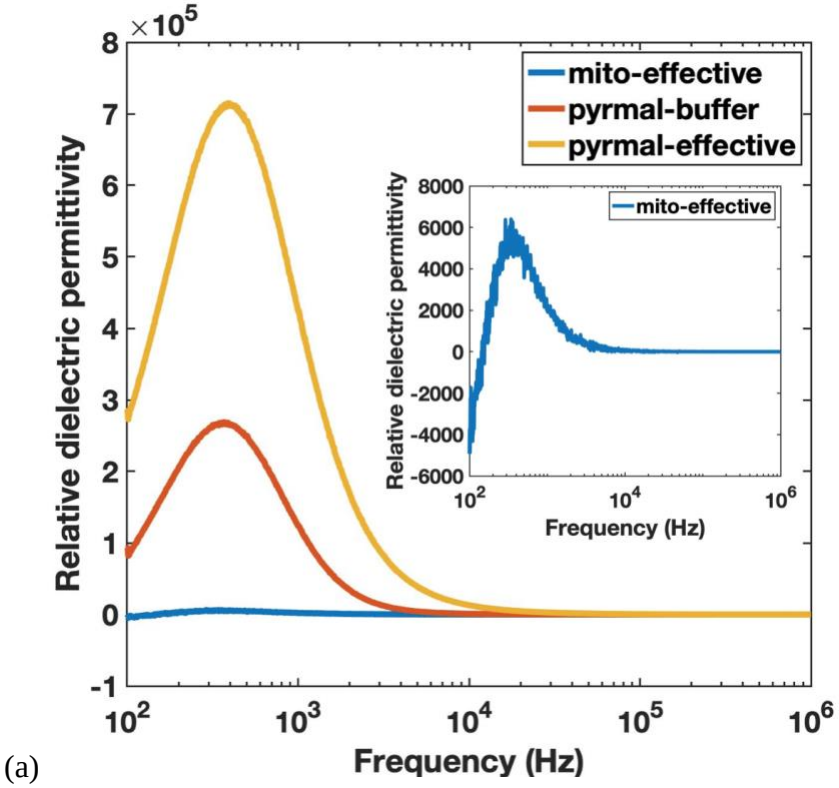

(a)

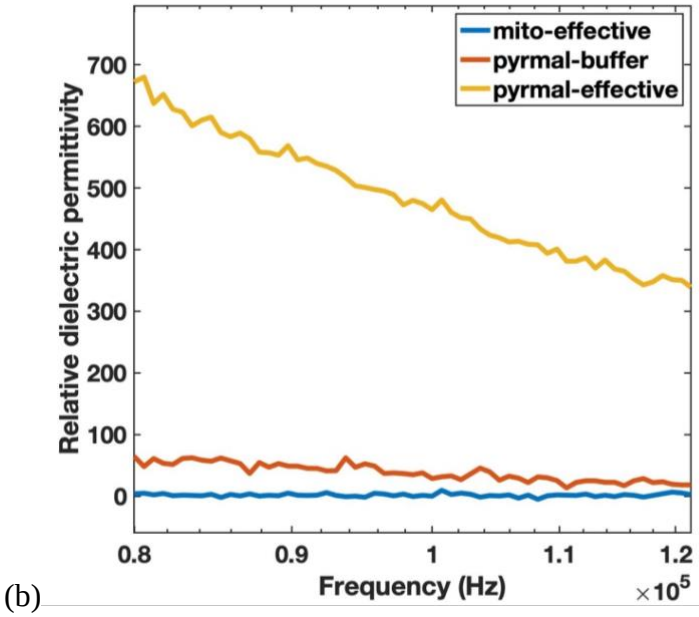

(b)

Figure 7.12: Relative dielectric permittivity calculated from admittance of effective admittance for mitochondria, and pyruvate and malate for a mitochondrial volume fraction of 0.09: (a) dispersion plot, and (b) dispersion plot magnified near 100 kHz frequency range.

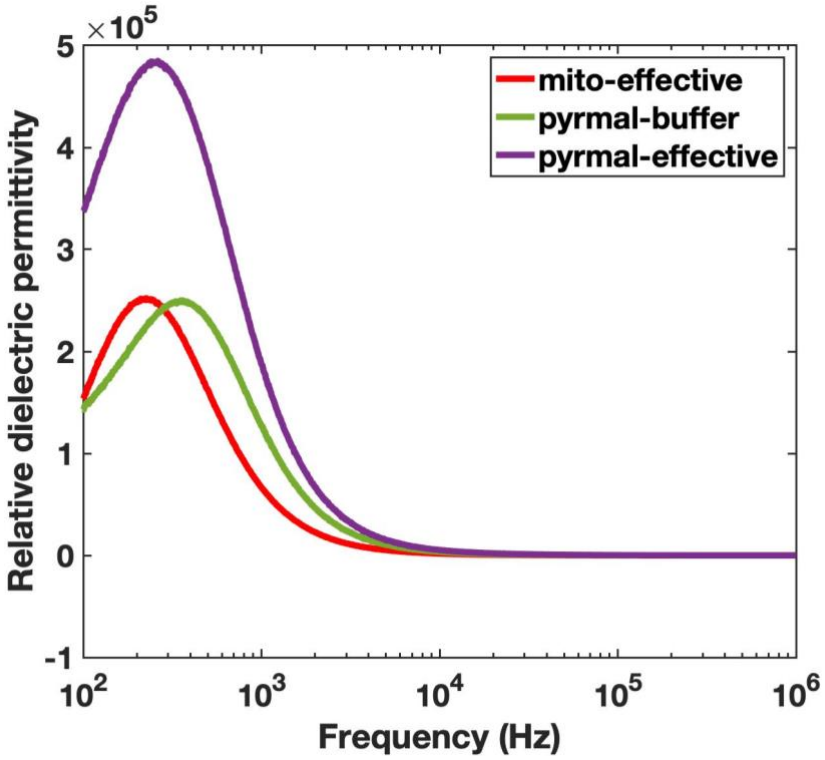

(a)

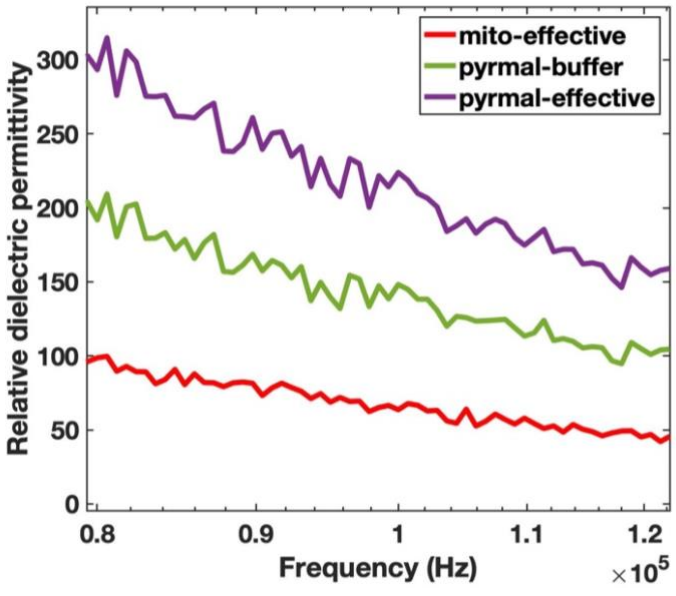

(b)

Figure 7.13: Relative dielectric permittivity calculated from admittance of effective admittance for mitochondria, and pyruvate and malate for a mitochondrial volume fraction of 0.33: (a) dispersion plot, and (b) dispersion plot magnified near 100 kHz frequency range.

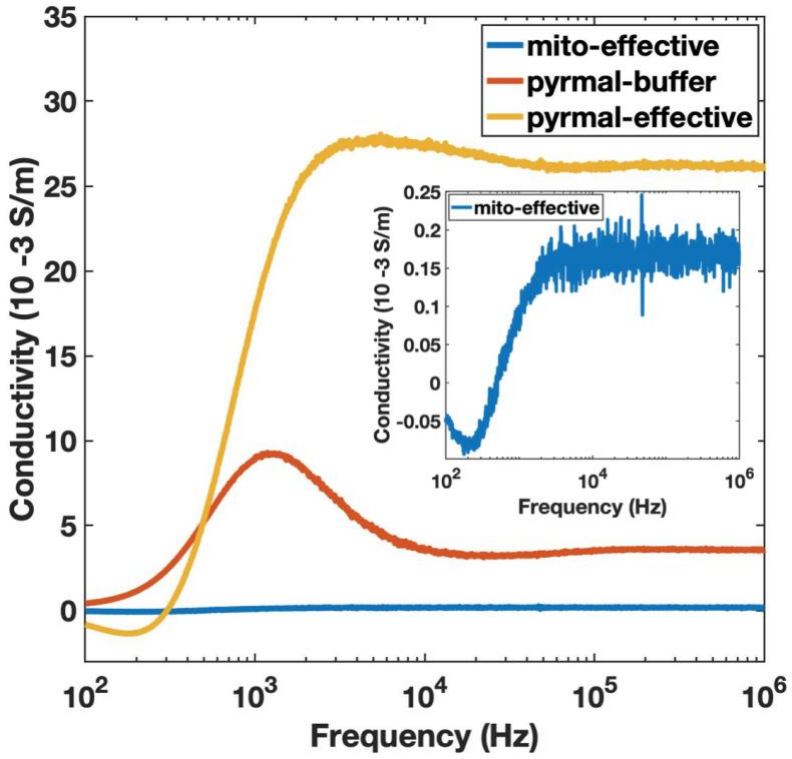

Figure 7.14: Conductivity calculated from admittance of effective admittance for mitochondria, and pyruvate and malate for a mitochondrial volume fraction of 0.09.

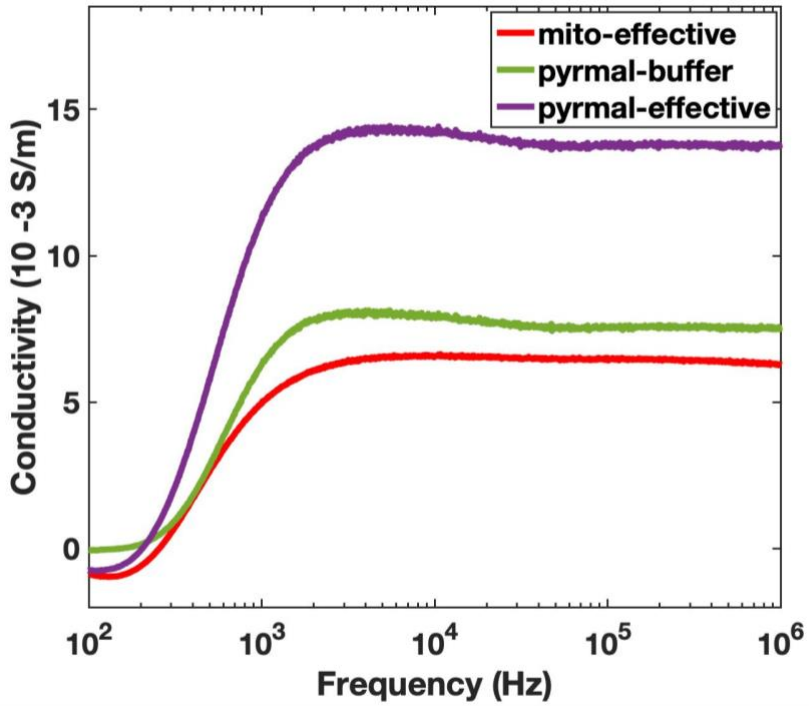

Figure 7.15: Conductivity calculated from admittance of effective admittance for mitochondria, and pyruvate and malate for a mitochondrial volume fraction of 0.33.

Chapter 8: Conclusions and Future work

In conclusion, a sensitive and effective probe was constructed for the purpose of real-time impedance spectroscopy studies of biological systems. Our results indicate that the probe was able to measure subtle changes in dielectric properties of biological media. For mitochondrial suspensions of various concentrations, the expected changes in membrane potential with titrations of different substrates, inhibitors, or uncouplers, were found to be congruent with some (though not all) of the dielectric and conductivity responses analyzed from impedance measurements. These expected changes were analyzed using basic bioenergetic respiratory protocols that provided insight into correlation between impedance changes and oxygen consumption in isolated mitochondria.

Biological systems interact with electromagnetic energy through the dielectric and conductivity properties of biological materials. The effective dielectric responses of mitochondrial suspensions provide information on the complex polarization processes that take place when an electric field is applied. Measuring the electrical properties provide understanding of the underlying biochemical processes that take place in these materials. However, such complex mitochondrial systems require extensive study to confidently identify and determine the exact processes that exhibit these behaviors. The investigation of biological specimens through the characterization of their electrical properties is a promising method from a diagnostic point of view. For complex mechanisms, such as mitochondrial electron transport pathways, the observed changes can be due to different properties and processes within the suspension being studied. These include, for example, the highly charged and polar properties of molecules such as ADP and ATP. In an electronic point of view, the changes in capacitive and resistive properties of mitochondrial suspensions can be determined, and modelled for detailed analysis.

Our technique for studying impedance measurements offers the ability to distinguish data accurately by removing the effect of electrode polarization. However, externally added substrates can be assumed to have electrode polarization effects as well, and need to be isolated by studying these substrates comprehensively to obtain more data. This method proves to be a sensitive and effective method for observing changes in dielectric properties of materials. The results obtained from this study show that changes in dielectric response can be correlated with changes in mitochondrial membrane potential in the presence of pyruvate and malate. Our calculations of admittance allowed the isolation of the effective change in dielectric constant when mitochondria responded to pyruvate and malate. These changes confirm that our method distinguishes the membrane potential change that affect the mitochondrial function.

For future developments building on this study, using extensive research and resources, this probe that was designed for the study of impedance spectroscopy can be used as a method to probe the changes in mitochondrial membrane potential and other aspects of mitochondrial activity. This probe was initially developed with the expectation of measuring impedance in four-terminal configuration to reduce effects of electrical polarization. Further studies using this device include solving the problem of instrumental measurement capability in four-terminal configuration, and observing the impedance for these mitochondrial systems. By developing this method, substantial information can be determined on these complex systems. Changes in membrane potential are closely correlated with the functionality and dysfunctionality of mitochondria, and by obtaining a broad range of information of frequency response of healthy mitochondria, methods can be developed to study dysfunctional and diseased mitochondria. As a non-invasive diagnostic technique in monitoring variations in biological functions, use of complex impedance to probe changes in mitochondrial membrane potential and other properties will likely become an increasingly powerful tool in biology, drug discovery, and medical diagnostics.

Bibliography

1. Prodan, C., Mayo, F., Claycomb, J. R., Miller Jr, J. H. and Benedik, M. J. Low-frequency, low-field dielectric spectroscopy of living cell suspensions. *Journal of Applied Physics*. 95(7):3754. 2004.
2. Prodan, E., Prodan, C. and Miller Jr, J. H. The dielectric response of spherical live cells in suspension: An analytic solution. *Biophysical Journal*. 95(9):4174-4182. 2008.
3. Bot, C. T. and Prodan, C. Probing the membrane potential of living cells by dielectric spectroscopy. *Eur Biophys J*. 38:1049-1059. 2009.
4. Mitra, R. C., Villagran, M. Y. S., Maric, S., Wosik J., Zagozdzon-Wosik, W. and Miller Jr, J. H. Evidence from Impedance Spectroscopy that Elevated Dopamine Reduces Mitochondrial Membrane Potential. *J Biosens Bioelectron*. 8(2). 2017.
5. Duchen, M. R. Mitochondria in health and disease: perspectives on a new mitochondrial biology. *Molecular Aspects of Medicine*. 25:365–451. 2004.
6. Mitra, R. C. Probing temporal changes in Mitochondrial Membrane Potential with Impedance Spectroscopy. *Doctoral Dissertation, University of Houston*. 2015.
7. Padmaraj, D., Pande, R., Miller, J. H. Jr, Wosik, J. and Zagozdzon-Wosik, W. Mitochondrial Membrane Studies Using Impedance Spectroscopy with Parallel pH Monitoring. *PLOS One*. 9(7). 2014.
8. Alberts, B., Bray, D., Lewis, J., Raff, M., Roberts, K. and Watson, J. D. *Molecular Biology of the Cell*. 3rd edition. New York: Garland Publishing. 1994.
9. Anderson, S., Bankier, A. T., Barrell, B. G., de Bruijn, M. H. L., Coulson, A. R., Drouin, J., Eperon, I. C., Nierlich, D. P., Roe, B. A., Sanger, F., Schreier, P. H., Smith, A. J. H., Staden, R. and Young, I. G. Sequence and organization of the human mitochondrial genome. *Nature*. 290:457-465. 1981.

10. Kühlbrandt, W. Structure and function of mitochondrial membrane protein complexes. *BMC Biology*. 13(89). 2015.

11. Siasos, G., Tsigkou, V., Kosmopoulos, M., Theodosiadis, D., Simantiris, S., Tagkou, N. M., Tsimpiktsioglou, A., Stampouloglou, P. K., Oikonomou, E., Mourouzis, K., Philippou, A., Vavuranakis, M., Stefanadis, C., Tousoulis, D. and Papavassiliou, A. G. Mitochondria and cardiovascular diseases—from pathophysiology to treatment. *Annals of Translational Medicine*. 6(12). 2018.

12. Concept of Biology: How Cells Obtain Energy. Digital image. https://slideplayer.com/slide/6529652/.

13. Lackner, L. L. Shaping the dynamic mitochondrial network. *BMC Biology*. 12 (35). 2014.

14. Frezza, C., Cipolat, S. and Scorrano, L. Organelle isolation: functional mitochondria from mouse liver, muscle and cultured fibroblasts. *Nat Protoc*. 2(2):287-295. 2007.

15. Picard, M., Taivassalo, T., Gouspillou, G. and Hepple, R.T. Mitochondria: isolation, structure and function. *J Physiol*. 589(18):4413-4421. 2011.

16. Mitchell, P. Coupling of Phosphorylation to electron and hydrogen transfer by a chemi-osmotic type of mechanism. *Nature*. 191:144-148. 1961.

17. Senior, A. E. ATP Synthesis by Oxidative Phosphorylation. *Physiological Reviews*. 68(1). 1988.

18. Nicholls, D. G. and Ferguson, S. J. *Bioenergetics 2*. 2nd edition. San Diego: Academic Press. 1992.

19. Electron transport chain and oxidative phosphorylation. Digital image. *Biology Dictionary*. 2019. https://biologydictionary.net/electron-transport-chain-and-oxidative-phosphorylation/.

20. The ATP cycle. Digital image. *Chemistry Libretexts*. 5 Jun 2019. https://chem.libretexts.org/.

21. Citric acid cycle with aconitate. Digital image. https://commons.wikimedia.org/wiki/File:Citric_acid_cycle_with_aconitate_2.svg.

22. Experiment Cm-3 Mitochondrial Respiration. *iwork Systems*. 2003. http://www.iworx.com/documents/LabExercises/MitoRespiration.pdf.

23. Rich, P. R. and Maréchal, A. The mitochondrial respiratory chain. *Biochemical Society*. 47:1-23. 2010.

24. Hüttemann, M., Lee, I., Pecinova, A., Pecina, P., Przyklenk, K. and Doan, J. W. Regulation of oxidative phosphorylation, the mitochondrial membrane potential, and their role in human disease. *J Bioenerg Biomembr*. 40:445-456. 2008.

25. H.M. Berman, J. Westbrook, Z. Feng, G. Gilliland, T.N. Bhat, H. Weissig, I.N. Shindyalov, P.E. Bourne. The Protein Data Bank. *Nucleic Acids Research*. 28:235-242. 2000. http://www.rcsb.org/.

26. Neupane, P., Bhuju, S., Thapa, N. and Bhattarai, H. K. ATP Synthase: Structure, Function and Inhibition. *BioMol Concepts.* 10:1-10. 2019.

27. Weber, J. and Senior, A. E. ATP synthesis driven by proton transport in F1F0-ATP synthase. *FEBS Letters.* 545(1):61-70. 2003.

28. Grimnes, S. and Martinsen, O. G. *Bioimpedance and Bioelectricity Basics.* London, UK: Academic Press. 2000.

29. Zorov, D. B., Juhaszova, M. and Sollott, S. J. Mitochondrial reactive oxygen species (ROS) and ROS-induced ROS release. *Physiol Rev*. 94(3):909-950. 2014.

30. Zorov, D. B., Juhaszova, M. and Sollott, S. J. Mitochondrial ROS-induced ROS release: an update and review. *Biochim Biophys Acta.* 1757(5-6):509-517. 2006.

31. Zorova, L. D., Popkov, V. A., Plotnikov, E. Y., Silachev, D. N., Pevzner, I. B., Jankauskas, S. S., Babenko, V. A., Zorov, S. D., Balakireva, A. D., Juhaszova, M., Sollott, S. J. and Zorov, D. B. Mitochondrial Membrane Potential. *Anal Biochem*. 552:50-59. 2018.

32. Labajova, A., Vojtiskova, A., Krivakova, P., Kofranek, J., Drahota, Z. and Houstek, J. Evaluation of mitochondrial membrane potential using a computerized device with a tetraphenylphosphonium-selective electrode. *Anal Biochem.* 353(1):37-42. 2006.

33. Perry, S. W., Norman, J. P., Barbieri, J., Brown, E. B. and Gelbard, H. A. Mitochondrial membrane potential probes and the proton gradient: a practical usage guide. *Biotechniques.* 50(2):98-115. 2011.

34. Liberman, E. A., Topaly, V. P., Tsofina, L. M., Jasaitis, A. A. & Skulachev, V. P. Mechanism of Coupling of Oxidative Phosphorylation and the Membrane Potential of Mitochondria. *Nature.* 222:1076–1078. 1969.

35. Ling, G. and Gerard, R. W. The normal membrane potential of frog sartorius fibers. *J Cell Comp Physiol.* 34(3):383-396. 1949.

36. Molleman, A. *Patch Clamping: An Introductory Guide To Patch Clamp Electrophysiology*. West Sussex, England: John Wiley & Sons. 2002.

37. Stuart, G. J. and Palmer, L. M. Imaging membrane potential in dendrites and axons of single neurons. *Pflugers Arch.* 453(3):403-410. 2006.

38. González, J. E. and Tsien, R. Y. Improved indicators of cell membrane potential that use fluorescence resonance energy transfer. *Chem Biol.* 4(4):269-277. 1997.

39. Padmaraj, D., Miller, J. H. Jr, Wosik, J. and Zagozdzon-Wosik, W. Reduction of electrode polarization capacitance in low-frequency impedance spectroscopy by using mesh electrodes. *Biosens Bioelectron.* 29(1):13-7. 2011.

40. Fernyhough, P., Roy Chowdhury, S. K. and Schmidt, R. E. Mitochondrial stress and the pathogenesis of diabetic neuropathy. *Expert Rev Endocrinol Metab.* 5(1):39-49. 2010.

41. Ferreira, I. L., Resende, R., Ferreiro, E., Rego, A. C. and Pereira, C. F. Multiple defects in energy metabolism in Alzheimer's disease. *Curr Drug Targets.* 11(10):1193-1206. 2010.

42. Haas R. H. Autism and mitochondrial disease. *Dev Disabil Res Rev.* 16(2):144-153. 2010.

43. Jarett, S. G., Lewin, A. S. and Boulton, M. E. The importance of mitochondria in age-related and inherited eye disorders. *Ophthalmic Res.* 44(3):179-190. 2010.

44. Kawamata, H. and Manfredi, G. Mitochondrial dysfunction and intracellular calcium dysregulation in ALS. *Mech Ageing Dev.* 131(7-8):517-526. 2010.

45. Kones, R. Parkinson's disease: mitochondrial molecular pathology, inflammation, statins, and therapeutic neuroprotective nutrition. *Nutr Clin Pract.* 25(4):371-389. 2010.

46. Ren, J., Pulakat, L., Whaley-Connell, A. and Sowers, J. R. Mitochondrial biogenesis in the metabolic syndrome and cardiovascular disease. *J Mol Med.* 88(10):993-1001. 2010.

47. Rocha, M., Apostolova, N., Hernandez-Mijares, A., Herance, R. and Victor, V. M. Oxidative stress and endothelial dysfunction in cardiovascular disease: mitochondria-targeted therapeutics. *Curr Med Chem.* 17(32):3827-3841. 2010.

48. Rosenstock, T. R., Duarte, A. I. and Rego, A. C. Mitochondrial-associated metabolic changes and neurodegeneration in Huntington's disease - from clinical features to the bench. *Curr Drug Targets.* 11(10):1218-1236. 2010.

49. Scaglia, F. The role of mitochondrial dysfunction in psychiatric disease. *Dev Disabil Res Rev.* 16(2):136-143. 2010.

50. Waldbaum, S. and Patel, M. Mitochondrial dysfunction and oxidative stress: a contributing link to acquired epilepsy? *J Bioenerg Biomembr.* 42(6):449-455. 2010.

51. Suomalainen, A. and Battersby, B. J. Mitochondrial diseases: the contribution of organelle stress responses to pathology. *Nature Reviews Molecular Cell Biology*. 19:77–92. 2018.

52. Brand, M. D., Chien, L. F., Ainscow, E. K., Rolfe, D. F. and Porter, R. K. The causes and functions of mitochondrial proton leak. *Biochim Biophys Acta.* 1187(2):132-139. 1994.

53. Feeney, C. J., Pennefather, P. S. and Gyulkhandanyan, A. V. A cuvette-based fluorometric analysis of mitochondrial membrane potential measured in cultured astrocyte monolayers. *Journal of Neuroscience Methods.* 125(1-2):13-25. 2003.

54. Rottenberg, H. and Wu, S. Quantitative assay by flow cytometry of the mitochondrial membrane potential in intact cells. *Biochim Biophys Acta.* 1404(3):393-404. 1998.

55. Zoratti, M. and Szabò, I. The mitochondrial permeability transition. *Biochim Biophys Acta.* 1241(2):139-176. 1995.

56. Capuano, F., Guerrieri, F. and Papa, S. Oxidative phosphorylation enzymes in normal and neoplastic cell growth. *J Bioenerg Biomembr.* 29(4):379-384. 1997.

57. Pedersen, P. L. and Morris, H. P. Uncoupler-stimulated adenosine triphosphatase activity. Deficiency in intact mitochondria from Morris hepatomas and ascites tumor cells. *J Biol Chem.* 249(11):3327-3334. 1974.

58. Brand, M. D. and Nicholls, D. G. Assessing mitochondrial dysfunction in cells. *Biochem J.* 435:297–312. 2011.

59. Heidari, R. and Niknahad, H. The Role and Study of Mitochondrial Impairment and Oxidative Stress in Cholestasis. *Methods in Molecular Biology*. Vol.1981. New York: Humana Press. 2019.

60. Kuznetsov, A. V., Veksler, V., Gellerich, F. N., Saks, V., Margreiter, R. and Kunz, W. S. Analysis of mitochondrial function in situ in permeabilized muscle fibers, tissues and cells. *Nat Protoc.* 3(6):965-976. 2008.

61. Saks, V. A., Belikova, Y. O. and Kuznetsov, A. V. In vivo regulation of mitochondrial respiration in cardiomyocytes: specific restrictions for intracellular diffusion of ADP. *Biochim Biophys Acta.* 1074(2):302-311. 1991.

62. Picard, M., Taivassalo, T., Ritchie, D. Wright, K. J., Thomas, M. M., Romestaing, C. and Hepple, R. T. Mitochondrial structure and function are disrupted by standard isolation methods. *PLOS One.* 6(3). 2011.

63. Eigentler A., Fontana-Ayoub M., Fasching M., Lassnig B., Stadlmann S., Rieger G., Haffner B., Lemieux H., Gnaiger E. Selected Media and Chemicals for Respirometry with Mitochondria and Permeabilized Cells. *Mitochondrial Physiology Network.* 3(2):1-9. 2012.

64. Wollenman L.C., Vander Ploeg M.R., Miller M.L., Zhang Y., Bazil J.N. The effect of respiration buffer composition on mitochondrial metabolism and function. *PLOS One.* 2017.

65. Gnaiger E. Mitochondrial Pathways and Respiratory Control - An Introduction to OXPHOS Analysis. *OROBOROS MiPNet Publications.* 4. 2014.

66. Gnaiger E., Fasching M., Gradl L., Gradl P. Oxygraph-2k: Start High-Resolution Respirometry. *Mitochondrial Physiology Network.* 12(6):1-18. 2012.

67. Gnaiger E. The Oxygraph for High-Resolution Respirometry. *Mitochondrial Physiology Network.* 6(1):1-18. 2011.

68. Bandarenka, A. S. Exploring the interfaces between metal electrodes and aqueous electrolytes with electrochemical impedance spectroscopy. *The Royal Society of Chemistry*. 138:5540–5554. 2013.

69. Palmeira, C. M. and Moreno, A. J. Methods in Molecular Biology. *Mitochondrial Bioenergetics: Methods and Protocols*. 810:Ch.3 Springer Science+Business Media. 2012.

70. Lesnefsky, E. J. and Hoppel, C. L. Oxidative phosphorylation and aging. *Aging Research Reviews*. 5(4):402-433. 2006.

71. Zivkovic, I. and Murk, A. Free-Space Transmission Method for the Characterization of Dielectric and Magnetic Materials at Microwave Frequencies. *Microwave Materials Characterization.* IntechOpen. 2012.

72. Siddabattuni, S. Interfacial effects on dielectric properties of polymer-particle nanocomposites. *Doctoral Dissertations*. 1954. 2011.

73. Kao, K. C. Dielectric Phenomena in Solids With Emphasis on Physical Concepts of Electronic Processes. *Academic Press Publications*. 2004.

74. Pradhan, R., Mitra, A. and Das, S. Impedimetric characterization of human blood using three-electrode based ECIS devices. *J Electr Bioimp*. 3:12-19. 2012.

75. Prodan, C. and Prodan, E. The dielectric behavior of living cell suspensions. *J Phys D: Appl Phys*. 32(3):335. 1998.

76. Schwan, H. P. Electrical properties of tissues and Cell Suspensions: Mechanisms and Models. *IEEE*. 1994.

77. Pauly, H. and Packer, L. The Relationship of Internal Conductance and Membrane Capacity to Mitochondrial Volume. *J Biophys Biochem Cytol.* 7:603-612. 1960.

78. Asami, K., Irimajiri, A., Hanai, T., Shiraishi, N. and Utsumi, K. Dielectric Analysis of Mitochondria Isolated from Rat Liver I. Swollen Mitoplasts as Simulated by a Single-shell Model. *Biochimica et Biophysica Acta*. 778:559-569. 1984.

79. Bot, C. T. and Prodan, C. Quantifying the membrane potential during *E. coli* growth stages. *Biophysical Chemistry*. 146:133-137. 2010.

80. Prodan, C. and Bot, C. T. Correcting the polarization effect in very low frequency dielectric spectroscopy. *J Phys D: Appl Phys.* 42:175505. 2009.

81. Claycomb, J. R. and Tran, J. Q. P. Introductory Biophysics Perspectives on the Living State. *Jones and Bartlett.* 2011.

82. Macdonald, J. R. Impedance Spectroscopy. *Annals of Biomedical Engineering.* 20:289-305. 1992.

83. Barsoukov, E. and Macdonald, J. R. Impedance Spectroscopy Theory, Experiment, and Applications. *John Wiley & Sons.* 2. 2005.

84. Padmaraj, D. Biomems for Mitochondria Medicine. *Doctoral Dissertation, University of Houston.* 2010.

85. Krishnamoorthy, S. *Nanomaterials: A Guide to Fabrication and Applications*. 1st edition. New York: CRC Press. 2016.

86. Dean, D.A., Ramanathan, T., Machado, D. and Sundararajan, R. Electrical Impedance Spectroscopy Study of Biological Tissues. *J Electrostat.* 66(3-4):165-177. 2008.

87. Gesteland, R. C., Howland, B., Lettvin, J. Y. and Pitts, W. H. Comments on Microelectrodes. *IEEE.* 47(11):1856-1862. 1959.

88. Impedance Measurement Handbook - A guide to measurement technology and technique. *Keysight Technologies.* 6. 2016.

89. Dean, D. A., Ramanathan, T., Machado, D. and Sundararajan, R. Electrical Impedance Spectroscopy Study of Biological Tissues. *J Electrostat.* 66(3-4):165–177. 2007.

90. Ellappan, P. and Sundararajan, R. A simulation study of the electrical model of a biological cell. *J Electrostat.* 63:297–307. 2005.

91. Radke S. M., Alocilja E. C. Design and Fabrication of a Microimpedance Biosensor for Bacterial Detection. *IEEE Sensors Journal.* 4(4):434-440. 2004.

92. Bannwarth, S., Darestani, M., Coster, H. and Wessling, M. Characterization of hollow fiber membranes by impedance spectroscopy. *Journal of Membrane Science*. 473:318-326. 2015.

93. Cai, X., Zhang, Y., Yin, L., Ding, D., Jing, W. and Gu, X. Electrochemical impedance spectroscopy for analyzing microstructure evolution of NaA zeolite membrane in acid water/ethanol solution. *Chemical Engineering Science*. 153:1-9. 2016.

94. Schoenbach, K. H., Katsuki, S., Stark, R. H., Buescher, E. S. and Beebe, S. Bioelectrics - New applications for pulsed power technology. *IEEE Transactions on Plasma Science*. 30(1):293-300. 2002.

95. Margo, C., Katrib, J., Nadi, M. and Rouane, A. Four electrode embedded bioimpedance measurement system. *IEEE.* 2013.

96. Margo, C., Katrib, J., Nadi, M. and Rouane, A. A four-electrode low frequency impedance spectroscopy measurement system using the AD5933 measurement chip. *Physiological Measurement.* 34:391-405. 2013.

97. Sarróa, E., Lecina, M., Fontova, A., Solà, C., Gòdia, F., Cairó, J. J. and Bragós, R. Electrical impedance spectroscopy measurements using a four-electrode configuration improve on-line monitoring of cell concentration in adherent animal cell cultures. *Biosensors and Bioelectronics.* 31:257-263. 2012.

98. Karlapudi, U. K. Bio-Impedance Spectrometer for Electrical Characterization of Mitochondria. *Doctoral Dissertation, University of Houston*. 2018.

99. Ayliffe, H. E., Frazier, A. B. and Rabbitt, R. D. Electric Impedance Spectroscopy Using Microchannels with Integrated Metal Electrodes. *IEEE Journal of Mitcroelectromechanical Systems.* 8(1):50-57. 1999.

100. Dielectric Constants of Liquids. Engineering ToolBox. https://www.engineeringtoolbox.com/liquid-dielectric-constants-d_1263.html. 2018.